ABSTRACT

Title of Dissertation:	COORDINATED TRAFFICKING OF HEME TRANSPORTERS BY CARGO SORTING COMPLEXES IS ESSENTIAL FOR ORGANISMAL HEME HOMEOSTASIS
	Sohini Dutt, Doctor of Philosophy, 2024
Dissertation directed by:	Professor Iqbal Hamza, Department of Animal and Avian Sciences

Heme, an iron-containing organic ring, is a vital cofactor responsible for diverse biological functions and is the major source of bioavailable iron in the human diet. As a hydrophobic and cytotoxic cofactor, heme must be transported in a highly controlled manner through membranes via specific intra- and inter-cellular pathways. However, the genes and pathways responsible for heme trafficking remain poorly understood. Unlike other metazoans, *Caenorhabditis elegans* cannot synthesize heme but requires heme for sustenance. Thus, *C. elegans* is an ideal animal model to identify heme trafficking pathways as it permits organismal heme homeostasis to be directly manipulated by controlling environmental heme. Heme is imported apically into the intestine by HRG-1-related permeases and exported basolaterally by MRP-5/ABCC5 to extra-intestinal tissues. Loss of *mrp-5* causes embryonic lethality that can be suppressed by dietary heme supplementation raising the possibility that MRP-5-independent heme export pathways must exist. Here we show, by performing a forward genetic screen in *mrp-5* null mutants, that loss of the vesicular cargo sorting Adaptor Protein complexes (AP-3) fully rescues *mrp-5* lethality and

restores heme homeostasis. Remarkably, intestinal heme accumulation due to *mrp-5*-deficiency causes a concomitant deficit in the lysosomal heme importer HRG-1 abundance and localization. Loss of both MRP-5 and AP-3 subunits resurrects HRG-1 levels and localization, thus underscoring the crucial role of HRG-1 in dictating *mrp-5* mutant phenotypes. In the absence of MRP-5, heme is exported by SLC49A3 homolog, a previously uncharacterized transporter. Live-cell imaging reveals vesicular coalescence that facilitates heme transfer between the importers and exporters at the interface of lysosomal-related organelle. These results define a mechanistic model for metazoan heme trafficking and identifies SLC49A3 as a promising candidate for heme export in mammals.

COORDINATED TRAFFICKING OF HEME TRANSPORTERS BY CARGO SORTING COMPLEXES IS ESSENTIAL FOR ORGANISMAL HEME HOMEOSTASIS

by

Sohini Dutt

Dissertation submitted to the Faculty of the Graduate School of the
University of Maryland, College Park, in partial fulfillment
of the requirements for the degree of
Doctor of Philosophy
2024

Advisory Committee:
Professor Iqbal Hamza, Chair
Dr. Tom Porter
Dr. Nishanth Sunny
Dr. Antony Jose
Dr. Michael Krause

Dedication

In the loving memory of my grandpa,

Who never missed a chance to cheer me on.

I wish you could be here to see this,

but I know you are cheering for me from up above

Acknowledgements

The journey towards my PhD would not have been possible without the support, guidance, and love from many incredible people. At the forefront of this journey stands my advisor and mentor Dr. Iqbal Hamza. Your invaluable guidance, mentorship, and unwavering support have been instrumental throughout my doctoral studies. Your ability to push me to my limits and think critically about research forced me to improve continuously. Yet, at the same time, your unwavering belief in my potential and your enthusiastic celebration of all my small successes fueled my determination. I am amazed by your boundless energy and infectious enthusiasm, that motivates all of us to push harder and achieve more! Thank you for fostering my scientific curiosity and for the lasting impact you have had on my journey.

I am also incredibly grateful to my thesis committee, Dr. Tom Porter, Dr. Nishanth Sunny, Dr. Antony Jose and Dr. Michael Krause. Your insightful feedback and your diverse perspectives helped me shape my research throughout the course of this dissertation. Thank you for bearing with me through all those long committee meetings! A special thanks goes to Dr. Nishanth Sunny for being a great mentor and friend, and for always having your office doors open to welcome me.

Thank you to all the past and present Hamza Lab members, who created a supportive and collaborative research environment that made coming to the lab a joy. Simon Beardsley, thank you for your incredible piece of work that paved the way to my entire

dissertation. Rini thank you for being a dear friend even after you graduated. Ian, thanks for all fruitful discussions during the middle of my PhD journey. The IGC energy was dearly missed in the last couple of years. Thank you, Andrew, Audrey, and Indira, for the countless stimulating discussions and shared experiences. Thank you Sandeepan, Ran, and Jonathan for being an amazing bunch of “Team Wormies”! Thank you, Dr. Xiaojing Yuan, for all your valuable insights and scientific support throughout this whole journey. To Melissa and Xuedi, this journey would not have been possible without the friendship and love from the both of you. Thank you for being the absolute best and for forming friendships that go way beyond the bench.

To my incredible graduate school friends- this journey would not have been the same without you. To my first roommate, Daphne thank you for giving me not just your unwavering friendship, but also a family in the US. Ahana and Bidisha, thank you for giving me some of the best graduate school memories since 2018 and for celebrating milestones together. Roni, Parama, Rishov, Upamanyu, Adway, Darshan, Sagnik, Samarpan, and Agniv thank you for making my days in Graduate Hills filled with endless laughter and for reminding me the importance of a life outside of academia. Maria, Aashli, Spandan, and Nikhil, thank you for your love and friendship.

A special debt of gratitude goes to Dr. Arnab Gupta, my mentor during my post-baccalaureate studies, whose guidance and encouragement during that formative time instilled the spark within me to pursue a PhD.

A heartfelt thank you to my grandparents, throughout my life. Your presence, even if from afar, has always meant the world to me.

To my parents-in-law, I am incredibly grateful for your understanding, support and warm welcome to your family. Thank you for being the best in-laws and for celebrating all my successes and for sticking by my side through the failures.

To my uncle, whose own path in academia has been a constant source of motivation for me. Thank you for always lending a patient ear, ready to hear about my struggles and successes.

To my parents, thank you for giving me the unwavering foundation that supported me throughout my life. Thank you for believing in me when I did not. This achievement is a testament to the foundation you have built on me, and I am forever grateful for your constant love and encouragement. Thank you for everything.

To my sister, a special thank you. Thank you for being my confidante, my cheerleader, and for always believing in me. You were always there to pick me up during every setback. This achievement feels even more special, knowing I could share it with you. You are, and will always be, my biggest strength.

And last but not least, to my dearest husband, Sankha, this journey took an unexpected turn for the best when you became my permanent roommate during PhD. You

celebrated my successes, empathized with my setbacks, while always offering me a comforting shoulder and a listening ear. I consider myself extremely fortunate to have a husband who is in the same boat as me, having shared camaraderie, frustrations, triumphs, and memories I will forever cherish through the ups and downs of graduate school. Thank you for being my partner in crime during this challenging yet rewarding journey. This dissertation is as much mine as it is yours.

Table of Contents

List of Figures

List of Abbreviations

ABC	ATP binding cassette
ALA	δ-aminolevulinic acid
ALAS	δ-aminolevulinic acid synthase
ANOVA	Analysis of variance
AP	Adaptor protien
APX	Ascorbate peroxidase
ATP	Adenosine triphosphate
BBB	Blood brain barrier
BCS	Bathocuproine disulphonate
BLOC	Biogenesis of lysosome-related organelles complex-1
BMP	Bone morphogenetic protein
BSA	Bovine serum albumin
COX	Cytochrome C oxidase
CPM	Counts per million
CYC	Cytochrome C
CRISPR	Clustered regularly interspaced short palindromic repeats
cryo-EM	Cryogenic electron microscopy
DIC	Differential interference contrast
DMEM	Dulbecco’s modified Eagle’s medium
DMT	Divalent metal transporter
DNA	Deoxyribonucleic acid
DPBS	Dulbecco's phosphate-buffered saline
DTT	Dithiothreitol
ECL	Extracellular loop
EDTA	Ethylenediaminetetraacetic acid
EE	Early endosome
ER	Endoplasmic reticulum
FBS	Fetal bovine serum
FECH	Ferrochelatase
FLVCR	Feline leukemia virus, subgroup C, receptor
GAPDH	Glyceraldehyde 3-phosphate dehydrogenase
GaPPIX	Gallium protoporphyrin
GFP	Green fluorescent protein
GTP	Guanosine-5'-triphosphate
HA	Hemagglutinin
HD	Heme depleted
HEPES	4-(2-hydroxyethyl)-1-piperazineethanesulfonic acid
HMOX	Heme oxygenase
Hp	Haptoglobin
HRG	Heme responsive gene
HRP	Horseradish peroxidase
Hx	Hemopexin
IMM	Inner mitochondrial membrane

IMS	Intermembrane space
IPTG	Isopropyl β-D-1-thiogalactopyranoside
LB	Luria-Bertan
LE	Late endosome
KO	Knockout
LAMP1	Labile heme pool
LHP	Labile heme pool
LOF	Loss of function
LRO	Lysosomal associated membrane protein 1
MAM	Mitochondrial-associated membrane
MARP	Membrane associated progesterone receptor
mCeHR	Modified *C. elegans* habitation and reproduction
MAM	Mitochondria associated membrane
MCS	Membrane contact site
MDCK	Madin-Darby canine kidney
MEF	Mouse embryonic fibroblasts
MICOS	Mitochondrial contact site and cristae organizing system
mRNA	Messenger RNA
MRP	Multidrug resistance-associated protein
MSD	Membrane spanning domain
NGM	Nematode growth medium
NRK	Normal rat kidney
OD	Optical density
OMM	Outer mitochondrial membrane
ORF	Open reading frame
PBG	Porphobilinogen
PBGD	Porphobilinogen deaminase
PBS	Phosphate buffered saline
PC	Phosphatidylcholine
PCR	Polymerase chain reaction
PFA	Paraformaldehyde
PGRMC	Progesterone receptor membrane component
PM	Plasma membrane
PPIX	Protoporphyrin IX
QKO	Quadruple knockout
RBC	Red blood cell
RNA	Ribonucleic acid
RNAi	RNA interference
SA	Succinyl acetone
SDS-PAGE	Sodium dodecyl sulfate polyacrylamide gel electrophoresis
SEM	Standard error of the mean
SLC	Solute carrier
TCA	Tricarboxylic acid
TGN	Trans-Golgi network
TMD	Transmembrane domain
UROS	Uroporphyrinogen III synthase

UROD	Uroporphyrinogen III decarboxylase
UTR	Untranslated region
WGA	Wheat germ agglutinin
WT	Wildtype
ZnMP	Zinc mesoporphyrin

Chapter 1: Introduction

Heme is an iron containing porphyrin, which acts as an essential cofactor for a multitude of biological functions. Hemoproteins are involved in oxygen binding and transport (globins), xenobiotic detoxification (cytochrome P450s), oxidative metabolism (succinate dehydrogenase, cytochrome c oxidase), gas sensing, (nitric oxide synthase, guanyl cyclase) and microRNA processing (DGCR8). Transcription factors can bind heme and regulate functions of downstream target genes, which in turn effects several pathways including mitochondrial respiration, circadian rhythms, apoptosis, cell proliferation, antioxidant stress response and ion channel activity. While heme is critical for all these biological processes it is also cytotoxic and hydrophobic, making it a necessary evil for the cell. Free heme generates reactive oxygen species because of its peroxidase activity. Additionally, heme can intercalate into membranes and bind non-specifically to proteins. Hence cellular heme levels need to be tightly regulated to maintain homeostasis. While great strides have been made in understanding heme synthesis and degradation, heme trafficking pathways remain poorly understood [1].

Section 1: Heme synthesis and degradation

Heme biosynthesis in most eukaryotes occurs via the Shemin/C4 pathway, which involves eight enzymatic steps shared between the mitochondria and cytosol [2]. The

first and rate limiting step of heme synthesis involves the condensation of glycine and succinyl-coenzyme A to form 5-aminolevulinate (ALA), catalyzed by the enzyme ALA synthase (ALAS) in the mitochondrial matrix. This ALA is then shuttled from the mitochondrial matrix to the cytosol, where ALA dehydratase (ALAD) converts ALA to porphobilinogen (PBG). Hydroxymethylbilane synthase or PBG deaminase (PBGD) then condenses four molecules of PBG to form hydroxymethylbilane, which in turn is cyclized to form uroporphyrinogen III by uroporphyrinogen synthase (UROS). In the final cytosolic step, uroporphyrinogen decarboxylase (UROD) catalyzes the decarboxylation of uroporphyrinogen III to coproporphyrinogen III. This is transported back into the mitochondrial inter-membrane space (IMS) where it gets oxidized to protoporphyrinogen IX by coproporphyrinogen oxidase (CPOX). In the matrix, protoporphyrinogen oxidase (PPOX) converts protoporphyrinogen IX to protoporphyrin IX (PPIX). Finally, ferrous ion is inserted into the PPIX ring to form heme by ferrochelatase (FECH) on the matrix side of the mitochondrial inner membrane [3]. FECH has been demonstrated to form complexes with ALAS, protoporphyrinogen oxidase, α-ketoglutarate dehydrogenase, succinyl-CoA-synthase, and the porphyrinogen transporter TMEM14C [4,5]. Further, FECH is involved in protein-protein interactions with mitoferrin, ATP binding cassette (ABC) transporters ABCB7 and ABCB10, heme chaperones progesterone receptor membrane component 1 and 2 (PGRMC1 and PGRMC2) [6]. Together, these discoveries endorse a model of an intricate metabolon for heme synthesis that safeguards the cellular milieu from the toxic intermediates of the pathway while facilitating efficient substrate channeling between the mitochondria and the cytosol [7]. Heme synthesis needs to be tightly

regulated at multiple levels since defects in this pathway cause toxic accumulation of intermediates, ultimately resulting in a group of diseases called porphyria. Additionally, there is a metabolic interplay between heme synthesis and oxidative phosphorylation, tricarboxylic acid cycle (TCA), as well as iron-sulfur cluster biogenesis. Recent research suggests that heme synthesis via ALAS1 and heme export by feline leukemia virus subgroup C receptor-related (FLVCR) protein FLVCR1a dictates the TCA cycle and oxidative phosphorylation flux, thereby impacting ATP distribution between the mitochondria and cytosol [8]. Further evidence of this crosstalk comes from studies showing that ALAD coordinates with an Fe_4S_4 cluster that is essential for its enzymatic activity [9]. The tight coupling of heme synthesis and other metabolic pathways underscores the need for precise regulation because any disruption in this finely tuned system can have cascading negative effects.

Heme is degraded enzymatically by heme oxygenases HO-1 and HO-2 to biliverdin, carbon monoxide and free iron. While HO-1 is induced by heme, metal ions, hormones and oxidative stress, HO-2 is constitutively expressed, primarily in the brain and testis [10].

Despite significant progress in understanding heme synthesis and degradation, there are several gaps in knowledge including those related to the transport of key components like glycine and protoporphyrinogen IX into the mitochondria, and shuttling of ALA into the cytosol. It is also unclear as to how heme oxygenases get

their heme, and if there are other proteins that donate heme to heme oxygenases for degradation [4].

Section 2: Intracellular heme trafficking

The terminal step of heme synthesis involves the insertion of iron into protoporphyrin ring, which occurs within the mitochondrial matrix. This heme then needs to be transported across both the inner and outer mitochondrial membranes, for incorporation into several hemoproteins present in different cellular compartments including the cytosol, endoplasmic reticulum, Golgi complex, nucleus, peroxisomes, and plasma membrane.

In the cytosol, the canonical glycolytic enzyme, glyceraldehyde phosphate dehydrogenase (GAPDH) is proposed to mediate the insertion of heme into nitric oxide synthase and soluble guanyl cyclase [11]. Despite elucidating the kinetics and key residues involved in heme binding to GAPDH, we currently lack understanding of the mechanism by which GAPDH interacts with client hemoproteins and transfers heme. Glutathione-S-transferases, known for conjugating glutathione to electrophilic compounds, also interacts with heme and porphyrins [12]. HBP23/PRX1 is a thiol peroxidase that loses its activity upon heme binding, while p22HBP is another cytosolic heme binding protein that binds to protoporphyrin IX (PPIX) [13]. Fatty acid binding protein has also been shown to bind heme [14]. The progesterone receptor membrane component (PGRMC) proteins, PGRMC1 and PGRMC2 forms complexes with ferrochelatase, the last enzyme in heme biosynthesis [15]. PGRMC1, PGRMC2,

Neurodesin, and Neuferricin, all of which belong to a family of Membrane Associated Progesterone Receptor (MAPR) proteins, share a cytochrome b5-like domain, and can bind heme. PGRMC2 has been demonstrated to mobilize heme from the ER to the nucleus and regulate thermogenesis [16]. Cytochrome P450s, despite being ER-anchored have their heme containing globular domain facing the cytosol. These cytosolic heme binding proteins play a general role in heme detoxification via sequestration or transfer. The cytosol constitutes the largest cellular labile heme pool of 20-340 nM, in contrast to mitochondria and nucleus, both of which have less than 1 nM [17,18].

The nuclear heme-binding proteins include transcription factors BACH1, REV-ERB-α, HAP1p, p53, and the micro-RNA processing protein DGCR8 [4]. BACH1 and p53 bind heme leading to their ubiquitination and proteasomal degradation. REV-ERB-α acts as a transcription repressor after binding to heme, thus effecting its stability and gas-sensing activity [19]. Additionally ferric heme regulates micro-RNA processing by activating the RNA binding protein DGCR8 [20,21].

In the secretory pathway, hemoproteins synthesized, processed, and folded in the ER and Golgi complex need to be correctly targeted to lysosomes, peroxisome, and plasma membrane. Some of the secretory pathway hemoproteins including the prostaglandin synthases COX1 and COX2 in the ER, myeloperoxidase in lysosome-like azurophil granules, catalase in peroxisomes, eosinophil peroxidase in eosinophil granules, and thyroperoxidase and ferric reductase on the plasma membrane [4,22]. Inter-organellar

membrane contact sites (MCSs) are physical contacts between two membrane-bound organelles that have been demonstrated to play critical roles in cell signaling and metabolite exchange including phospholipids transfer [23]. Given that the ER forms MCSs with mitochondria, the site for heme synthesis, we have previously proposed that the ER network can facilitate intra-cellular heme trafficking [3]. Indeed, experiments using genetically encoded fluorescent heme sensors in *Saccharomyces cerevisiae* revealed an ER-mitochondria network regulating heme trafficking to the nucleus along with identification of the GTPases involved in nuclear heme trafficking [24]. Recent studies also demonstrated that yeast ferrochelatase forms an oligomeric complex with Mic60, a component of the mitochondrial contact site and cristae organization system (MICOS). In the absence of Mic60, ferrochelatase activity is perturbed, leading to accumulation of toxic tetrapyrrole precursors. Interestingly the oxidative stress caused because of this can be mitigated by synthetic reconstruction of intermembrane connection [25]. In mammals, ER-mitochondrial membrane sites remain poorly understood, and their roles in heme trafficking and mobilization are yet to be defined.

The intestine heme exporter MRP-5, initially discovered in *Caenorhabditis elegans*, regulates heme levels within the secretory pathway. Worms with deletions in *mrp-5* experience a heme-dependent lethality, indicating a crucial role of *mrp-5* in exporting heme from the intestine to extra-intestinal tissues [26]. Interestingly, mice lacking Mrp5 do not exhibit heme-related phenotype. However, absence of Mrp5 and its close homolog Mrp9 in mice leads to male reproductive problems, mitochondrial

dysfunction and aberrant levels of the heme precursor succinyl-coenzyme A. Notably, both Mrp5 and Mrp9 are localized to MAMs within the testis, but whether they transport heme in MAMs is yet to be investigated [27].

Section 3: Intercellular heme trafficking

The dogma in heme biology states that cellular heme homoeostasis is maintained solely by heme synthesis and degradation in a cell autonomous manner [28]. However, the discovery and characterization of cellular heme importers and exporters challenge this long-standing belief, implying that cellular heme homeostasis is not only maintained cell-autonomously, but also by an inter-tissue communication to ensure systemic heme homeostasis. In fact, multiple studies have unraveled regulators of the paradigm-shifting inter-organ heme homeostasis.

Using the heme auxotroph *C. elegans*, HRG-3 was identified as an inter-cellular heme chaperone, which binds to and delivers maternal heme to the developing oocytes [29]. Under low heme conditions, *hrg-3* is transcriptionally upregulated, secreted from the mother's intestine into the pseudocoelom, thus aiding in heme mobilization to extra-intestinal tissues including oocytes. Loss of *hrg-3* results in intestinal heme unable to reach the oocytes, which become heme deficient and post-fertilization, the embryos get developmentally arrested.

Another key player in heme homeostasis is HRG-2, a putative heme reductase, that facilitates heme utilization in the hypodermis of *C. elegans*. HRG-2 is a heme binding type-I membrane protein, residing in the ER and apical plasma membrane of hypodermal cells [30].

The discovery of intercellular regulators of heme homeostasis raises an intriguing question. Are there systemic signaling pathways that can communicate the heme status between distant organs or cell types? We can draw an analogy from iron metabolism, where hepcidin functions as a master regulator for maintenance of systemic iron homeostasis [31]. In fact, studies using *C. elegans* identified HRG-7, a homolog of A1 aspartic proteases, as a secreted signaling molecule that communicates long-range signaling at the intestine-neuron axis to promote systemic heme homeostasis [32]. Under heme deficient conditions, HRG-7 is secreted from the intestine, and perceived by the anterior and posterior neurons. The neurons, in turn communicate via a feedback signal mediated by DBL-1, the worm homolog of bone morphogenetic protein 5 (BMP5), which represses intestinal HRG-7 through a transcription factor SMA-9 [32]. Given that human homologs exist for HRG-7, DBL-1 and SMA-9, genetic and biochemical studies in *C. elegans* can potentially open doors to unravel similar inter-organ mediators for maintenance of systemic heme homeostasis in mammals.

Section 4: Heme import by HRG-1 and its paralogs

Given that most metazoan cells possess the machinery for heme synthesis and degradation, it would be paradoxical for cells to utilize heme importers and exporters

to maintain homeostasis [28]. Interestingly, red blood cells are capable of exporting iron, despite being the major consumer of iron for hemoglobin synthesis [33]. Drawing parallels between iron and heme biology, one can assume that metazoan cells can import and/or export exogenous heme and not rely solely on de novo heme synthesis. However, since heme synthesis and transport are tightly coupled it is difficult to genetically and cell biologically separate heme transport and trafficking from heme synthesis without pleiotropic effects [1].

The soil dwelling nematode *C. elegans* is a heme auxotroph that completely relies on dietary heme for sustenance. This offers a clean genetic background to study heme trafficking, without any confounding factors from heme synthesis [34]. A microarray study in *C. elegans* identified 288 heme responsive genes (HRGs) when worms were grown axenically in low (4 µM), optimal (20 µM), and high heme (500 µM) concentrations [35].

The first *bona fide* heme importer identified was HRG-1 [36]. In *C. elegans* HRG-1 and its paralogs HRG-4,-5,-6 mediate intestinal heme uptake. While HRG-4 localizes to the apical membrane of the intestine and imports dietary heme, HRG-1 is present on the endolysosomal membrane facilitating heme import from these subcellular compartments into the cytosol. By contrast, mammals have a single homolog termed HRG1/SLC48A1 [36]. This redundancy in *C. elegans* highlights potential adaptations for maximizing dietary heme acquisition as heme is essential for their survival. Both *hrg-1* and *hrg-4* are transcriptionally upregulated under low heme conditions, unlike

hrg-5 and *hrg-6*. This suggests that HRG-5 and -6 may play a role in heme import when heme is replete, since HRG-4 is repressed under these conditions. HRG-1 binds heme in a pH dependent manner, and the mammalian homolog was shown to interact with the c subunit of vacuolar proton ATPase pump [37]. An essential role for HRG-1 in iron and heme homeostasis was established using biochemical, functional, and genetic assays in worms, *Xenopus* oocytes, yeast, zebrafish, and murine erythroleukemia cell lines. Mechanistic studies in *Saccharomyces cerevisiae* identified the key residues within HRG-1 and HRG-4 that are essential for heme transport [38]. The carboxy terminus of both *C. elegans* and humans HRG1 has a tyrosine (YRAF in *C. elegans* and YRAD in humans) and di-leucine (ESQPLL in *C. elegans* and DISILS in humans) based sorting motifs. Interestingly, the hydrophobic residue (Ø) in the final position of the tyrosine-based sorting signal is absent in worm HRG-4 and HRG-5. HRG-6 on the other hand possesses YGKL, which fits the canonical motif. The di-leucine based sorting signal is present only in HRG-1 but is absent in HRG-4, -5, and -6. The differences in sorting motifs between HRG-1 and its paralogs HRG-4 and -6 fit with their intracellular location. HRG-4 and -6, lacking the acidic di-leucine motif, are found on the plasma membrane. Conversely, HRG-1 possessing this motif resides on the endolysosomal membranes, indicating that these motifs play a critical role in membrane trafficking [38].

The trafficking of cargo proteins between organelles or between organelles and the plasma membrane is primarily mediated by vesicles. Vesicles are formed when cargo proteins packed into a nascent vesicle pinch-off from a donor membrane. They are then

transported through the cytosol where they fuse with the target membrane compartment, finally docking and coalescing to release their cargo. A crucial group of regulators that play a role in this sorting are adaptors [39]. Adaptor protein (AP) complexes bind to sorting signals on the cytoplasmic tails of cargo proteins, recruit clathrin, and other accessory proteins, and then sort the cargo proteins from the donor compartment to the correct target organellar membrane. In mammals, there are five AP complexes that have been identified so far: AP-1, AP-2, AP-3, AP-4, and AP-5. However, *C. elegans* only has three AP complexes. Adaptor proteins are heterotetrametric complexes, each containing four core subunits- one small (σ), one medium (μ) and two large (β and δ), and two globular appendages (ear) connected by flexible linkers (hinge). The δ subunit interacts with the target membrane, β subunit recruits the clathrin coat protein, μ subunit is responsible for cargo recognition and σ subunit is involved in stabilization of the complex [39]. AP complexes specifically recognize short, linear consensus sequences of amino acids in the cytoplasmic region of the cargo proteins. AP complexes recognize a tyrosine-based sorting motif YXXϕ (where X represents any amino acid and ϕ represents an amino acid with a bulky hydrophobic side chain) and a di-leucine based sorting motif [DE]XXXL[LI]. While the tyrosine-based sorting motif directs the cargo to endosomal, lysosomal as well as the basolateral membrane of polarized epithelial cells, the di-leucine based sorting motif targets the cargo to the trans-Golgi network (TGN) or endosome. These sorting signals need not always be identical and can show some variation while retaining their functionality. They typically consist of 4-7 amino acids, with 2-3 crucial residues essential for proper function. These keys residues are very often bulky hydrophobic as

well as charged residues, which dictate signal specificity and targeted membrane trafficking [40].

The mechanism of AP-3 dependent protein sorting relies on a small GTPase ARF1, which facilitates recruitment of adaptor proteins, coat, and accessory proteins [40]. Binding of ARF1 with AP-3 induces a conformational change from closed to open, which exposes the binding sites to allow simultaneous interactions between clathrin and cargo proteins, finally bringing the complex in close contact with the membrane. AP-3 is involved in transport of membrane and cargo from the trans-Golgi network (TGN) and/or endosome or lysosomes or lysosome-related organelle (LRO) (Figure 1.2). AP-3 physically interacts with biogenesis of lysosome-related organelles complex-1 (BLOC-1). In humans, mutations of these genes cause Hermansky-Pudlak syndrome-10 (HPS10), which is characterized by abnormal biogenesis and function of the LROs including melanosomes and platelet granules [40]. *C. elegans* have orthologs of AP-3 and BLOC-1, and their knockdowns lead to abnormal gut granule formation thereby affecting trafficking to the gut granules [41].

Section 5: SLC49 family of transporters: heme or choline?

5.1: SLC49 family of transporters in heme transport

5.1.1. SLC49A1 (FLVCR1)

FLVCR1 is the cell surface receptor for Feline leukemia virus subgroup C (FeLV-C). The retrovirus infects all hematopoietic cells where the FeLV-C envelope protein binds to the receptor FLVCR1, thus disrupting its function. Consequently, infected cats develop red blood cell aplasia, a condition marked by lack of circulating reticulocytes due to arrested erythropoiesis [42]. FLVCRs belong to major facilitator superfamily (MFS), but the specific function of this transporter in heme homeostasis was first revealed in 2004. This study demonstrated that FLVCR1 is a cell surface heme exporter, thereby protecting erythroid cells from the toxic effects of heme synthesis during erythropoiesis. Experiments using K562 cells showed that inhibiting FLVCR1 decreased heme export, hindered red blood cell maturation, ultimately leading to apoptosis. Furthermore, FLVCR1 levels were high in erythroid progenitors, suggesting that heme export must be critical during erythropoiesis [43]. Subsequent studies showed that mice lacking FLVCR1 die embryonically due to impaired red blood cells formation. Neonatally deleted murine FLVCR1 exhibits severe macrocytic anemia due to arrested erythroid differentiation. Beyond red blood cells, FLVCR1 acts as a heme exporter in macrophages during erythrophagocytosis, thus playing a critical role in heme-iron recycling [44]. Functional studies in NRK (normal rat kidney) epithelial cells validated the function of FLVCR1 as a heme exporter using fluorescent heme analog ZnMP as well as radioactively labelled [^{55}Fe]-hemin [43]. Heme export by FLVCR1 was shown to require extracellular heme binding proteins- in the absence of

extracellular heme binding proteins hemopexin and albumin, FLVCR1 is unable to export heme [45].

In 2012, Chiabrando et. al. identified FLVCR1b, a mitochondrial isoform of *Flvcr1*, which transports heme from the mitochondria to the cytosol and contains six transmembrane domains [46]. The plasma membrane isoform previously identified was renamed as FLVCR1a. Overexpression of FLVCR1b increased intracellular heme content, while its knockdown resulted in heme accumulation within the mitochondria. FLVCR1b was also demonstrated to be crucial for erythroid differentiation in vitro and in vivo. Together, this study dissected the role of the two isoforms of *Flvcr1* to demonstrate that both the isoforms play a key role to complete differentiation of erythroid progenitors. While FLVCR1b is essential for erythropoiesis by regulating the mitochondrial heme efflux, FLVCR1a is important for preventing edema, hemorrhage, and skeletal deformities [47]. A follow-up study by the same research group, further revealed that FLVCR1a is required for proliferation and expansion of committed erythroid progenitors, while FLVCR1b is essential during all phases of erythropoiesis including proliferation and differentiation [48]. Subsequent studies using tissue-specific knockout mouse models unraveled the heme export function of FLVCR1a in liver, intestine, and endothelial cells [49-51].

Several lines of evidence have shown a strong link between heme synthesis and export by FLVCR1a. Silencing of FLVCR1a leads to dampening of ALAS1 activity and/or expression in several cell types including HUVEC (human umbilical vein endothelial

cell), Caco2, C80, and SKCO cells [8,51,52]. Conversely overexpression of FLVCR1a increased ALAS1 levels in Caco2 cells [8]. A recent study further corroborated these results in skeletal muscle, where FLVCR1a deficiency in skeletal muscle reduces heme biosynthesis impairing overall muscle performance [53].

5.1.2. SLC49A2 (FLVCR2)

Mutations in *SLC49A2/FLVCR2* gene has been associated with Fowler syndrome, a rare brain disorder characterized by cerebral proliferative vasculopathy [54]. Investigations have revealed that FLVCR2 functions as a cell surface heme importer. FLVCR2 bound to hemin-conjugated agarose and overexpressing FLVCR2 in CHO cells showed an enhanced uptake of ZnMP, a fluorescent heme analog. *Xenopus* oocytes injected with FLVCR2 cRNA increased [^{55}Fe]- hemin import [55]. Conversely, silencing of FLVCR2 reduced heme uptake into cells. However, expression of FLVCR2 in yeast failed to restore growth in heme-deficient yeast strains, raising questions about its heme import function [38]. Another study implicated the role of FLVCR2 in thermogenesis by regulating the coupling of mitochondrial respiration in response to heme [56]. In conclusion, the role of FLVCR2 in heme import remains unclear, and warrants further investigation.

5.1.3. SLC49A3 and SLC49A4

The functions of *SLC49A3* and *SLC49A4* remain poorly understood. Both contain 12 TMDs and show ~30% amino acid (aa) identity with FLVCR1. SLC49A3 has been predicted to have a short ~20 aa N-terminal segment and a comparatively long ~100 aa long C-terminal segment, with no published studies on their localization and/or function. SLC49A4 has been shown to localize in the lysosomes in HeLa cells, with mutations in the N-terminal resulting in plasma membrane expression [57]. To date, the specific substrates and functioning of SLC49A3 and SLC49A4 remain unknown.

5.2: SLC49 family of transporters: the choline connection

While a significant amount of research over the past two decades has established the role of FLVCRs in heme metabolism, there has been a recent controversy on its substrate. Several recent publications in the past year have suggested the role of FLVCRs in choline import, which has raised questions about the substrate for FLVCR transporters.

To investigate human genes involved in phosphatidylcholine (PC) metabolism, a study combined organelle-selective click-labeling of PC with flow cytometry and identified FLVCR1 as one of the top hits [58]. This strategy involved metabolic incorporation of azido-choline (N_3-Cho) in live cells, followed by an organelle-targeted clickable dyes (OCDs) reaction to generate dye-labeled PC in the corresponding organelle. This allowed PC in different organelles to be simultaneously tagged with different colored fluorescent dyes, thus enabling live tracking of PC dynamics and trafficking. One of

the top hits was FLVCR1a, whose depletion reduced the PC levels in K562, HeLa, and A549 cells.

A parallel study conducted an integrative genetic analysis to associate serum metabolites to membrane transporters revealed a connection between FLVCR1a and choline metabolism. Further experiments reported that cells lacking FLVCR1a exhibit reduced levels of choline, as well as its downstream metabolites phosphocholine and betaine. Complementation assays with FLVCR1a but not FLVCR1b restored the phosphocholine levels in knockout cells. Additionally, radiolabeled choline uptake experiments showed that FLVCR1a facilitates choline import into cells. Finally, their results demonstrated that choline supplementation could partially rescue the embryonic lethality observed with FLVCR1-null embryos, hence confirming the role of FLVCR1-mediated choline import in murine development [59].

In accordance with these studies, additional research by the Nguyen group strengthens the evidence for FLVCR1a's role as a choline transporter [60]. Using A549 cells, they showed that silencing of FLVCR1a reduced choline uptake along with a modest decrease in PC and sphingomyelin levels. They further showed that the choline transport function of FLVCR1a is conserved across diverse species, and independent of a cation gradient. Importantly, their work revealed that FLVCR1a imports choline down its concentration gradient, suggesting that intracellular choline levels and its catabolizing enzymes regulate FLVCR1a-mediated flux.

The Kennedy pathway synthesizes the two most abundant phospholipids in cells - phosphatidylcholine (from choline) and phosphatidylethanolamine (from ethanolamine). A recent structural study demonstrated that FLVCR1 engages a common binding site comprising aromatic and polar amino acid residues to bind both choline and ethanolamine [61]. Radiolabeled ethanolamine uptake experiments in WT and FLVCR1-KO HEK293T cells revealed FLVCR1 as an ethanolamine importer as well. The Michaelis constant (K_m) for choline and ethanolamine is 8 μM and 2.8 μM respectively, indicating that FLVCR1 is a high affinity transporter for both choline and ethanolamine, thus providing substrates for both branches of the Kennedy pathway.

As far as FLVCR2 is concerned, two studies have implicated FLVCR2 in choline metabolism. First, research by Nguyen's group demonstrated FLVCR2 as a choline transporter at the blood brain barrier (BBB) [62]. Metabolomics performed on brains of *FLVCR2*-null embryos revealed elevated levels of choline and choline metabolites. Overexpression of FLVCR2 in HEK293 cells increased choline uptake, and this import is electrogenic, as revealed by radiolabeled choline import and single-cell patch clamp analysis, respectively. While mice deficient in FLVCR2 in the endothelial cells of the central nervous system showed reduced import of exogenous choline, brain choline levels were surprisingly elevated. Consistent with this finding, another independent study identified FLVCR2 as a BBB choline transporter using both in vitro and in vivo assays, and that the choline uptake is driven by a proton gradient [63]. Additionally, this group deployed cryo-electron microscopy to illustrate the structures of choline-

bound FLVCR2 in both inward and outwards facing conformations, shedding light into the specific amino-acid residues that are involved in substrate coordination.

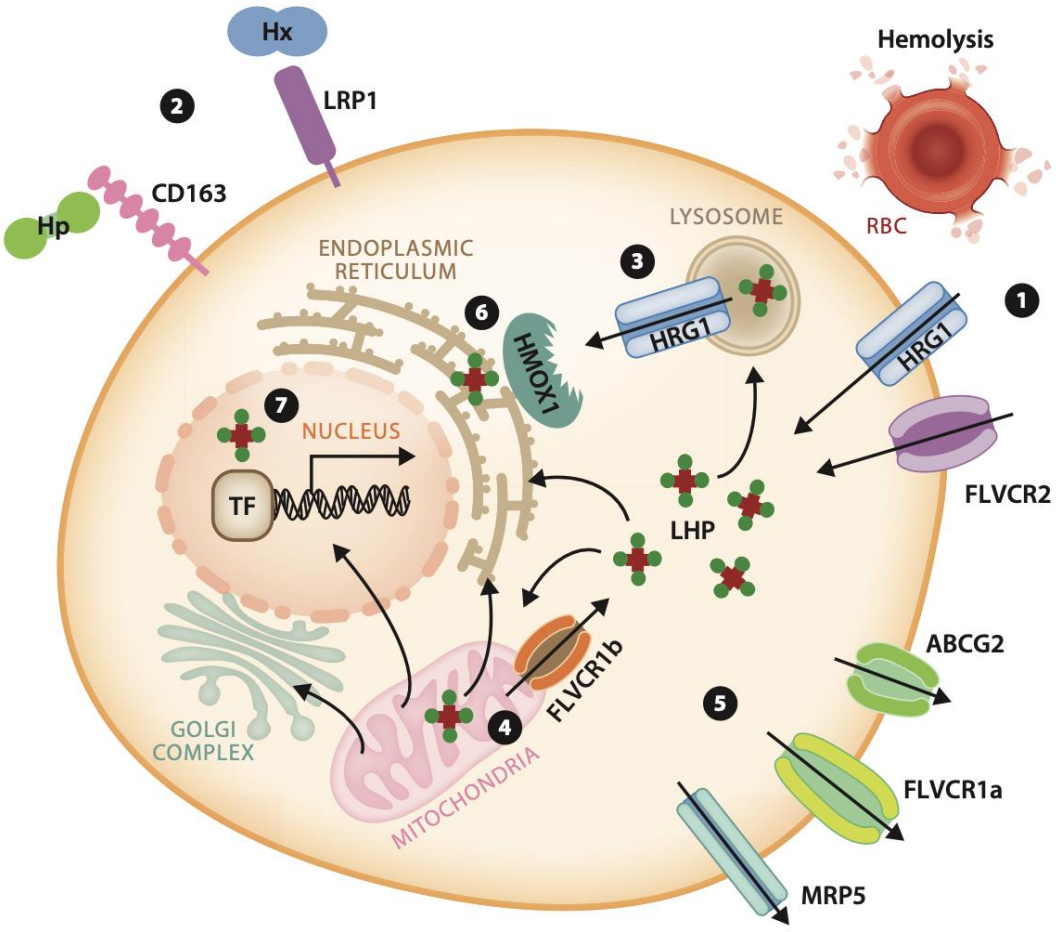

Figure 1.1. Consensus model of known mediators of heme transport and pathways for intercellular heme trafficking

Most metazoan cells can meet their heme requirements autonomously by de novo synthesis in the mitochondria. (1) Cells can import heme through the plasma membrane transporters HRG1, FLVCR2, or via endocytosis of senescent red blood cells. (2) Hemopexin (Hx) and Haptoglobin (Hp) are scavenged by membrane-bound CD163 and CD91 receptor-mediated endocytosis, respectively. (3) Intracellular heme is

imported into the cytosol by HRG1 residing on endolysosomal membrane and (4) FLVCR 1b on mitochondrial membrane. (5) Heme export is mediated by plasma membrane heme exporters FLVCR1a, ABCG2, and MRP5. (6) Heme degradation is mediated by HMOX1, to prevent cytotoxicity. (7) Cellular labile heme pool (LHP) may facilitate intracellular heme trafficking. (8) In the nucleus, transcription factors (TF) directly bind to heme and regulate transcription of downstream target genes. Abbreviations: ABCG2, ATP-binding cassette subfamily G member 2; FLVCR, feline leukemia virus subgroup C receptor; HMOX1, heme oxygenase 1; HRG, heme responsive gene; MRP, multidrug resistance protein; RBC, red blood cell. Figure directly taken from Dutt et al [1].

A

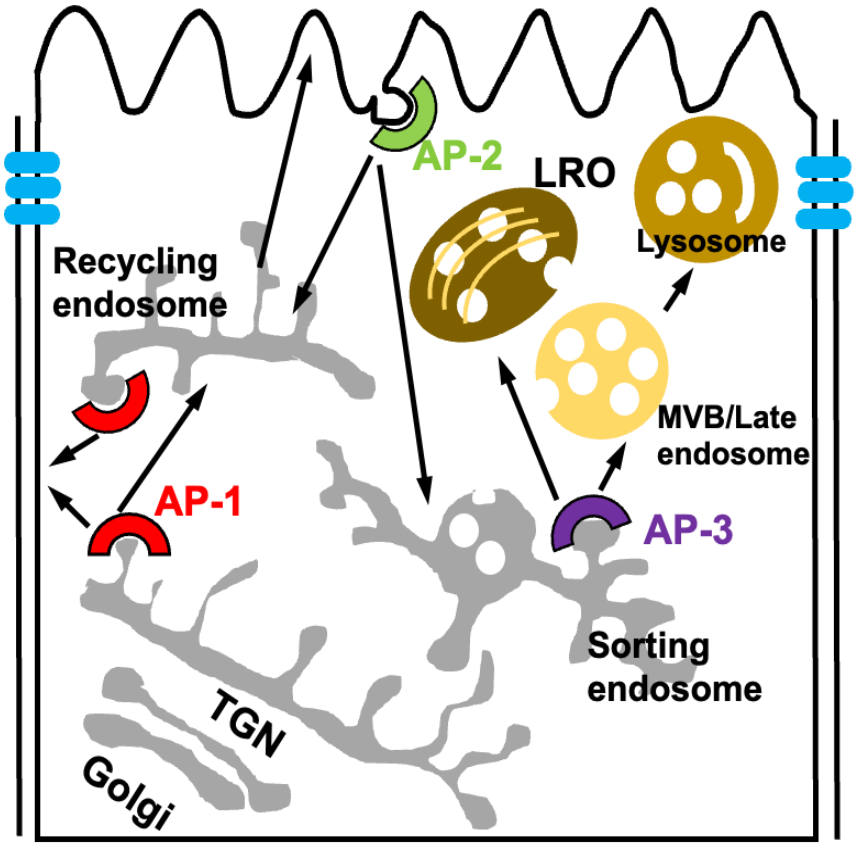
AP-2
LRO
Lysosome
Recycling endosome
MVB/Late endosome
AP-1
AP-3
Sorting endosome
TGN
Golgi

B

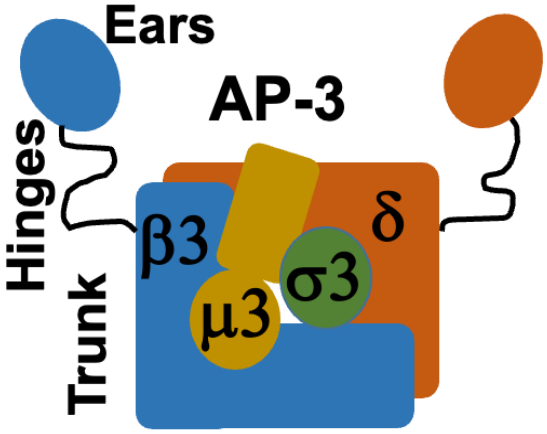
Ears
AP-3
Hinges
β3
δ
σ3
μ3
Trunk

Figure 1.2. Schematic of Adaptor protein (AP) complexes

A. Schematic representation of intracellular localization of AP complexes, and the trafficking mediated by them. AP-1 mediates bidirectional transport between trans-Golgi network (TGN) and recycling endosomes. AP-2 mediates clathrin-dependent endocytosis from plasma membrane. AP-3 is responsible for trafficking of cargo proteins from the TGN and/or endosomes to lysosomes or lysosome related organelles (LRO). The corresponding trafficking pathways for each AP complex are indicated by arrow lines.

B. Diagram of hetero-tetrameric AP-3 complexes. Subunit names are indicated. AP-3 consists of a trunk, hinge and ear domains. The trunk domain binds to membranes and to different cargos via the μ and β subunits. The ear or appendage domains bind to different accessory proteins. The hinge domains bind to clathrin terminal domain.

Section 6: MRP-5 and its role in heme export

MRP5 (ABCC5) belongs to a family of Multidrug resistance associated proteins (MRPs), which are a type of ATP-binding cassette (ABC) transporter. Researchers have extensively investigated MRPs for their role in cancer drug resistance, owing to their ability to export drugs out of the cells.

In *C. elegans,* MRP-5/ABCC5 has been identified as the primary heme exporter. Microarray studies identified 288 heme-responsive genes (HRGs), of which 41 genes encoded transmembrane-containing proteins [26]. The heme sensor strain (IQ6011) has a transcriptional fusion of the heme responsive gene *hrg-1,* fused to green fluorescent protein (GFP). The fluorescence intensity of GFP is inversely correlated with the heme status of the worms; more GFP indicates low heme concentrations. RNAi depletion of each of these 288 HRGs in IQ6011 uncovered *mrp-5* as one of the key regulators of heme homeostasis since knockdown of *mrp-5* resulted in significant increase in GFP signal [35]. Remarkably, this increase of GFP signal could not be rescued even with high heme (500 μM), unlike *hrg-4* RNAi, which could be rescued by 50 μM. In fact, microarrays and qRT-PCR studies revealed a three-fold upregulation of *mrp-5* mRNA under low heme conditions. Interestingly, worms lacking *mrp-5* show embryonic lethality, which could be restored by heme supplementation. Tissue-specific RNAi of *mrp-5* showed that depletion of *mrp-5* from the intestine alone could phenocopy the whole organism RNAi, thus indicating that the intestine is the primary tissue responsible for this lethality. Worm translational fusion strain of *mrp-5* ($P_{vha\text{-}6}$*::MRP-*

5::GFP) demonstrated that MRP-5 protein primarily localizes on the basolateral membranes of the intestine as well as intracellular compartments. Additionally, RNAi depletion of *mrp-5* resulted in increased ZnMP accumulation within the intestine, and resistance to the toxic heme analog gallium protoporphyrin IX (GaPPIX), indicative of the potential role of *mrp-5* in exporting porphyrins. Zebrafish injected with morpholinos against *mrp-5* showed severe anemia, as reflected by decreased o-dianisidine staining and globin expression of RBCs, suggestive of defective erythropoiesis caused by lack of *mrp-5*. Confocal microscopy studies in murine embryonic fibroblasts (MEFs) revealed MRP5 localized to plasma membranes, Golgi and endosomal recycling organelles. Functional assays in yeast and mammalian cells showed MRP5 functions as a heme exporter, translocating heme from cytosol into the lumen of the secretory pathway [26].

Section 7: Screening suppressors of mrp-5(ok2067) embryonic lethality

mrp-5 null mutant worms show embryonic lethality that can be rescued by heme supplementation indicating that, in the absence of *mrp*-5, alternate heme export pathways must exist to export heme from the intestine. To uncover these alternate pathways, Simon Beardsley, a former student in the lab conducted an ethyl methanesulfonate (EMS)-based forward genetic screen to identify suppressors of lethality using the *mrp-5 (ok2067)* null mutants. Before conducting a forward genetic screen it was necessary to investigate the precise heme requirements for *mrp-5 (ok2067)* worms, so that the growth conditions for the screen could be established [64].

About 20 % embryonic lethality was observed at ≤ 80 µM supplemented heme, and 100 % embryonic lethality was observed at ≤ 50 µM heme. At heme concentrations ≤ 50 µM, the *mrp-5 (ok2067)* worms hatched but did not lay viable progeny (Figure 1.3).

A forward genetic screen was conducted on ~20,000 early L4 P_0 *mrp-5(ok2067)* worms by exposing these worms to EMS, causing random mutations in their germ line. These mutant worms were allowed to self-fertilize, generating ~80,000 F1 worms, in which the mutations appeared somatically as heterozygous. This represented ~160,000 haploid genomes, or an eight-fold genomic coverage. Self-fertilization of F1 and subsequent screening of F2 on NGM plates supplemented with 30 µM heme, identified 32 suppressors which laid viable F3 progeny (Figure 1.4). The top three suppressors could completely bypass *mrp-5* lethality without the addition of any exogenous heme. We decided to focus on these three mutants and characterize them further.

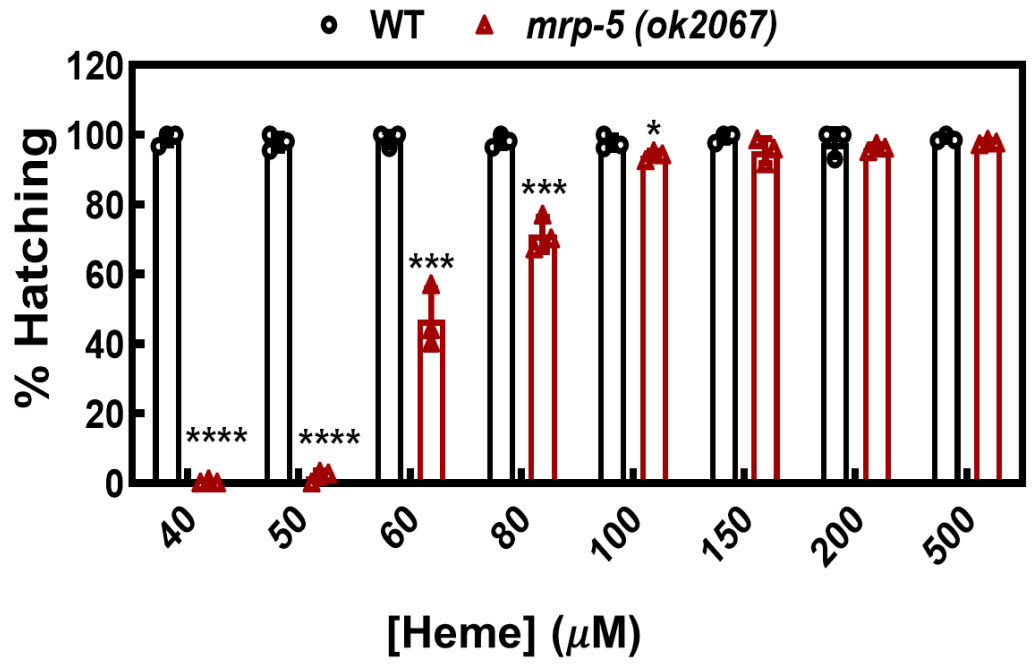

Figure 1.3 ***mrp-5 (ok2067)*** **worms can be rescued by heme supplementation.**

NGM agar plates were seeded with OP50 grown overnight in LB with indicated heme concentrations. Worms were maintained for one generation on 200 µM heme NGM plates, and their progeny were synchronized. Approximately 50 synchronized L1 (P_0) were seeded onto each plate and observed daily. Once F_1 embryos were observed on a plate, P_0 were removed, and hatching was scored 24 h later. No embryos were observed at 10 or 20 µM heme (experiment performed by Simon Beardsley). Unpaired t test (*, $p<0.05$; **, $p< 0.01$; and ***, $p< 0.001$) [64]

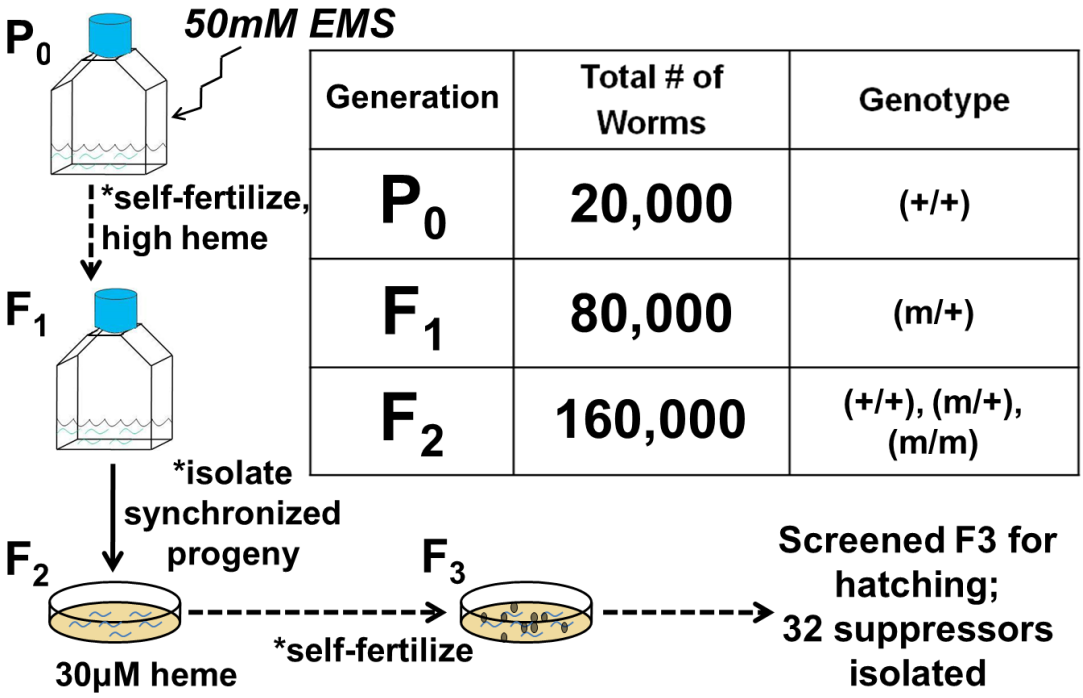

Generation	Total # of Worms	Genotype
P_0	20,000	(+/+)
F_1	80,000	(m/+)
F_2	160,000	(+/+), (m/+), (m/m)

Figure 1.4. EMS mutagenesis screen identified *mrp-5* suppressors

mrp-5(ok2067) worms were maintained in axenic mCeHR-2 media supplemented with 200 µM heme. Following EMS treatment, mutagenized P_0 animals were moved back to axenic mCeHR-2 media supplemented with 200 µM heme and allowed to lay F_1 progeny. Gravid F_1 were bleached to isolate and synchronize the F_2 generation, which were then placed on 38 plates supplemented with 30 µM heme. Viable F_3 were picked to fresh NGM plates seeded with 30 µM heme OP50. Only lines capable of laying viable progeny after seven days were called *mrp-5* suppressors (experiment performed by Simon Beardsley) [64].

Early characterization of unmapped suppressor mutants revealed that suppressor alleles could restore intestinal heme efflux. Exposing worms to the toxic heme analog GaPPIX results in lethality [65]. However, *mrp-5* mutants are resistant to GaPPIX toxicity due to a decrease in GaPPIX export to extra-intestinal tissues [26]. Suppressor strains phenocopy WT worms and succumb to GaPPIX, indicating restoration of intestinal heme efflux despite the absence of *mrp-5* [64] (Figure 1.5).

Treatment of worms with the fluorescent heme analog Zinc mesoporphyrin (ZnMP), resulted in a distinct phenotype among the suppressor mutants. WT worms show ZnMP accumulation within intestinal LROs, while loss of *mrp-5* results in hyper-accumulation of intestinal ZnMP. The three suppressor mutants (IQ1003, IQ1004, IQ1005) showed a complete loss of detectable ZnMP signal within the intestine, suggesting that heme exits the intestine through an alternate pathway [64] (Figure 1.6).

All three suppressor lines were determined to be recessive mutations and a variant-based deep sequencing was employed to identify the suppressor mutations in these suppressor lines. Suppressor alleles were mapped to 2 Mb regions, and candidates were identified based on missense, nonsense, splicing, or frameshift mutations induced by EMS (Figure 1.7). Surprisingly, three distinct subunits of adapter protein complex 3 (AP3), *aps-3*, *apd-3*, and *apm-3* were identified as candidates in the three suppressor mutants.

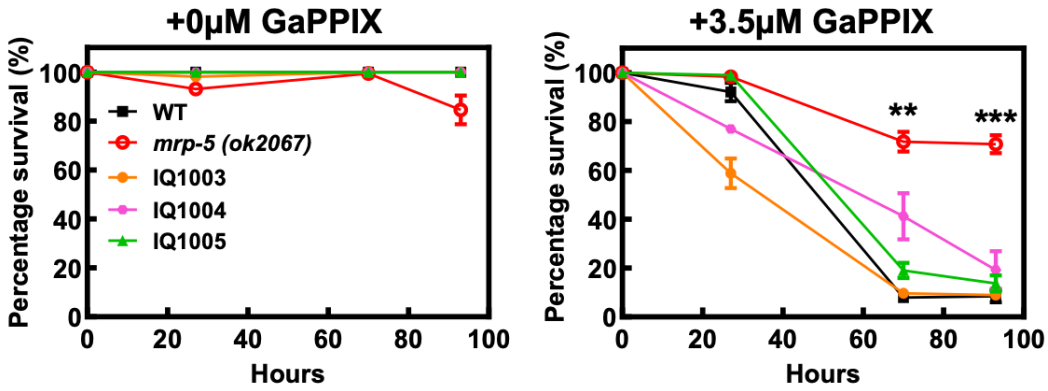

Figure 1.5. Suppressor mutants restored intestinal heme efflux.

Gallium Protoporphyrin IX (GaPPIX) was directly supplemented to 35mm NGM agar plates, which were then seeded with 200 µL OP50. All strains were maintained for one generation on NGM plates supplemented with 100 µM heme, and their progeny were synchronized by bleaching and 50 synchronized L1 worms were placed on plates at time zero, and lethality was scored at the indicated time points. Lethality was determined by a complete lack of movement and failure of a worm to respond to tactile stimulus (experiment performed by Simon Beardsley).

*p<0.05; **p<0.01, ***p<0.001 (One-way ANOVA, Dunnett's multiple comparison test).

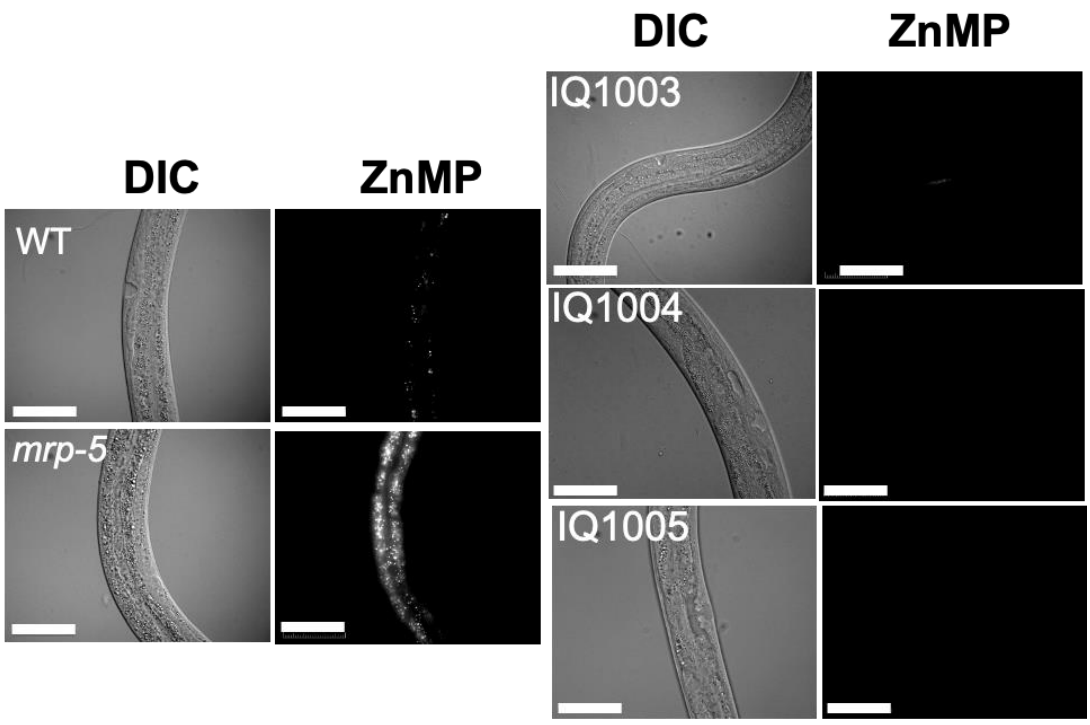

Figure 1.6. *mrp-5* suppressor mutants altered ZnMP accumulation within the intestine.

The indicated strains were grown and treated with ZnMP as described. WT refers to N2 worms, while *mrp-5* refers to *mrp-5(ok2067)*. Images were taken using a DMIRE2 epifluorescence microscope (Leica) connected to a Retiga 1300 cooled mono 12-bit camera, and ZnMP signal was detected by rhodamine filter. Exposure time was calibrated with worms not exposed to ZnMP. At least 30 worms were analyzed for each strain. Scale bar, 50 µm (experiment performed by Simon Beardsley).

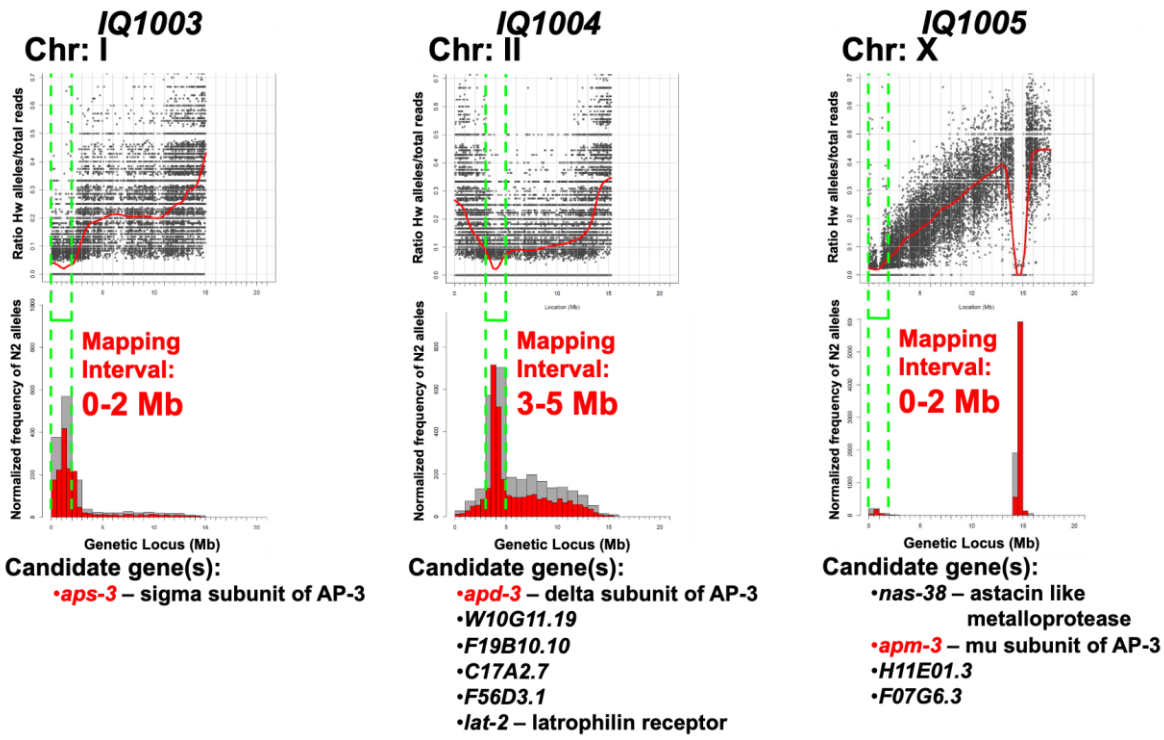

Figure 1.7. Summary of mapping intervals for *mrp-5* suppressors

All mapping plots were generated using "CloudMap Hawaiian Variant Mapping with WGS and Variant calling workflow" on the Galaxy Web server. For a given chromosome (linkage group, LG), the top plot represents the ratio of Hawaiian to N2 versions of a single nucleotide polymorphism (SNP), where each black dot represents an individual SNP. The red line represents a LOESS regression line of the frequency of Hawaiian SNPs as a function of genetic locus. The bottom plot represents the frequency of pure N2 alleles over a given interval. Red bars represent bin size of 1Mb. Table shows candidate genes generated by compiling all genes containing missense, nonsense, frameshift, or splicing variants (predicted by snpEff function) within the indicated mapping intervals for each suppressor mutant (experiment performed by Simon Beardsley).

Problem statement:

As described herein, heme is an essential yet cytotoxic cofactor for cells, but its trafficking remains poorly understood. While the SLC49 family of transporters have been shown to function as heme exporters (*SLC49A1/FLVCR1*) and importers (*SLC49A2/FLVCR2*), research in the past year has questioned these findings by implicating these transporters in choline import [59,61,63,66]. Do *SLC49A1* and *SLC49A2* function as antiporters importing choline and exporting heme? What are the functions of its paralogs, *SLC49A3* and *SLC49A4*?

The fact that the embryonic lethality of *mrp-5* null mutants can be rescued by heme supplementation suggests that there must be alternate mechanisms for heme export. To uncover these pathways, we conducted a forward genetic screen using *mrp-5(ok2067)* worms and identified that loss of adaptor protein -3 (AP-3) subunits can completely bypass the embryonic lethality of *mrp-5* deficiency without the addition of any exogenous heme. What is the mechanism of this suppression? Are there other heme exporters in *C. elegans*, apart from the already identified MRP-5? The present study shows that adaptor proteins play a key role in maintaining systemic heme homeostasis by maintaining a fine balance between heme import, storage, and export. Additionally, we identify and characterize the worm homologs of *SLC49A3* and delineate their roles as bona fide heme exporters in *C. elegans* and mammalian cells. Our results demonstrate a novel role for *SLC49A3* homologs as heme exporters.

Chapter 2: Materials and Methods

Section 1: Worm Methods

2.1.1. Worm Culture

C. elegans were maintained in axenic cultures, where worms were grown in continuously shaken liquid mCeHR2 medium [67]. Alternatively, worms were cultured on nematode growth medium (NGM) plates seeded with either OP50 or HT115(DE3) bacteria at 15°C or 20°C unless noted otherwise. The composition of the NGM plates is provided for reference (3 g/L NaCl, 2.5 g/L peptone, 20 g/L agar, 5 mg/L cholesterol, 0.1 M $CaCl_2$, 0.1 M $MgSO_4$, and 25 mM KH_2PO_4). Routine maintenance procedures, synchronization of worm lifecycles, crosses, and general observations followed established methods described by Epstein and Shakes [68]

2.1.2. Synchronization of Worms

For harvesting worms on NGM plates, M9 buffer was used to wash them off the agar and remove any bacteria, repeated three times. Worms grown in liquid mCeHR-2 medium were harvested by centrifugation at low speed (800 x g) for 5 minutes [67]. After removing the supernatant, the worms were resuspended in a salt solution (0.1 M NaCl) and allowed to settle on ice for 5 minutes. Supernatant was then aspirated. Gravid worms were exposed to a solution of sodium hypochlorite and sodium hydroxide to release the embryos. The mixture was then centrifuged again at low speed

(800 x g) for 1 minute. After removing the supernatant, the embryos were washed twice with sterile water and resuspended in M9 buffer for overnight hatching.

2.1.3. Worm strains

Worm strains used in this study are listed in Appendix I.

2.1.4. RNA interference

RNAi was performed by feeding worms bacteria engineered to express double-stranded RNA (dsRNA) complementary to the target gene. For RNAi feeding all clones were obtained from the established Ahringer library. The RNAi bacteria were grown and spotted onto NGM plates containing antibiotics (50 μg/mL carbenicillin and 12 μg/mL tetracycline) and 2 mM isopropyl-β-D-thiogalactopyranoside (IPTG) to induce dsRNA production. L1 stage larvae were then placed on these RNAi plates and incubated at the desired temperature (15°C or 20°C). After at least 72 h, we investigated the resulting phenotypes in the worms.

2.1.5. Hemin chloride preparation

To prepare a 10 mM hemin chloride solution, 130 mg of hemin chloride powder (Frontier CAS# 16009-13-5) was added in 15 mL of 0.3 M NH_4OH. The pH of the solution was then adjusted to 8.00 (+/- 0.05) using concentrated HCl. Finally, the solution was brought to a final volume of 20 mL with an additional 0.3 M NH4OH (pH 8.0).

2.1.6. RNAi bacteria Heme Supplementation

The LB broth used for *E. coli* culture was directly supplemented with the required heme chloride concentration, and then shaken at 37°C.

2.1.7. Embryonic lethality assay

Worms were synchronized and placed on RNAi plates (NGM plates with Noble Agar (Difco CAS 214320)) with bacterial cultures grown in 1/4 Luria-Bertani broth (LB) (2.5 % tryptone, 1.25 % yeast extract, and 10 % NaCl weight by volume, 50 μg/mL carbenicillin, 12 μg/mL tetracycline, and 2 mM IPTG) with no added heme or different concentrations of added heme. After 48 h, young adult worms were clonally picked to fresh RNAi plates and allowed to lay embryos for 24 h. After another 24 h, these worms were then moved to new RNAi plates and hatched worms and unhatched embryos were counted from the previous plate.

2.1.7. Immunoblotting

5000 gravid worms were harvested and lysed in a buffer containing 150 mM NaCl, 50 mM HEPES, and 1 % Triton X, with protease inhibitor (complete Protease Inhibitor Cocktail EDTA-free, 1 mM phenylmethylsulfonyl fluoride, 4 mM benzamidine, 2μg/ml leupeptin, and 1μg/ml pepstatin, Roche Diagnostics, CAS 1187358001),

Lysing Matrix C beads (MP Biomedicals) in a FastPrep-24 Beadbeater (MP Biomedicals). Worm lysates were centrifuged 3 times at 10,000 x g for 10 minutes, then total protein concentration in the supernatants was measured using Bradford assay (Bradford Reagent Protein Assay Dye Reagent, Bio-Rad, CAS 5000006). Protein samples were then mixed with 4X Laemmli sample buffer and loaded on to a 10 % SDS PAGE gel. Separated proteins were transferred from the gel to a nitrocellulose membrane, cross-linked by UV-treatment, and stained for 5 minutes with Ponceau S solution for protein loading, following by blocking (5 % nonfat dry milk in 0.05 % PBS-Tween 20 [PBS-T] for 1 hour at room temperature. Blots were then incubated overnight at 4°C in blocking buffer containing mouse anti-GFP (monoclonal, Biolegend CAS 902603) or rat anti-RFP (monoclonal, Chromotek CAS 5F8-100) at concentration of 1:1000. Rabbit anti-mouse HRP conjugated secondary was used for anti-GFP, or goat anti-rat HRP conjugated secondary for anti-RFP, at a 1:10,000 dilution. Blots were developed in SuperWest Pico Chemiluminescent Substrate (Thermo Scientific). BioRad Image Lab software was used to quantify blots.

2.1.8. Microscopy

Representative confocal worm images were taken using Zeiss LSM710 and Nikon A1 with a 63X oil immersion objective. After worms were harvested, they were added to slides with 2% agar pads. Worms were immobilized using 10 mM Levamisole (MP Bio, CAS 155228), and then mounted on cover slips before visualization. For images

of GABA neuron synapses, dorsal cord of the middle part of the animals are shown. The dorsal cord number of GABA synapses were counted.

2.1.9. Zinc Mesoporphyrin treatment

10mM zinc mesoporphyrin (ZnMP) stock solution was prepared by dissolving in 0.3M NH_4OH, pH adjusted to 8 by addition of HCl. To visualize ZnMP uptake, synchronized L1 worms were seeded on RNAi NGM plates, and allowed to grow until young adult stage, after which they were harvested, and washed thrice with M9. Worms were incubated with 10 μM ZnMP in mCeHR2 media, while shaking overnight at 15°C. They were then collected and co-stained with Lysotracker.

2.1.9. LysoTracker staining

50 μM Lysotracker (LysoTracker Blue DND-22 CAS L7525) solution was prepared in M9. Worms were incubated in this solution for 15 minutes at 20°C in the dark. They were then washed and allowed to de-stain for another one hour at 20°C in the dark, followed by imaging.

2.1.10. Single worm PCR

For single worm PCR, worms were lysed in a buffer containing 50 mM KCl, 10 mM Tris- HCl, 2.5 mM $MgCl_2$, 0.45% NP-40, 0.45% Tween-20, 0.01% gelatin, 1 mg/ml

Proteinase K. These lysates were incubated for 2 hours at -80°C, 1 hour at 65°C, and 30 mins at 95°C. Worm lysates were added to PCR reactions containing appropriate primers to detect wildtype and transgenic worms. Genotyping primers for IQH01 and IQH02 are listed in Appendix II. For each PCR reaction 2 μL of template was used. Reaction steps:

1. 95°C, 2 mins
2. 95°C, 30 sec
3. 58°C, 40 sec
4. 72°C, 90 sec
5. 72°C, 10 mins
6. 12°C, forever

Section 2: Mammalian Cell Culture methods

2.2.1. Mammalian cell culture

Mammalian cell culture experiments were performed using HEK293 and HeLa cells. These cells were grown in a humidified incubator at 37°C with 5 % CO_2. Dulbecco's modified Eagle medium (DMEM) supplemented with 10 % FBS and 1 % penicillin/streptomycin/glutamine was used as the culture medium.

2.2.2. DNA cloning

Worm B0416.5 and C27A7.6 ORFs were synthesized using TWIST. HA epitope tag was added by PCR and then the construct was digested with XhoI and BamHI. This was then ligated into pEGFP-N1 cut with XhoI and BamHI.

2.2.3. Immunoprecipitation

Transfected cells were washed twice with PBS, and lysed with cold buffer containing 150 mM NaCl, 50 mM HEPES, and 1 % Triton X and protease inhibitors. The lysates wer incubated on ice for 10 minutes and then centrifuges at 11,000 g for 15 mins. The supernatant was collected, and total protein concentration determined by Bradford Assay. 20 μg was saved for input control, while 200 μg lysate was incubated for 2 h in agarose beads (for pre-clear). After this, the lysate was incubated with anti-GFP (GFP-TRAP agarose, CAS gta) or anti-HA beads (Pierce™ Anti-HA Agarose, ThermoFisher, CAS 26181) overnight at 4°C. The beads were then washed with PBS containing 0.01 % n-dodecyl-ß-D-maltoside (DDM) and the immunoprecipitated proteins were eluted by incubating with 4X Laemmli buffer at 55°C for 10 minutes. Proteins were detected by SDS-PAGE.

2.2.4. Immunoblotting

HEK293 cells were transfected with equal amounts of empty vector, CeHRG1-GFP, B0416.5-HA-GFP and C27A7.6-HA-GFP using PolyJet transfection reagent (SignaGen, CAS SL100688). Media was changed the following day. Again, a day later cells were harvested and lysed using a buffer containing 150 mM NaCl, 50 mM HEPES, and 1 % Triton X, with protease inhibitor (complete Protease Inhibitor Cocktail EDTA-free, 1mM phenylmethylsulfonyl fluoride, 4 mM benzamidine, 2μg/ml leupeptin, and 1μg/ml pepstatin, Roche Diagnostics, CAS 1187358001). Total protein concentration for each sample was measured using Bradford assay (Bradford Reagent Protein Assay Dye Reagent, Bio-Rad, CAS 5000006). Protein samples were then mixed with 4X Laemmli sample buffer and loaded on to a 10 % SDS PAGE gel. Separated proteins were transferred from the gel to a nitrocellulose membrane, cross-linked by UV-treatment, and stained for 5 minutes with Ponceau S solution for protein loading, following by blocking (5 % nonfat dry milk in 0.05 % PBS-Tween 20 (PBS-T)) for 1 hour at room temperature. Blots were then incubated overnight at 4°C in blocking buffer containing mouse anti-GFP (monoclonal, Biolegend CAS 902603) or mouse anti-actin at a concentration of 1:1000. Rabbit anti-mouse HRP conjugated secondary was used for anti-GFP and anti-actin, at a 1:10,000 dilution. Blots were developed in SuperWest Pico Chemiluminescent Substrate (Thermo Scientific) and imaged using Azure imaging systems.

2.2.5. Heme arginate preparation

Fresh 1 mM solution of heme:arginate was made with 10 mM arginine, prepared by dilution in 0.2 M KOH/100 % ethanol (1:1, v/v).

2.2.6. Oxalic acid heme quantification assay

Transfected cells treated with 10 μM heme arginate were harvested and lysed using 2 M oxalic acid solution by vortexing. Protein concentration was determined using Bradford assay. Samples along with porphyrin and heme standards were incubated in heating block at 100°C for 1 hour to convert heme to porphyrin. Porphyrin fluorescence was then measured at excitation 400nm and emission 660nm.

2.2.7. Horseradish/ascorbate peroxidase assay

HEK293 cells were transfected with equal amounts of empty vector, HRG-1, B0416.5 and C27A7.6 along with either ER-HRP or cytosol APX or mitochondria-APX using PolyJet transfection reagent. The following day, the media was changed to heme depleted (HD) media (DMEM with 10 % heme depleted FBS and 1 % PSG), and 0.5 mM succinylacetone (SA), along with different concentrations of heme arginate. The following day, cells were harvested and lysed using a buffer containing 150 mM NaCl, 50 mM HEPES, and 1 % Trition X, with protease inhibitor. Total protein concentration for each sample was measured using Bradford Assay. Peroxidase activity was

measured as described in [18]. Each sample was normalized to the peroxidase activity of empty vector at 1 μM and to the protein concentration.

2.2.8. Wheat Germ Agglutinin staining

1 mg/ml stock solution of Wheat Germ Agglutinin (WGA) was prepared in PBS. After cells were fixed with 4% parafolmaldehyde (PFA), they were washed. WGA stock concentration was diluted to 5 μg/ml using PBS, and then added to the cells and incubated for 10 minutes at room temperature. Cells were then washed with PBS thrice and proceeded with subsequent steps for imaging.

2.2.9. Microscopy of fixed cells

HeLa cells were transfected with B0416.5-HA-GFP or C27A7.6-HA-GFP by themselves or along with different markers (LAMP1-mCherry, or CeHRG1-mCherry). The following day the media was changed. The day after cells were fixed using 4 % parafolmaldehyde (PFA) for one hour, washed with PBS and sterile water and subsequently mounted using Antifade (ProLong Gold Antifade Reagent, Invitrogen, CAS P36934). Images were taken and processed using Zeiss Airyscan 980 SR confocal microscope.

2.2.9. Live cell imaging

HeLa cells were transfected with B0416.5-HA-GFP or C27A7.6-HA-GFP along with CeHRG-1-mCherry. The following day the media was changed to HD along with 0.5 mM SA. Again, the day after fresh HD+SA media was added and then taken for imaging using the Nikon W1 spinning disc. 50 μM heme was added while the cells were being imaged. Videos were processed and denoised by Nikon Elements software.

2.2.9. Radioactive heme uptake

HEK 293 cells were seeded at a 60 % confluency per 12-well plate in duplicates. The following day, cells were transfected with CeHRG1 or empty vector. Media was changed the next day. The following day (day of the experiment), cells were incubated with 5 μM [^{55}Fe]-heme prepared in DMSO for different durations ranging from 30 minutes to 30 h. After each time point, cells were harvested, washed with PBS containing 5 %BSA, lysed using buffer containing 150 mM NaCl, 50 mM HEPES, and 1% Triton X, and then transferred to a scintillation cocktail (Ecoscint A Scintillation Cocktail, CAS LS-273). Radioactivity was measured using a scintillation counter. Radioactivity was normalized to the total protein concentration for each sample.

2.2.10. Radioactive heme efflux

HEK 293 cells were seeded at a 60% confluency per 12-well plate in duplicates. The following day, cells were transfected with different DNA constructs (empty vector, CeHRG1, B0416.5, C27A7.6, HRG1+ B0416.5 and HRG1+ C27A7.6). Media was changed the next day. The following days cells were incubated with different concentrations of [^{55}Fe]-heme prepared in DMSO for 6 h. Cells were then washed with PBS containing 5% BSA, and media was changed to fresh OptiMEM without any added heme, and incubated for another 24 h at 37°C. After this, cells were harvested, lysed using buffer containing 150 mM NaCl, 50 mM HEPES, and 1% Triton X and then transferred to a scintillation cocktail (Ecoscint A Scintillation Cocktail, CAS LS-273). The media was also collected and transferred to a scintillation cocktail. Radioactivity was measured using a scintillation counter and was normalized to the total protein concentration for each sample.

Section 3: General methods

2.3.2. RNA-Seq Analysis

Synchronized L1 larvae of IQ1904 (WT brood-mate), IQ1903 (*mrp-5(ok2067*)), IQ1902 *(apb-3(ok429)),* and IQ1901 (*mrp-5(ok2067);apb-3(ok429*)) strains were grown on 10 cm NGM plates supplemented with OP50 bacteria and 10 µM heme. Worms were collected at late L4 stage in M9 buffer, followed by three additional washes with M9 buffer. Total RNA was extracted with RNeasy kit following the

manufactory's manual (Qiagen, Germany). A total of 12 samples were sequenced using Illumina's HiSeq-2500, with triplicate of each genotype. Single-end 50 base reads were sequenced and checked by FastQC, version 0.11.5. The reads were aligned to *C. elegans* UCSC reference genome ce10 using STAR, version 2.5.2b. Differentially expressed genes (DEGs) were identified using DESeq2, version 1.40.2 and R version 4.3.1. Log2 fold changes of gene expression was shrunk by the 'lfcShrink (ashr)' function of DESeq2. The False Discovery Rate (FDR) was used to determine the statistical significance with the cutoff value (adjusted p-value) of 0.05 set for DEGs. Enrichment analysis was performed using WormBase (https://wormbase.org). All the sequencing data including read counts per gene will be deposited to NCBI Sequence Read Archive (SRA).

2.3.1. Bioinformatics and Statistics

MEGA11 was used to make phylogenetic trees. Protein structure modelling was done using AlphaFold3. All data are presented as mean ± the standard error of the mean (SEM). Statistical significance was determined using one-way or two-way ANOVA or unpaired t test, as indicated in figure legends using GraphPad Prism, version 10.00 (GraphPad Software, Inc).

Chapter 3: Depletion of AP-3 components suppresses lethality caused by *mrp-5* deficiency

Summary

Heme is an essential cofactor for a plethora of biological functions. While heme synthesis has been well elucidated, the pathways governing heme trafficking within a cell and between different cell types remains poorly understood. We have leveraged the heme auxotrophy of *C. elegans* to identify and characterize various mediators of heme homeostasis pathways. Heme import occurs via the conserved permease HRG-1, located on the membrane of endolysosomal compartments, where it imports heme from these subcellular compartments into the cytosol. Heme export occurs via MRP-5, present on the basolateral membrane of the intestine. *mrp-5* null mutants show embryonic lethality which can be rescued by heme supplementation, hence suggesting that there are alternate heme export pathways, which function in the absence of *mrp-5*. To uncover these alternate heme export pathways, we conducted a forward genetic screen to identify mutants that can bypass the lethality caused by lack of *mrp-5*. We identified loss of function mutations in the subunits of adaptor protein-3 (AP-3) complex that can completely suppress the *mrp-5* lethality without any exogenous heme. The strong suppression mediated by AP-3 deficiency is primarily attributed to the intestine. Apart from the lethality, loss of AP-3 also rescues glial migratory and synaptic defects associated with weak loss of mutations of *mrp-5*. Genetic depletion of

mrp-5 and AP-3 subunits increases the systemic heme availability within the secretory pathway, without altering the cytosolic heme levels. The increase in intestinal heme levels due to *mrp-5* deficiency causes HRG-1 degradation, and HRG-1 overexpression rescues *mrp-5* lethality. Conversely, knocking down *hrg-1* in the suppressed strain (*apb-3;mrp-5*) leads to embryonic lethality. RNA-Seq analysis revealed upregulation of HRGs in the *mrp-5* null mutants, which is restored in the suppressor strain. Subsequent screening identified two worm homologs of SLC49A, *B0416.5* and *C27A7.6* as heme exporters. B0416.5 localizes to the basolateral membrane and intracellular compartments of the intestine, a pattern similar to MRP-5, while C27A7.6 localizes primarily to the plasma membrane and intracellular compartments in oocytes. AP-3 depletion disrupts the intracellular localization of B0416.5 and C27A7.6 indicating the importance of the dual localization of both these proteins for its function in the suppressor strain. In conclusion, our results demonstrate the cellular basis for how AP-3 deficiency bypasses the *mrp-5* lethality and identify B0416.5 and C27A7.6 as novel heme transporters.

Results

Depletion of AP-3 subunits can suppress the embryonic lethality associated with *mrp-5* null mutants

mrp-5(ok2067) worms cannot be grown on NGM plates unless supplemented with exogenous heme. An EMS-based forward genetic screen, performed by a previous lab

member, identified suppressors of *mrp-5* lethality that could be completely bypassed without any exogenous heme (Figure 3.1).

Although, the forward genetic screen in *mrp-5* identified three subunits of adaptor protein-3 (*apd-3*, *apm-3*, and *aps-3*), we included the fourth subunit *apb-3* in all our subsequent RNAi studies. We verified these as suppressors of *mrp-5* lethality since RNAi knockdown of any of the four subunits of adaptor protein -3 (AP-3) can suppress the embryonic lethality caused by *mrp-5* deficiency without any exogenous heme (Figure 3.2A).

We next sought to determine if this suppression is specific to AP-3 subunits or if this is a general feature of adaptins. Interestingly, knockdown of AP-2 subunits also suppressed *mrp-5* lethality. However, knockdown of AP-1 subunits results in lethality in both wildtype and *mrp-5* worms (Figure 3.2B).

To genetically evaluate the strength of this suppression, we compared the viability between wildtype and a heme sensitized quadruple mutant (QKO) strain. This QKO strain was generated by CRISPR/Cas9 by deleting all four known heme importers paralogs *hrg-1,-4,-5 and -6*, thus making it a heme-sensitized strain. RNAi of *mrp-5* in QKO resulted in complete lethality, which cannot be rescued even with heme supplementation. Importantly, co-depletion of any of the four AP-3 subunits along with *mrp-5* in the QKO strain led to ~30% rescue. Addition of 50 μM heme further showed that loss of AP-3 subunits can completely override the embryonic lethality caused by

mrp-5 deficiency even in a heme sensitized strain, suggesting that this is a strong suppression (Figure 3.3).

Using tissue-specific RNAi strains, we have previously shown that it is the loss of *mrp-5* primarily from the intestine that dictates the embryonic lethality [26]. Worms harboring mutations in the *rde-1* gene are resistant to RNAi. Expressing *rde-1* ectopically from a tissue-specific promoter in a *rde-1* mutant background targets RNAi silencing to a particular tissue [69]. To address the tissue contribution of AP-3 suppression, we performed RNAi against *mrp-5* and AP-3 subunits in the intestine-specific RNAi strain (VP303), which expresses *rde-1* from the intestinal promoter *nhx-2*. Loss of either of the four subunits of AP-3 from the intestine is sufficient to rescue the embryonic lethality caused by *mrp-5* deficiency, thus recapitulating the whole animal RNAi phenotype. Likewise, depletion of AP-2 subunits from the intestine also suppressed the *mrp-5* lethality. Together, these results indicate that reversion of *mrp-5* lethality caused by the loss of AP-2 or AP-3 subunits can be primarily attributed to the intestine (Figure 3.4).

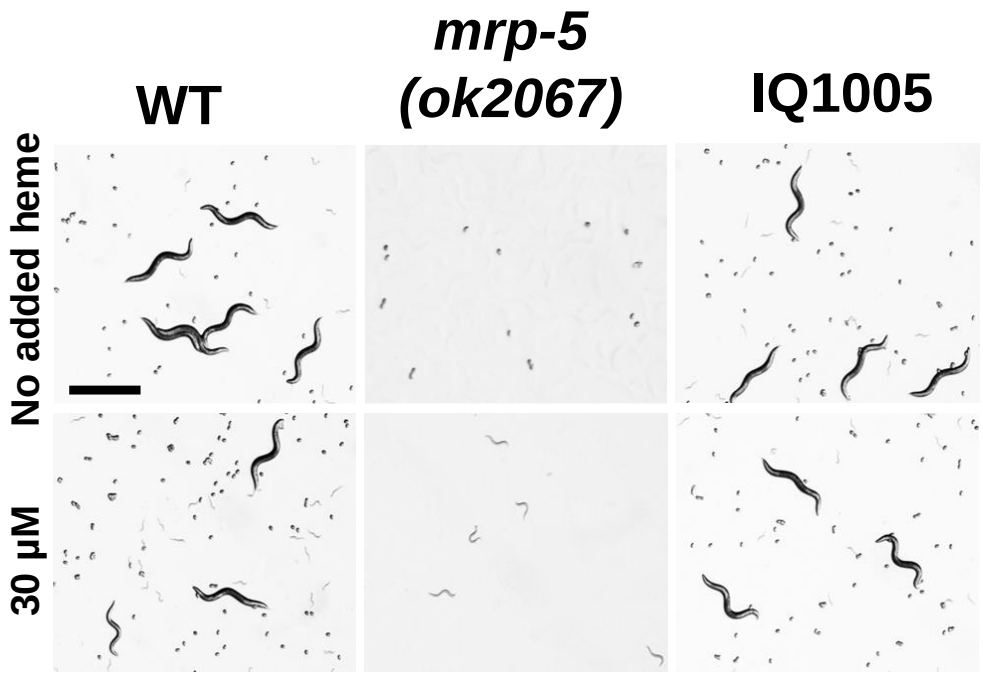

Figure 3.1. Representative images of wild-type, *mrp-5(ok2067)*, and suppressor strain *(IQ1005)*

Synchronized P0 worm strains were seeded on NGM plates with and without heme and allowed to lay F1 progeny. Photographs were taken 3 days after the P0 worms were seeded. Scale bar, 0.2 mm

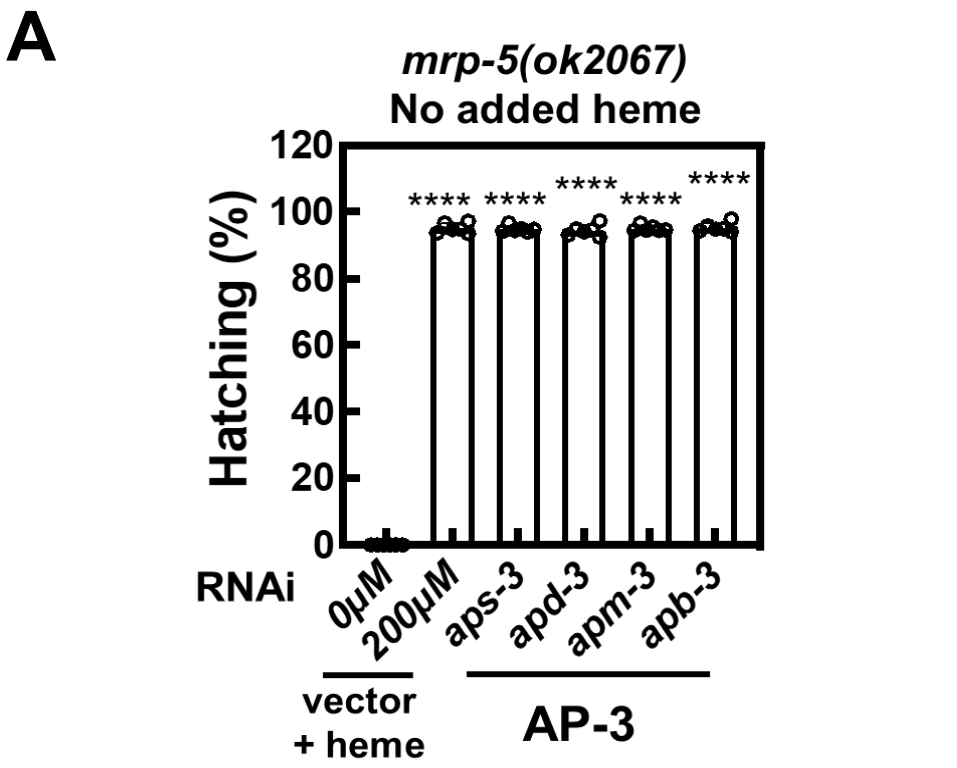
A
mrp-5(ok2067)
No added heme
Hatching (%)
120
100
80
60
40
20
0
****
****
****
****
****
RNAi
0μM
200μM
aps-3
apd-3
apm-3
apb-3
vector
+ heme
AP-3

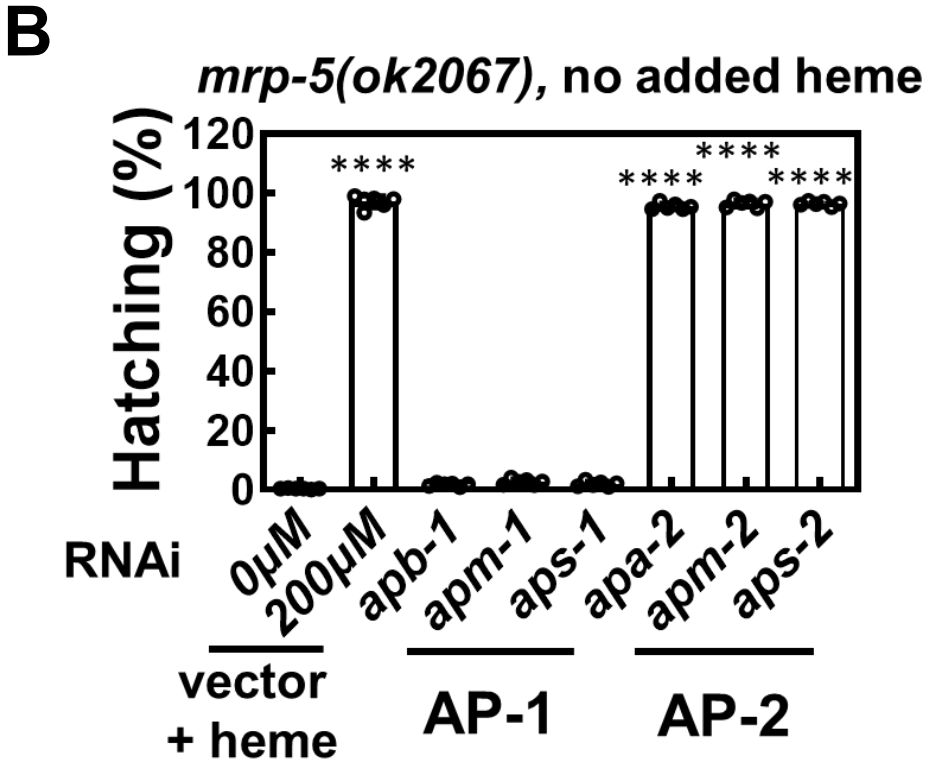
B
mrp-5(ok2067), no added heme
Hatching (%)
120
100
80
60
40
20
0
****
****
****
****
RNAi
0μM
200μM
apb-1
apm-1
aps-1
apa-2
apm-2
aps-2
vector
+ heme
AP-1
AP-2

Figure 3.2 Depletion of AP-3 or AP-2 subunits can rescue the embryonic lethality caused by loss of mrp-5 without the addition of exogenous heme.

RNAi against AP-3 subunits (A) and AP-2 /AP-1 subunits (B) was conducted using synchronized *mrp-5(ok2067)* worms on NGM plates, where five young adults were clonally moved to RNAi plates without heme supplementation. These P0 worms were allowed to lay eggs for 24 h, and then moved to new RNAi plates. The F1 eggs were scored for hatching after another 24 h, and the number of hatched worms and unhatched eggs were recorded. *mrp-5(ok2067)* seeded on 200 μM heme was used as a positive control and observed until the F1s reached adulthood.

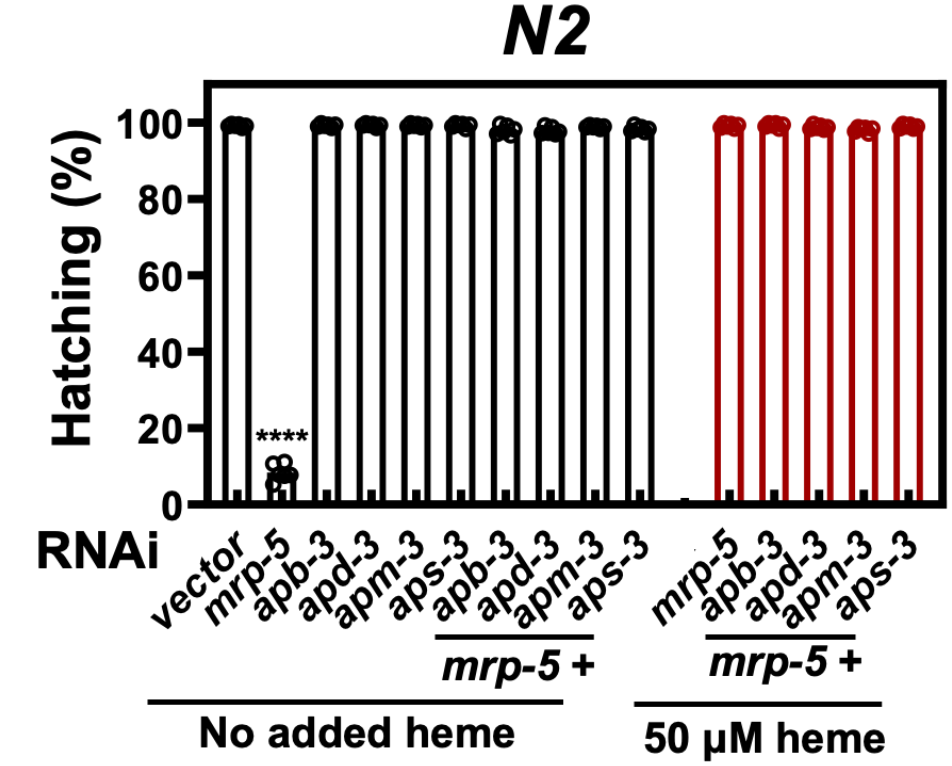
N2
Hatching (%)
100
80
60
40
20
0
****
RNAi
vector
mrp-5
apb-3
apd-3
apm-3
aps-3
apb-3
apd-3
apm-3
aps-3
mrp-5
apb-3
apd-3
apm-3
aps-3
mrp-5 +
mrp-5 +
No added heme
50 µM heme

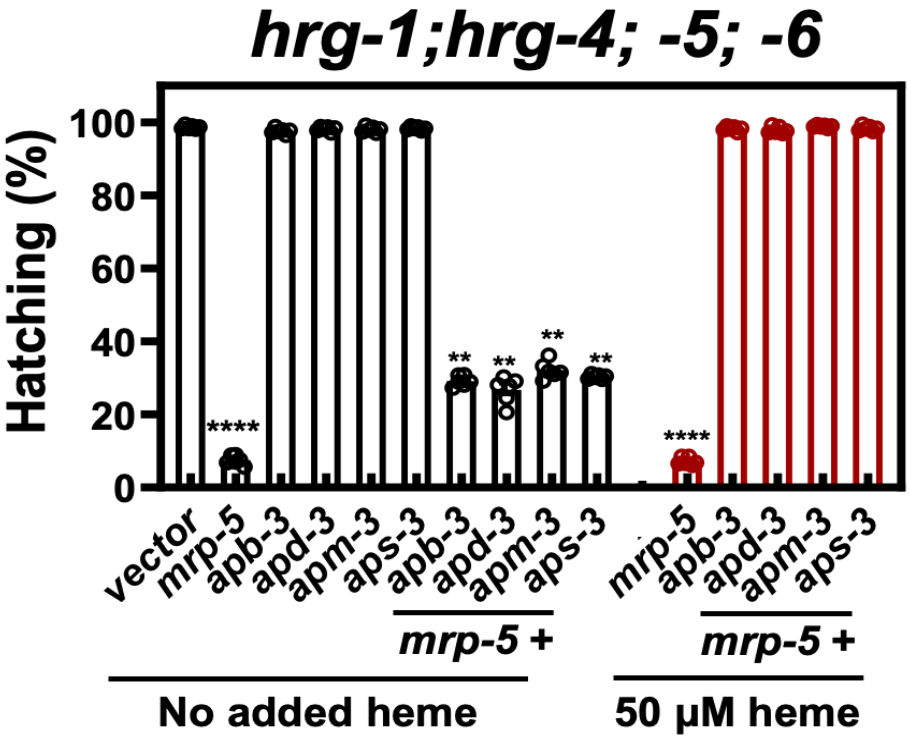
hrg-1;hrg-4; -5; -6
Hatching (%)
100
80
60
40
20
0
****
**
**
**
**
****
vector
mrp-5
apb-3
apd-3
apm-3
aps-3
apb-3
apd-3
apm-3
aps-3
mrp-5
apb-3
apd-3
apm-3
aps-3
mrp-5 +
mrp-5 +
No added heme
50 µM heme

Figure 3.3. Loss of AP-3 subunits act as strong suppressors of *mrp-5* lethality

Wildtype and quadruple mutant (*hrg-1; hrg-4,-5,-6*) worms were fed with dsRNA against *mrp-5* or *ap-3* subunits or both in presence and absence of 50 μM added heme. Synchronized P0 worms were first seeded on the indicated RNAi plates and allowed to grow till young adults. Five young adults were clonally moved to new RNAi plates, where they were left for 24 h to allow egg laying. After 24 h, these worms were transferred to new RNAi plates, while the eggs were scored for hatching after another 24 h.

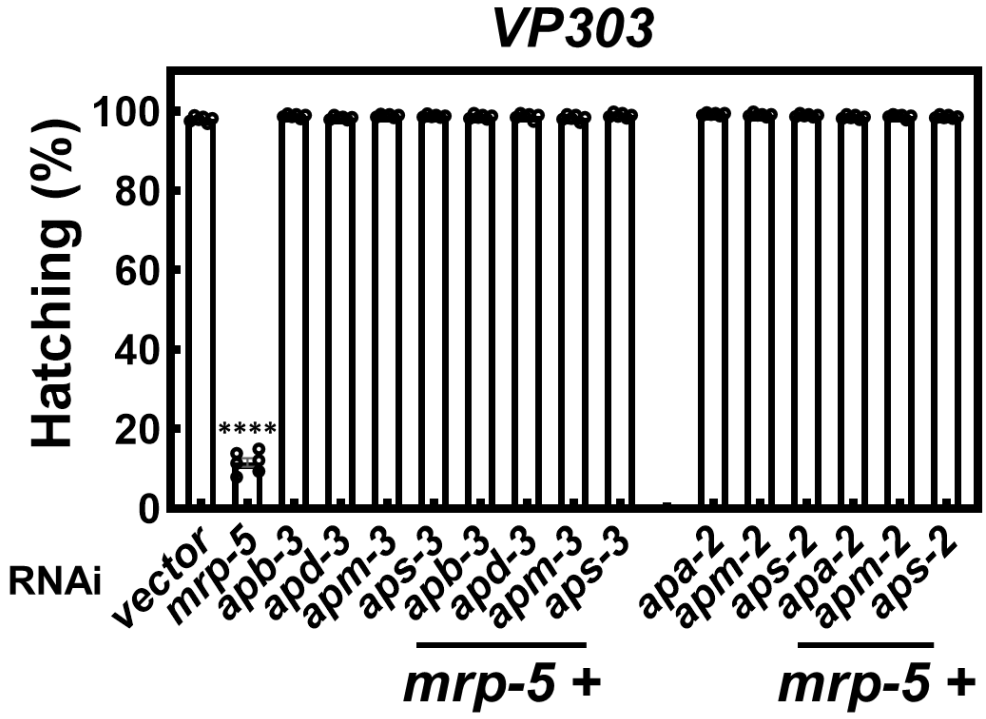

Figure 3.4. Depletion of AP-3/AP-2 subunits in the intestine is sufficient to fully restore the viability of *mrp-5* mutants.

Synchronized *VP303* worms were fed with dsRNA against *mrp-5* or *ap-3* subunits or both without any added heme on NGM plates. Once the P0 worms reached young adult stage, 5 worms were clonally picked and transferred to new RNAi plates, allowed to lay eggs for 24 h, and then removed. These worms were then transferred to new RNAi plates, and the eggs were scored for hatching after another 24 h.

Loss of AP-3 subunits can suppress the glial migratory defects caused by mutations in *mrp-5*

Building upon our results so far that AP-3 loss bypasses the embryonic lethality in *mrp-5* null mutants, we investigated its potential to restore other *mrp-5* related defects. To asses this, we exploited the $P_{F53F4.13}$*::GFP (NYL1269),* which is a transgenic amphid sheath glia reporter strain. The amphid sensilla, the largest sensory organ of the worm, is a pair of sensilla each consisting of 12 neurons and 2 glial cells. The glia, termed amphid sheath glia (AMsh), ensheathe the dendrites of sensory neurons in the amphid sensilla [70]. The cell bodies of these glia migrate from the tip of the nose to the pharyngeal bulb of the worm. A genetic screen performed by Zhang et. al. identified a weak loss of function (LOF) allele of *mrp-5 (NYL2499)* that exhibited glial migratory defects in which their amphid sheath glia over-migrated further down the body and failed to stop at the correct location. To determine if loss of AP-3 subunits can restore these glial migratory defects caused by mutations in *mrp-5*, we performed RNAi depletion of each of the AP-3 subunits in NYL1269 and NYL2499 with and without heme supplementation. Glial migratory index was calculated as described in Figure 3.5A. RNAi knockdown of any of the four AP-3 subunits in wildtype worms (NYL1269) caused glial over-migration that could be rescued by >50 μM heme. *mrp-5* (NYL2499) mutants required about 100 μM heme to exhibit normal glial migration, but as little as 10 μM heme was able to rescue the glial over-migration phenotype when AP-3 was depleted in these mutants. These results suggest that AP-3 subunits and low

levels of heme supplementation can rectify glial phenotypes observed in a weak *mrp-5* LOF (Figure 3.5).

Loss of AP-3 subunits can suppress *mrp-5* induced defects in GABA synapses

Zhang et al further reported that *mrp-5* (NYL2499) mutants show enlarged synapses and decreased synapse number. We next set to evaluate if loss of AP-3 subunits can rescue the defect in synapse formation caused by *mrp-5* mutation. To test this, we employed the GABA synapse reporter strain $P_{unc\text{-}25}$*::SNB-1::GFP* to visualize GABAergic synapses. Interestingly, AP-3 depletion alone decreased synapse numbers, suggesting a role for AP-3 in synapse formation. However, co-depleting AP-3 with *mrp-5* or supplementing with heme restored synapse numbers (Figure 3.6). These results indicate that heme or loss of AP-3 subunits can mitigate the synaptic defects caused by loss of *mrp-5*. In conclusion, our findings reveal that loss of AP-3 subunits can not only bypass embryonic lethality in *mrp-5* null mutants but also restore the glial migration and synaptic defects associated with *mrp-5* defects.

A

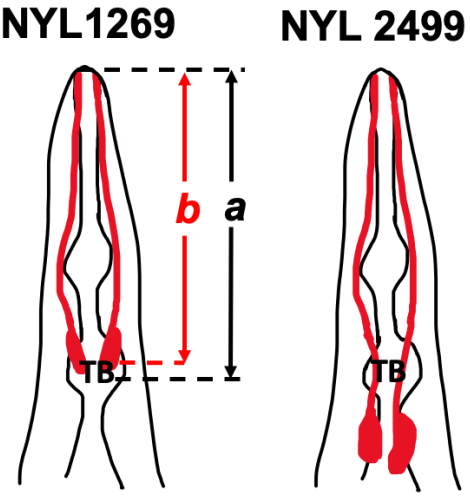

$$\text{Migration index (MI)} = \frac{b - a}{a} \times 100\%$$

B

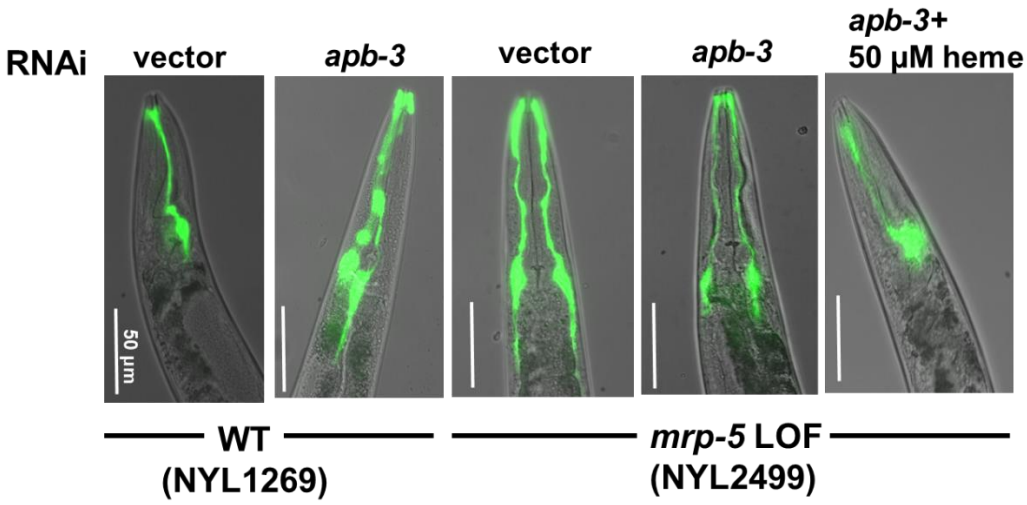

C

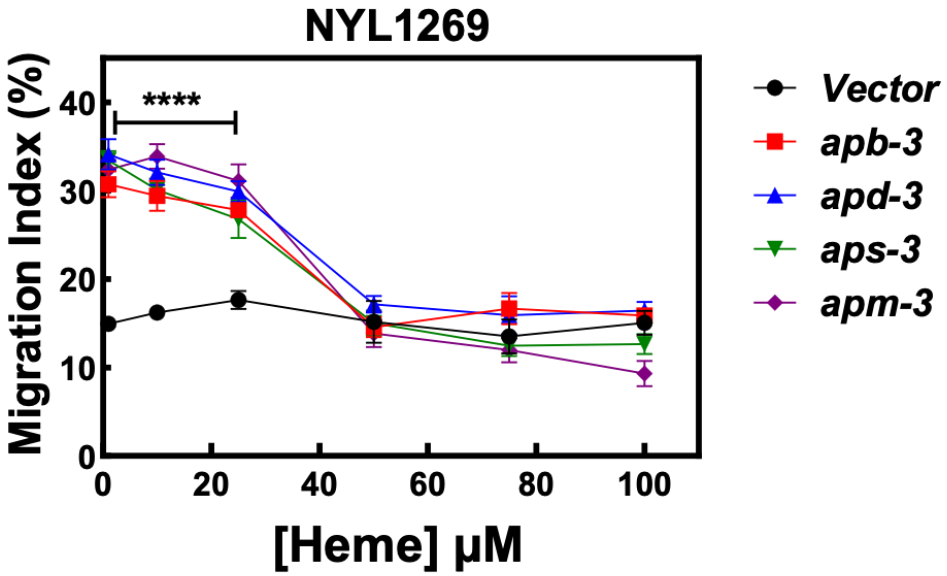
NYL1269
Migration Index (%)
****
0
10
20
30
40
0
20
40
60
80
100
[Heme] µM
Vector
apb-3
apd-3
aps-3
apm-3

D

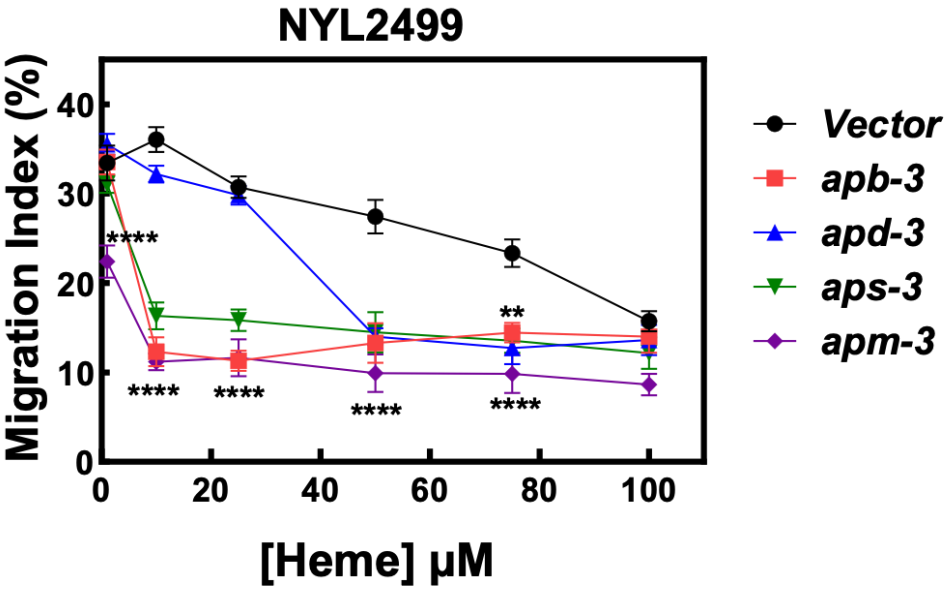
NYL2499
Migration Index (%)
****
****
****
**
****
0
10
20
30
40
0
20
40
60
80
100
[Heme] µM
Vector
apb-3
apd-3
aps-3
apm-3

Figure 3.5. AP-3 deficiency restores glial migratory defects associated with weak loss of function mutations of *mrp-5*.

(A) Representative schematic images of AMsh glia in wildtype (NYL1269) and *mrp-5* mutants (NYL24299) expressing *Pf53f4.13::GFP* (*yadIs48*). TB, terminal bulb. Migration index (MI) is calculated as b/(b-a) x 100%. Here "a" represents the distance between the tip of the nose and center of the pharyngeal terminal bulb and "b" represents the distance between the tip of the nose and center of the AMsh cell bodies.

(B) Representative confocal images of AMsh glia in wildtype (NYL1269) and *mrp-5* mutants (NYL24299) expressing *Pf53f4.13::GFP* (*yadIs48*) fed with dsRNA targeting *apb-3* with and without heme supplementation. Scale bar, 50 μm

(C) Quantification of migration index of AMsh glia in NYL1269 and (D) NYL2499 when supplemented with different heme concentrations. Data represented as mean ± SEM. One-way ANOVA test. **p<0.05, ***p<0.001, ****p<0.0001

A

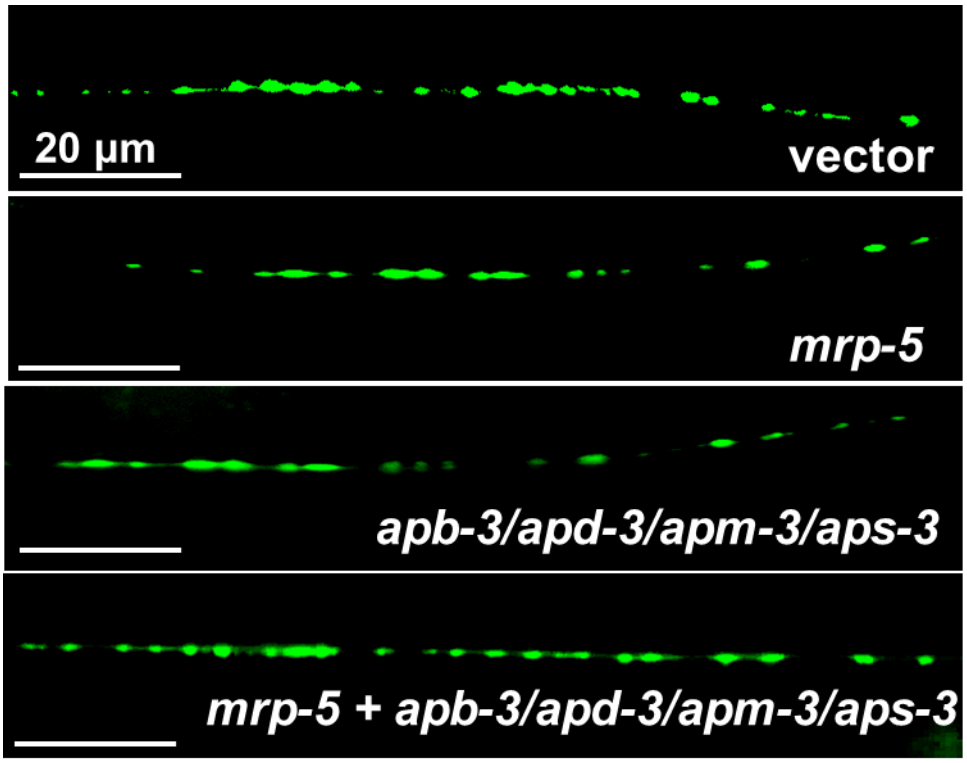
20 µm
vector
mrp-5
apb-3/apd-3/apm-3/aps-3
mrp-5 + apb-3/apd-3/apm-3/aps-3

B

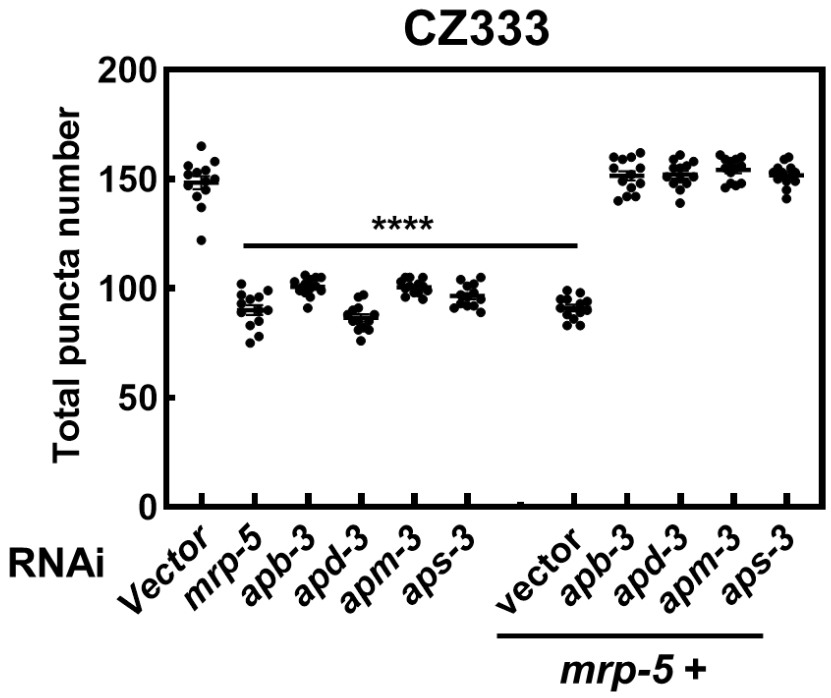
CZ333
Total puncta number
200
150
100
50
0
****
RNAi
Vector
mrp-5
apb-3
apd-3
apm-3
aps-3
vector
apb-3
apd-3
apm-3
aps-3
mrp-5 +

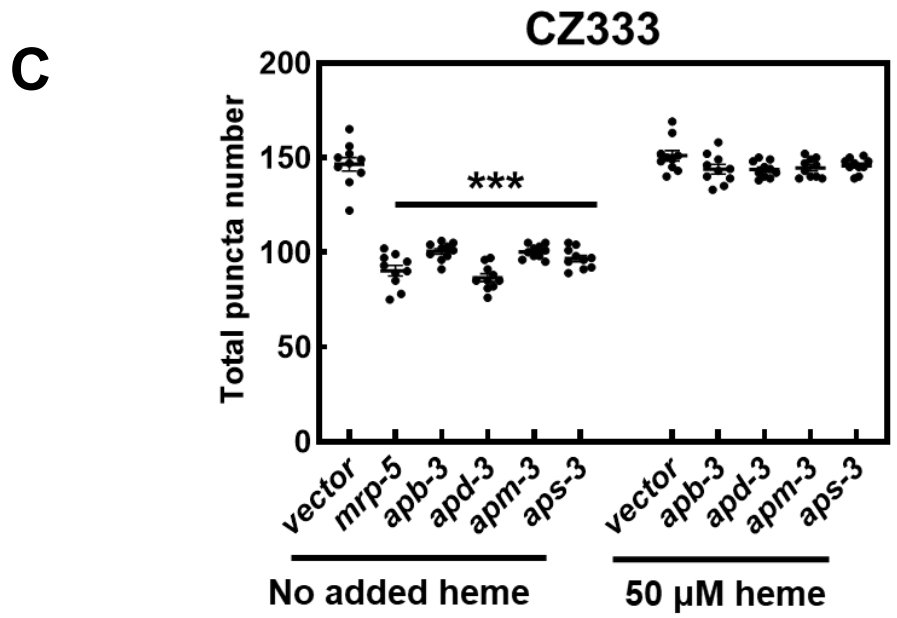

Figure 3.6. AP-3 deficiency rescues synaptic defects associated with weak loss of mutations of *mrp-5*.

(A) Representative confocal images show GABA neuron synapses visualized by SNB-1::GFP *(juls1)* at the dorsal cord after being fed the corresponding dsRNA, as labeled. Scale bar, 20 μm.

(B) Quantification of the GABA neuron synapses at the dorsal cord after RNAi depletion of AP-3 subunits by themselves, and by combining them with *mrp-5* RNAi.

(C) Quantification of the GABA neuron synapses at the dorsal cord after RNAi depletion of AP-3 subunits in the presence and absence of 50 μM heme.

In (B) and (C), data are represented as mean ± SEM. One-way ANOVA test. ***p<0.001, ****p<0.0001

Loss of AP-3 subunits increases systemic heme availability, specifically in the secretory pathway

To determine tissue heme levels, we deployed genetically encoded, tissue-specific peroxidase-based reporters. The enzymes horseradish peroxidase (HRP) and ascorbate peroxidase (APX) use heme as a prosthetic group for their peroxidase activity, thus making them robust reporters of labile heme levels when their expression is driven from tissue-specific promoters. We first assessed the heme levels in the secretory pathway using ER-targeted HRP reporters driven from the intestinal (*vha-6*), hypodermal (*dpy-7*) and pan-neuronal (*unc-119*) promoters [18]. Knockdown of *mrp-5* caused higher HRP activity consistent with heme accumulation within the intestine, while only a marginal increase in intestinal HRP activity was observed when AP-3 subunits were depleted. However, co-depletion of *mrp-5* along with AP-3 subunits resulted in a significant increase in HRP activity (Figure 3.5A). Conversely, knockdown of *mrp-5* in the hypodermis showed an expected decrease in HRP activity unless the AP-3 subunits were co-depleted (Figure 3.5B). In neurons, *mrp-5* RNAi resulted in lower HRP activity, as expected. Remarkably, co-depletion of *mrp-5* and AP-3 subunits caused a significant increase in HRP activity, similar to the intestine (Figure 3.5C). Importantly, cytosolic heme levels are unaffected, as the cytosol-targeted APX driven from the intestinal promoter showed no changes in the cytosolic APX activity (Figure 3.5D). These results together indicate that loss of AP-3 subunits in the *mrp-5* mutants lead to increased systemic heme levels specifically in the secretory pathway without altering intestinal cytosolic heme levels.

A

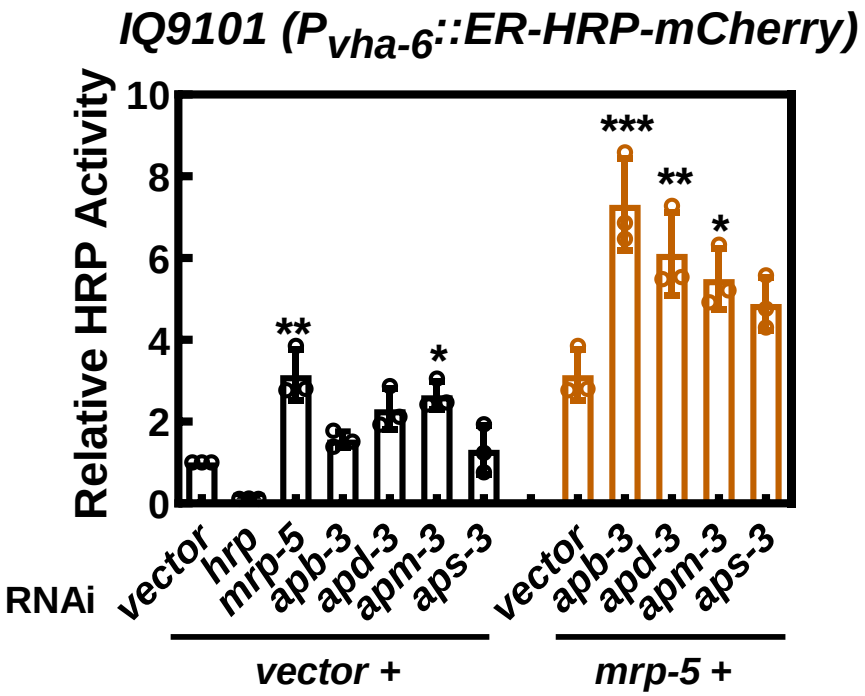
IQ9101 (Pvha-6::ER-HRP-mCherry)
Relative HRP Activity
10
8
6
4
2
0
**
*
***
**
*
RNAi
vector
hrp
mrp-5
apb-3
apd-3
apm-3
aps-3
vector
apb-3
apd-3
apm-3
aps-3
vector +
mrp-5 +

B

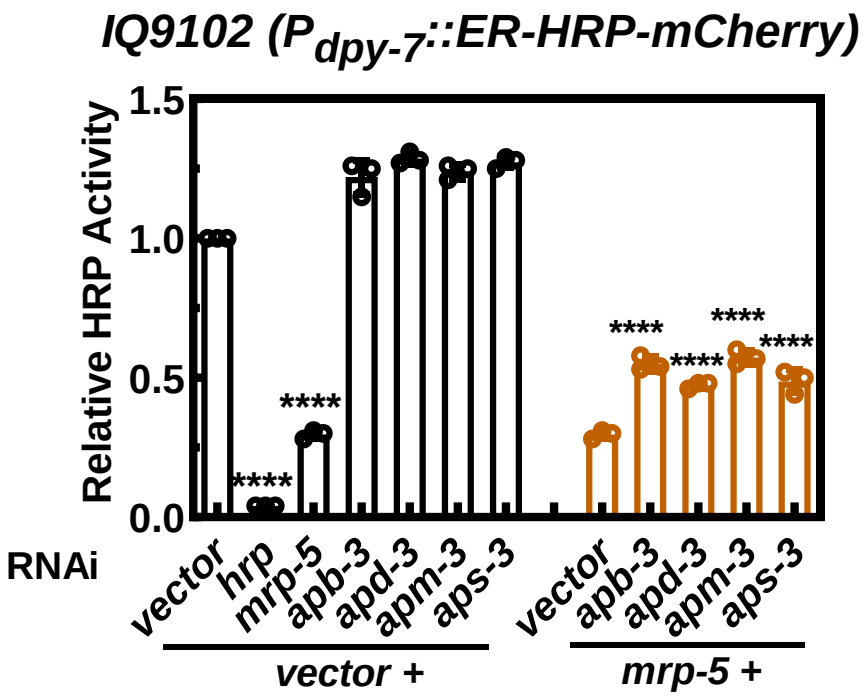
IQ9102 (Pdpy-7::ER-HRP-mCherry)
Relative HRP Activity
1.5
1.0
0.5
0.0
****
****
****
****
****
RNAi
vector
hrp
mrp-5
apb-3
apd-3
apm-3
aps-3
vector
apb-3
apd-3
apm-3
aps-3
vector +
mrp-5 +

C

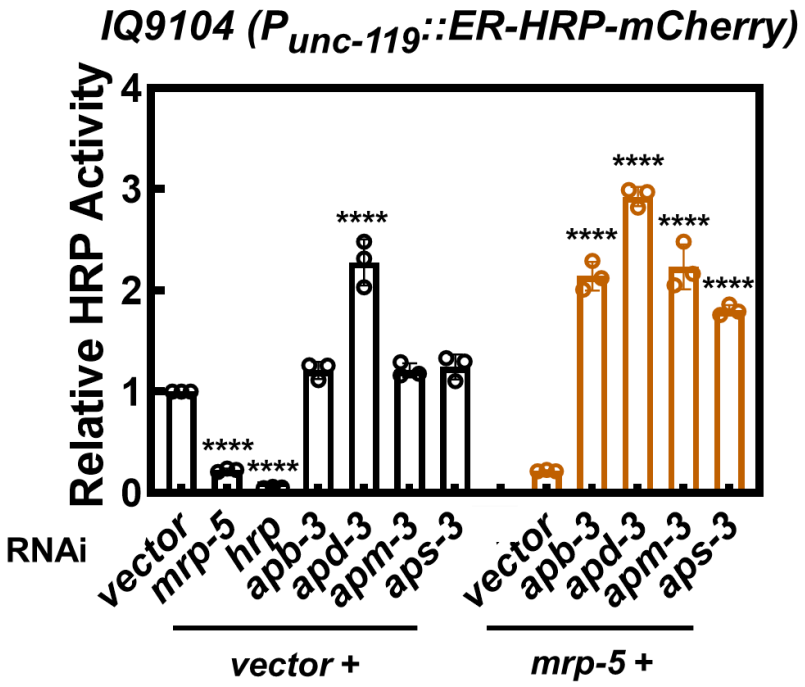
IQ9104 (Punc-119::ER-HRP-mCherry)
Relative HRP Activity
0
1
2
3
4
****
****
****
****
****
****
RNAi
vector
mrp-5
hrp
apb-3
apd-3
apm-3
aps-3
vector
apb-3
apd-3
apm-3
aps-3
vector +
mrp-5 +

D

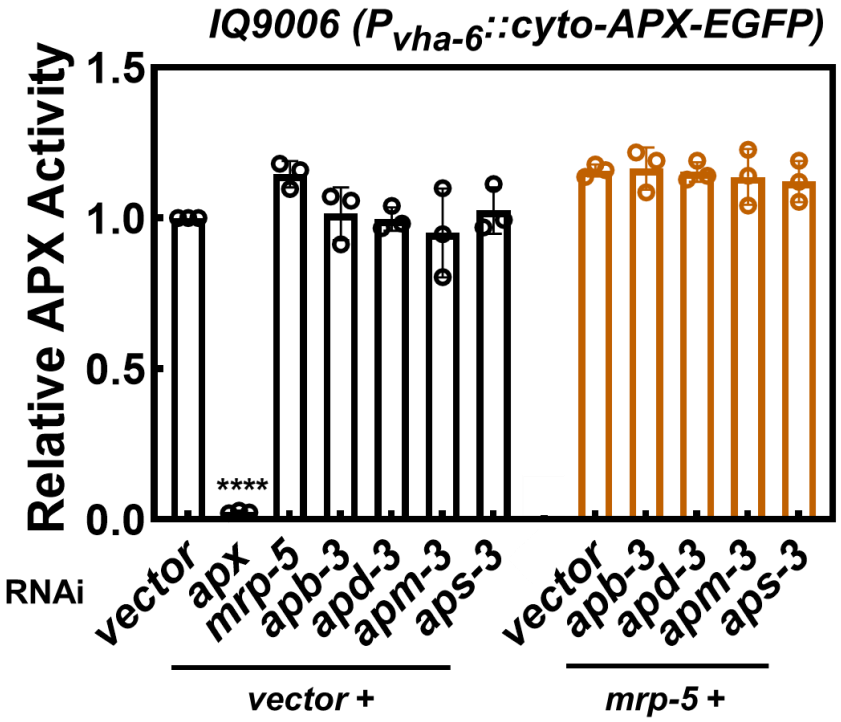
IQ9006 (Pvha-6::cyto-APX-EGFP)
Relative APX Activity
0.0
0.5
1.0
1.5
****
RNAi
vector
apx
mrp-5
apb-3
apd-3
apm-3
aps-3
vector
apb-3
apd-3
apm-3
aps-3
vector +
mrp-5 +

Figure 3.7. Loss of AP-3 subunits increases systemic heme availability, specifically in the secretory pathway.

Synchronized L1s of $P_{vha\text{-}6}$*::ER-HRP::mCherry* (A), $P_{dpy\text{-}7}$*::ER-HRP::mCherry* (B), $P_{unc\text{-}119}$*::ER-HRP::mCherry* (C) and $P_{vha\text{-}6}$*::cyto-APX-EGFP* (D) were seeded on indicated RNAi plates, harvested at young adult stage, lysed and subjected to reporter activity analysis using o-dianisidine and H_2O_2 as substrates. Peroxidase activity was determined using a plate reader (SynergyHT, BioTek) and normalized against *vector + vector* co-RNAi.

*p<0.05, **p<0.01, ***p<0.001 (one-way ANOVA with Dunnett's multiple comparison test)

Coordinated regulation of *mrp-5* and AP-3 regulate HRG-1 levels

Given that the AP-3 subunits are involved in the formation of LROs, and this is the same compartment where HRG-1 resides, we investigated how AP-3 influences HRG1 localization within the *C. elegans* intestine. To test this, we conducted RNAi experiments using the *P_{hrg-1}::HRG-1::GFP (IQ6111)* worms and stained them with zinc mesoporphyrin IX (ZnMP) and LysoTracker. While ZnMP is a fluorescent heme analog, lysotracker aids in visualization of acidic compartments. HRG-1 co-localized with both ZnMP and Lysotracker within the intestine, indicating its proper targeting to these compartments. Consistent with its role in heme export, *mrp-5* RNAi caused an accumulation of ZnMP due to increased heme within the intestine. Strikingly, *mrp-5* depletion resulted in a dramatic reduction in HRG-1 within the intestine. RNAi of *apb-3* led to diffused HRG-1 localization and reduced lysotracker and ZnMP staining characteristic of AP-3 involvement in LRO formation. Co-depletion of *apb-3* and *mrp-5* partially restored HRG-1 levels and localization (Figure 3.8). A similar phenotype was observed when other AP-3 subunits were co-depleted with *mrp-5* (not shown). These findings reveal that both *mrp-5* and *AP-3*, are essential for dictating HRG-1 localization and abundance (Appendix V).

To evaluate the contribution of HRG-1 in *mrp-5* mutants, we employed transgenic worms that expressed worm or human HRG-1 under the control of an intestine-specific promoter (*P_{vha-6}::HRG-1-mCherry*). These transgenic worms displayed no embryonic

lethality when *mrp-5* was knocked down suggesting that ectopic expression of HRG-1 mitigates *mrp-5* lethality (Figure 3.9A).

To further substantiate the role of HRG-1 in *mrp-5* mutants, we depleted *hrg-1* in the suppressed strain. *hrg-1* depletion resulted in embryonic lethality in the suppressor (*apb-3;mrp-5*) strongly supporting the notion that HRG-1 is essential for the survival of *apb-3;mrp*-5 suppressor (Figure 3.9B).

Taken together, these results highlight the importance of HRG-1 levels in determining the lethality observed in *mrp-5* null mutants. Increasing HRG-1 expression can compensate for the loss of *mrp-5* function, and conversely, depletion of *hrg-1* in the suppressor strain negates the rescue by AP-3 deficiency.

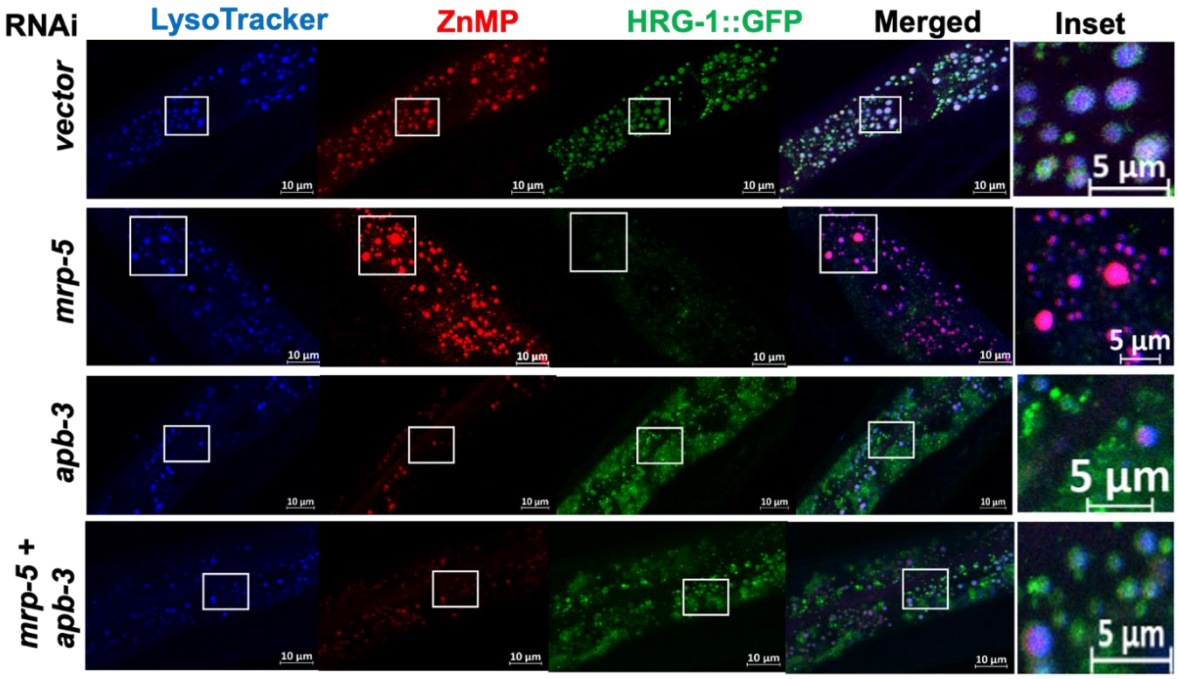

Figure 3.8. Coordinated regulation of *mrp-5* and *ap-3* dictates HRG-1 abundance.

Transgenic worms $P_{hrg\text{-}1}$*::HRG-1::GFP* (green) were fed with indicated dsRNA, co-stained with LysoTracker Blue and zinc mesoporphyrin (ZnMP) and visualized with confocal microscopy. White boxes indicate insets.

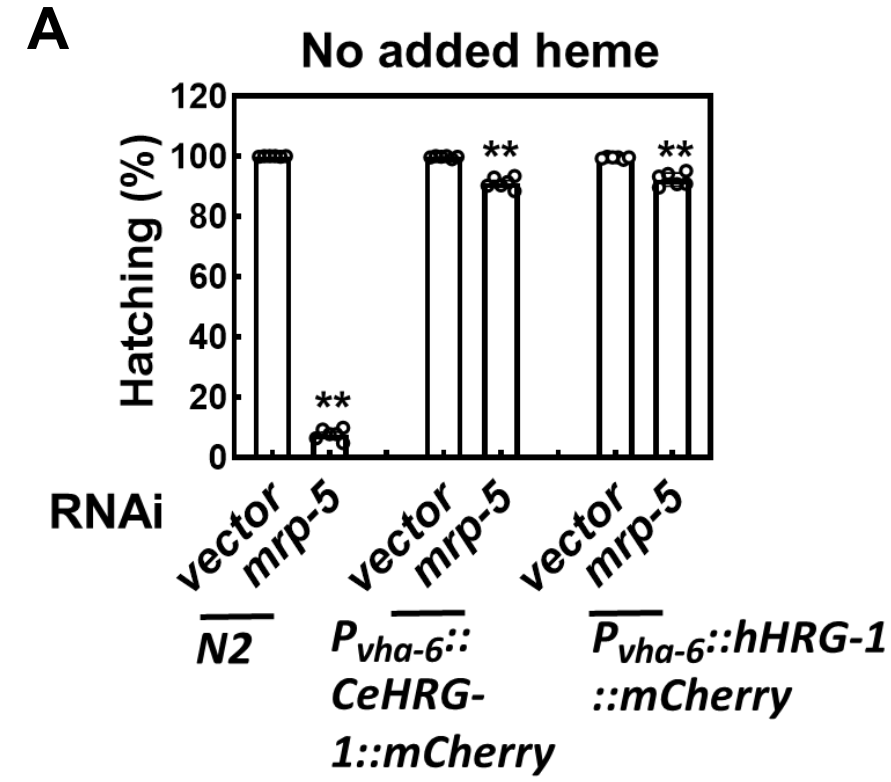
A
No added heme
Hatching (%)
120
100
80
60
40
20
0
**
**
**
RNAi
vector
mrp-5
vector
mrp-5
vector
mrp-5
N2
P vha-6 :: CeHRG-1::mCherry
P vha-6 ::hHRG-1 ::mCherry

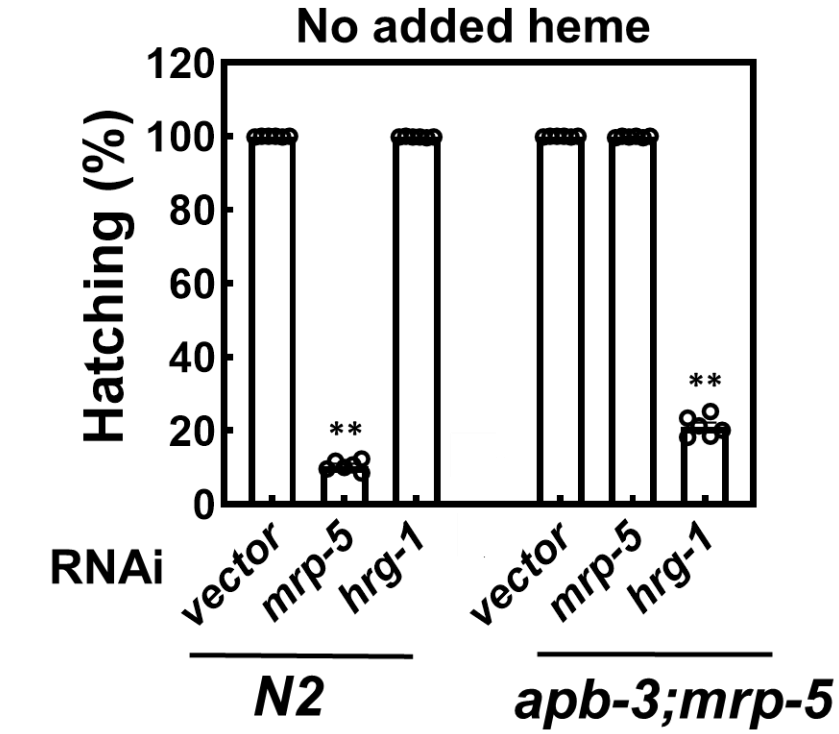
B
No added heme
Hatching (%)
120
100
80
60
40
20
0
**
**
RNAi
vector
mrp-5
hrg-1
vector
mrp-5
hrg-1
N2
apb-3;mrp-5

Figure 3.9. HRG-1 is essential for *mrp-5* lethality rescue.

(A) Indicated worm strains were synchronized and fed with dsRNA against *mrp-5* without any added heme on NGM plates. Once the P0 worms reached young adult stage, 5 worms were clonally picked and transferred to new RNAi plates, allowed to lay eggs for 24 h, and then removed. These worms were then transferred to new RNAi plates, and the eggs were scored for hatching after another 24 h. CeHRG-1 denotes *C. elegans* HRG-1, while hHRG-1 represents worms expressing human HRG-1.

(B) Wildtype (N2) and suppressor stains (*apb-3;mrp-5*) were synchronized and fed with dsRNA without any added heme on NGM plates. Once the P0 worms reached young adult stage, 5 worms were clonally picked and transferred to new RNAi plates, allowed to lay eggs for 24 h, and then removed. These worms were then transferred to new RNAi plates, and the eggs were scored for hatching after another 24 h.

Data are represented as mean ± SEM. Unpaired t test. **$p<0.05$.

Heme targeted turnover of HRG-1 protein

Our studies reveal that *mrp-5* deficiency leads to an increase in intestinal heme accumulation and a concomitant decrease in HRG-1 protein. To determine whether heme regulates HRG-1, we employed two *C. elegans* strains: one strain expressed HRG-1 under the control of its endogenous promoter ($P_{hrg\text{-}1}$*::HRG1::GFP*), while the other expressed HRG-1 ectopically from the intestine-specific promoter ($P_{vha\text{-}6}$*::HRG1::mCherry).* Both strains displayed a clear influence of heme concentration on HRG-1 protein abundance when grown with varying heme concentrations ranging from 1.5 - 200μM in axenic conditions. When expressed from its endogenous promoter, *hrg-1* is also subject to transcriptional repression by heme [36]. HRG-1 levels were highest at lower heme concentrations (1.5 μM and 4 μM) but began to decline significantly at concentrations exceeding 10 μM (Figure 3.10A, C). Conversely, in worms expressing *hrg-1* from the ectopic intestine-specific promoter but lacking transcriptional control by heme showed stable expression of HRG-1 till 100 μM heme before declining (Figure 3.10B, C). These results indicate that high intestinal heme contributes to HRG-1 degradation. Further investigation is needed to elucidate the specific mechanisms by which heme affects HRG-1 protein turnover.

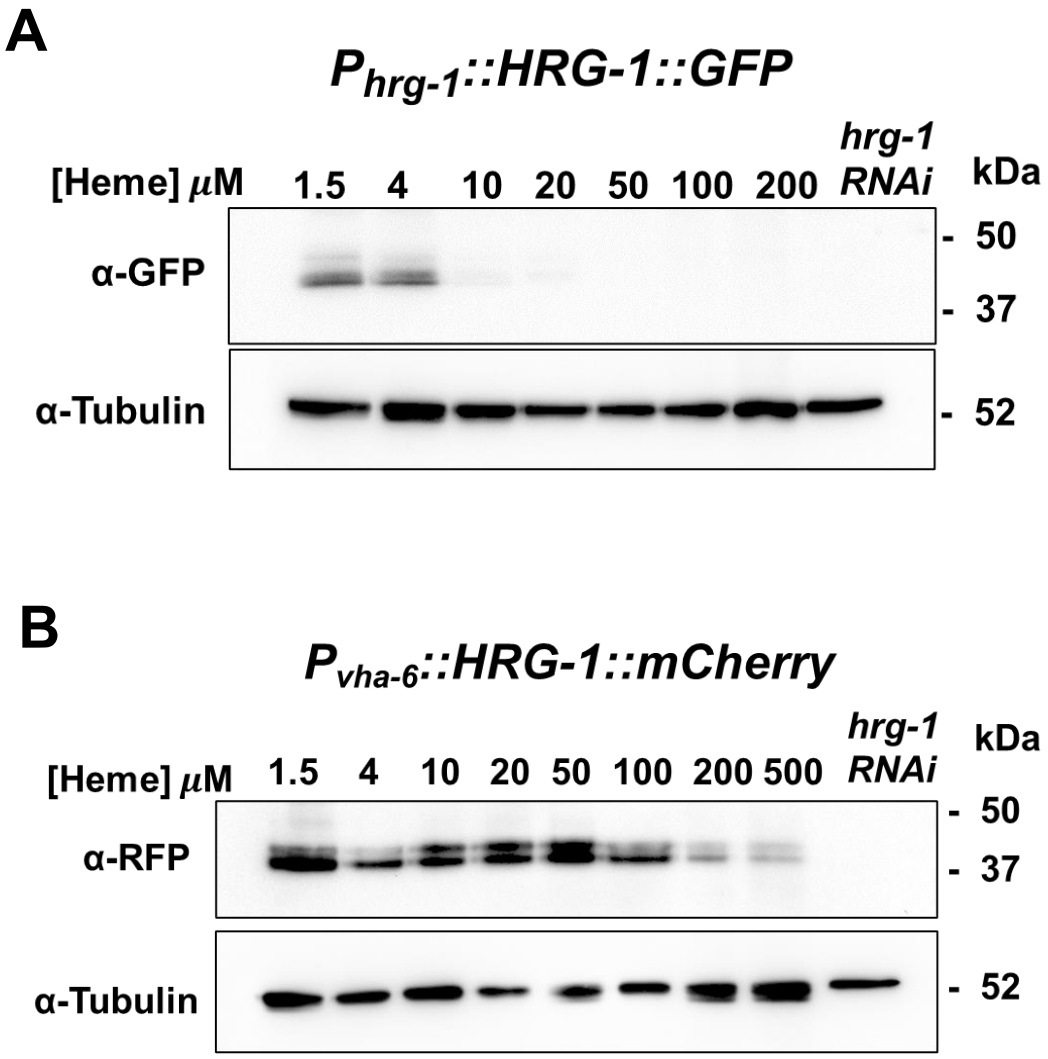
A
P_{hrg-1}::HRG-1::GFP
[Heme] μM
1.5
4
10
20
50
100
200
hrg-1 RNAi
kDa
α-GFP
- 50
- 37
α-Tubulin
- 52
B
P_{vha-6}::HRG-1::mCherry
[Heme] μM
1.5
4
10
20
50
100
200
500
hrg-1 RNAi
kDa
α-RFP
- 50
- 37
α-Tubulin
- 52

C

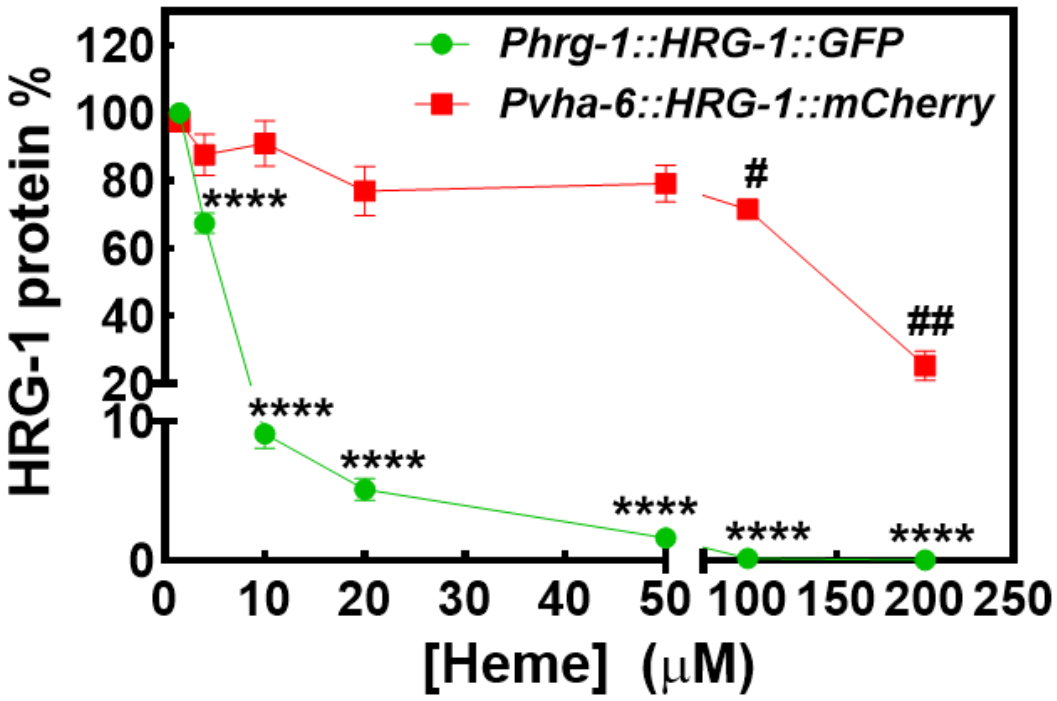

Figure 3.10. Post-translational heme-dependent turnover of HRG-1.

(A) Immunoblot analysis of HRG-1 expression in *$P_{hrg\text{-}1}$::HRG1::GFP* grown axenically in increasing heme concentrations. Membranes were probed with anti-GFP antibody, and then incubated with HRP conjugated with anti-mouse secondary antibody.

(B) Immunoblot analysis of HRG-1 expression in *$P_{vha\text{-}6}$::HRG1::mCherry* grown axenically in increasing heme concentrations. Membranes were probed with anti-RFP antibody, and then incubated with HRP conjugated with anti-mouse secondary antibody.

(C) Quantification of protein abundance in (A) and (B), across three independent experiments. HRG-1 protein levels were normalized against tubulin (loading control). Data represents mean ± SEM. One-way ANOVA, #$p<0.05$, ##$p<0.01$, ****$p<0.0001$, compared against 1.5 μM for each worm strain.

HRG-1 is a cargo protein of AP-3

To elucidate a potential physical interaction between HRG-1 and AP-3 complex, we leveraged the cargo recognition properties of AP-3. Since AP-3 subunits specifically recognize tyrosine and dileucine-based sorting motifs, and both these motifs are present within the C-terminus of HRG-1, we hypothesized that HRG-1 might be a cargo protein for AP-3. Furthermore, our previous findings demonstrated that loss of AP-3 subunits impacts HRG-1 protein localization. To test this hypothesis, we performed a co-immunoprecipitation (co-IP) assay. We co-expressed human AP-3 μ subunit, since this subunit is responsible for cargo recognition and binding with human HRG1 in HEK293 cells. Pull-down with GFP and HA antibodies revealed a physical interaction between HRG-1 and AP-3 complex. This interaction was specific as an ER-localized CD3δ-GFP did not interact with either HRG-1 or AP-3 suggesting that HRG-1 is indeed a cargo protein for AP-3 complex (Figure 3.11).

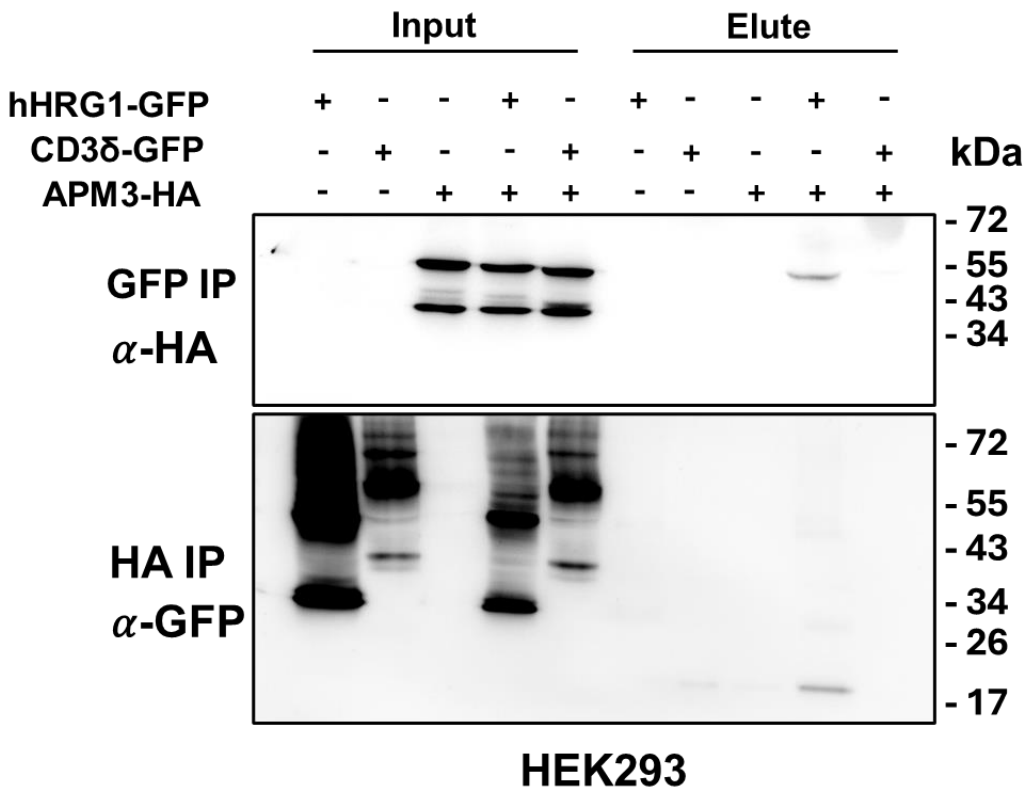

Figure 3.11. AP-3 physically interacts with HRG-1.

HEK293 cells were transfected with plasmids encoding human HRG1 tagged with GFP (hHRG1-GFP), human AP-3 subunit μ tagged with HA (APM3-HA), and ER marker CD3δ tagged with GFP (CD3δ-GFP), used as a negative control. Cell lysates were immunoprecipitated (IP) with either anti-GFP or anti-HA antibodies, followed by immunoblot analysis of these co-IP experiments. Input represents whole cell lysates before immunoprecipitation and is 10 % of the total protein that was immunoprecipitated. Elute represents proteins eluted from immunoprecipitations using either anti-GFP or anti-HA antibodies and represents 20 % of the total protein eluted.

Suppression of *mrp-5* lethality by AP-3 is a heme-specific phenomenon

Similar to *mrp-5*, loss of the copper transporting P-type ATPase *cua-1* is lethal as CUA-1 traffics between the gut granules and basolateral membranes [71]. This resemblance between heme and copper trafficking made copper homeostasis an attractive system to explore the universality of AP-3 mutant suppression on export of essential micronutrients. WT worms show reduced growth under low copper conditions when grown in the presence of bathocuproinedisulfonic acid disodium salt (BCS), a copper chelator. *cua-1* or *apb-3* depletion significantly reduced viability unless copper was supplemented. However, copper was unable to restore growth when *cua-1* and *apb-3* were co-depleted (Figure 3.12). Additionally, RNA-Seq analysis revealed that genes involved in other metabolic pathways are not altered between the wildtype and suppressor strain (Appendix IV). These results suggest that AP-3 deficiency does not universally suppress lethality caused by defects in micronutrient export.

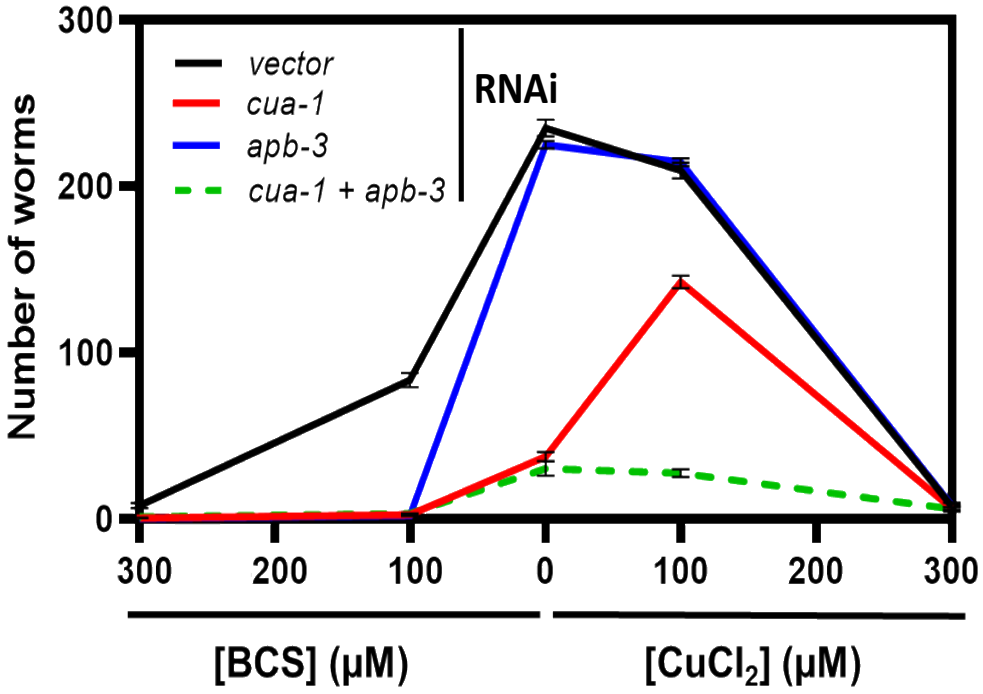

Figure 3.12. AP-3 does not suppress lethality associated with *cua-1*.

Synchronized N2 worms were plated on NGM plates seeded with HT115(DE3) for RNAi against *vector*, *cua-1*, *apb-3*, and co-RNA of *cua-1* and *apb-3*. Once gravid, four P_0 worms were picked clonally on NGM plates supplemented with BCS or CuCl2 and seeded with HT115(DE3) for RNAi against indicated genes. P_0 worms were allowed to lay F1 and then removed after 24 h. Once F1 were hatched as L1s for vector, all plates were scored for the number of hatched worms. Data are represented as mean ± SEM.

RNA-Seq analysis revealed homologs of human SLC49A3 as backup transporters in the suppressor strain

To identify how intestinal heme export is restored in the suppressor, we performed RNA-seq analyses of WT, *mrp-5*, *apb-3* and *mrp-5;apb-3* worms. A strong negative correlation was observed of differentially expressed mRNA transcripts in *mrp-5* and *mrp-5;apb-3* mutants, while *apb-3* and *mrp-5;apb-3* showed no correlation (Figure 3.13). Notably, heat maps reveal an upregulation of all the HRGs in *mrp-5* mutants compared to WT worms. This upregulation was significantly mitigated in the suppressed strain, where HRG expression levels were restored nearly to normal levels (Figure 3.14).

To identify the heme exporter, we focused on SLC49A (or FLVCR) homologs in *C. elegans*, since human SLC49A1 has been previously established as a heme exporter [43]. As four *SLC49A* homologs were significantly upregulated in the suppressor strain (Figure 3.15 and 3.16), we RNAi depleted all the *SLC49A* homologs. Knockdown of *B01416.5* and *C27A7.6* caused near-complete lethality in the suppressor (Figure 3.17); heme supplementation fully rescued the embryonic lethality caused by *C27A7.6* depletion (100 %) but not for *B0416.5* depletion (< 20 %). (Figure 3.18B). By contrast, only a minor heme-dependent growth phenotype was observed for *B01416.5* depletion in WT and QKO worms (Figure 3.18A and 3.18C), while knockdown in *mrp-5* mutants resulted in a severe phenotype that was only partially rescued by heme (~40 %) (Figure 3.18D). Together our data suggest that *B0416.5* is indispensable when the primary

heme exporter MRP-5 is compromised, while the role of *C27A7.6* becomes more prominent only in the suppressor strain when both *apb-3* and *mrp-5* are missing. Our results support a role for *B0416.5* and *C27A7.6* as alternate transporters in the suppressor strain.

Given the recent publications implicating human FLVCR1 and FLVCR2 in choline import, we tested if choline supplementation could rescue the lethality associated with *B0416.5* or *C27A7.6* (Figure 3.19) [59-63,66]. Choline had no impact on embryonic lethality caused by RNAi depletion of either *B0416.5* or *C27A7.6* in any of our assays.

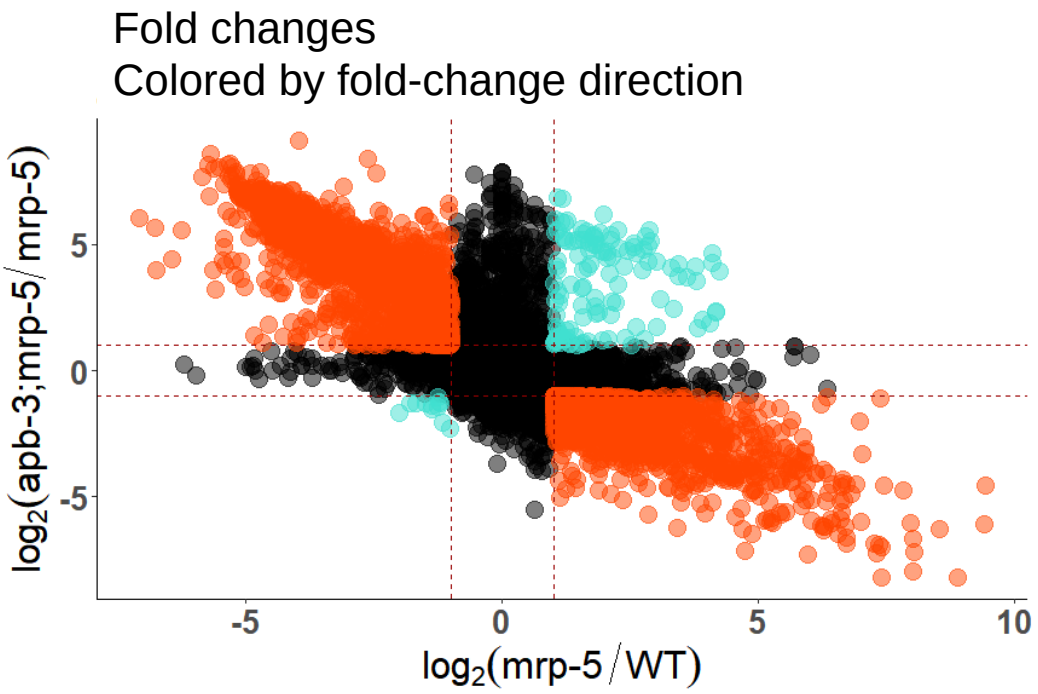
Fold changes
Colored by fold-change direction
log2(apb-3;mrp-5/mrp-5)
log2(mrp-5/WT)
5
0
-5
-5
0
5
10

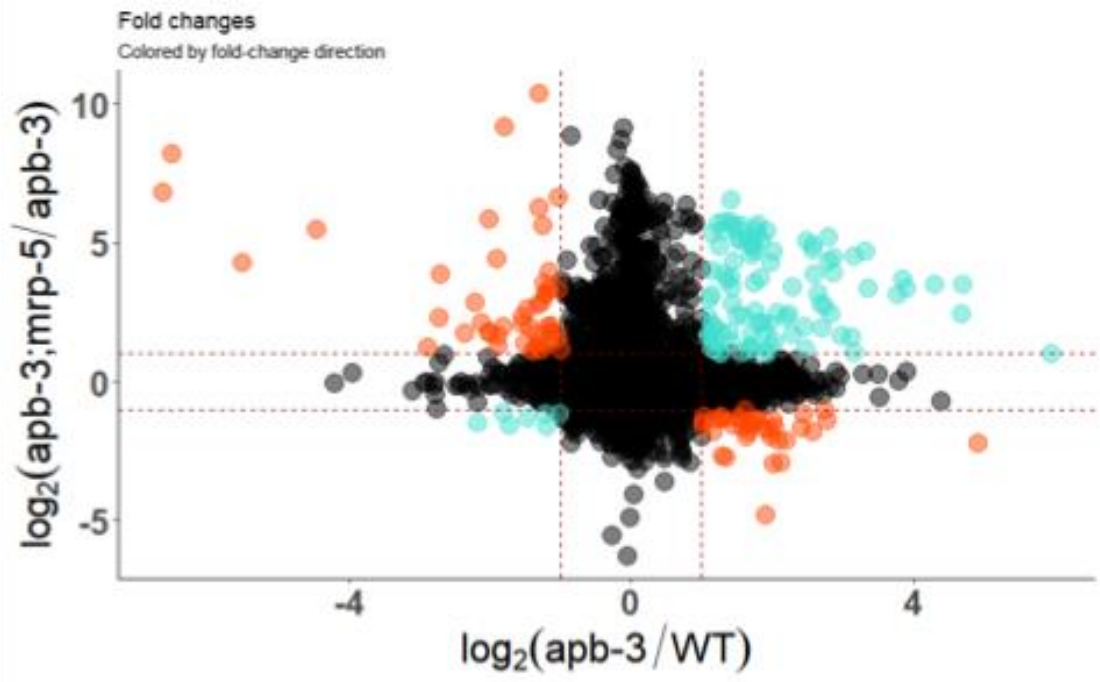
Fold changes
Colored by fold-change direction
log2(apb-3;mrp-5/apb-3)
log2(apb-3/WT)
10
5
0
-5
-4
0
4

Figure 3.13. Scatter-plots show differentially expressed transcripts, as revealed by RNA-Seq.

Scatter plots reveal negative correlation of transcripts that were differentially expressed in *mrp-5(ok2067)* and *mrp-5(ok2067);apb-3(ok429)* mutant worms. Top: Plot $\log_2$ fold change (LFC) of *mrp-5(ok2067)* vs. WT (x-axis) against LFC of *mrp-5(ok2067);apb-3(ok429)* vs. *mrp-5(ok2067)* (y-axis). Bottom: Plot LFC of *apb-3(ok429)* vs. WT (x-axis) against LFC of *mrp-5(ok2067);apb-3(ok429)* vs. *apb-3(ok429)* (y-axis). Upper right and lower left quadrants contain positively co-regulated transcripts (cyan). Upper left and lower right quadrants contain negatively co-regulated transcripts (orange). Co-regulated transcripts had an absolute LFC change higher than 1 in both pairwise comparisons. Broken red lines marks LFC = 1. Correlation analysis was performed using Pearson method (Top: R=-0.78, Bottom: R=-0.05).

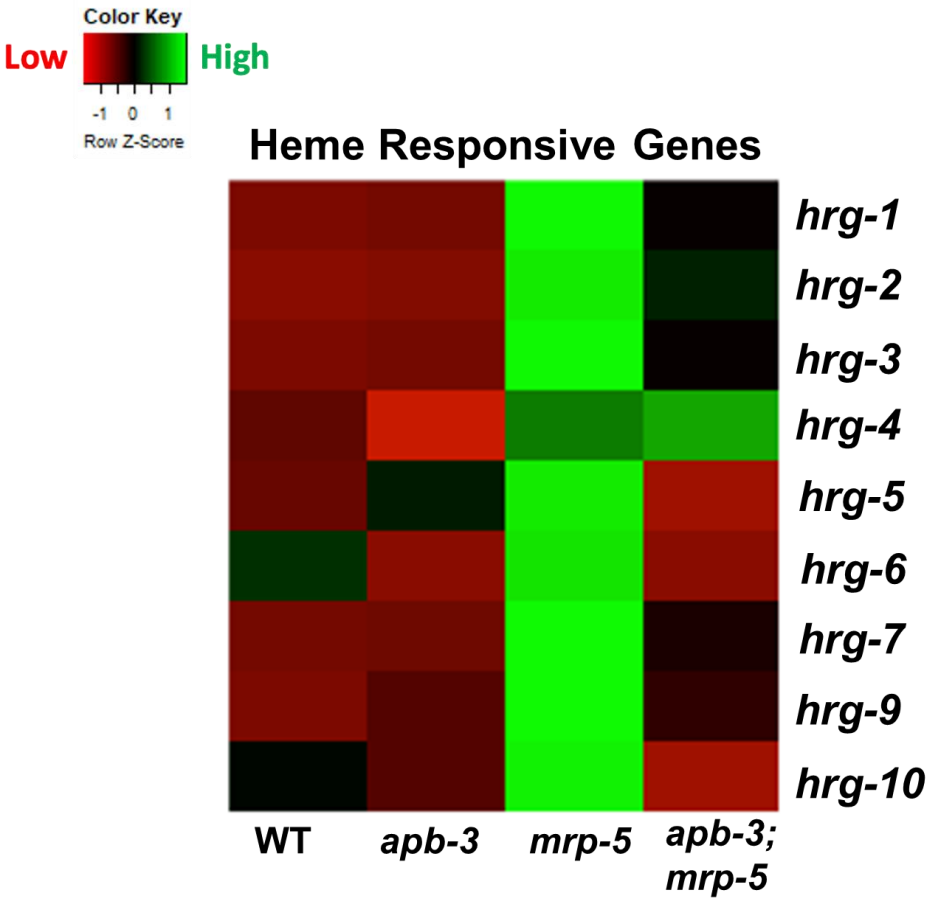

Figure 3.14. RNA-Seq analysis revealed upregulation of HRGs in the *mrp-5* mutants which is restored in the suppressor strain.

Expression of heme responsive genes in WT, *apb-3(ok429)*, *mrp-5(ok2067)* and *mrp-5(ok2067);apb-3(ok429)* worms.

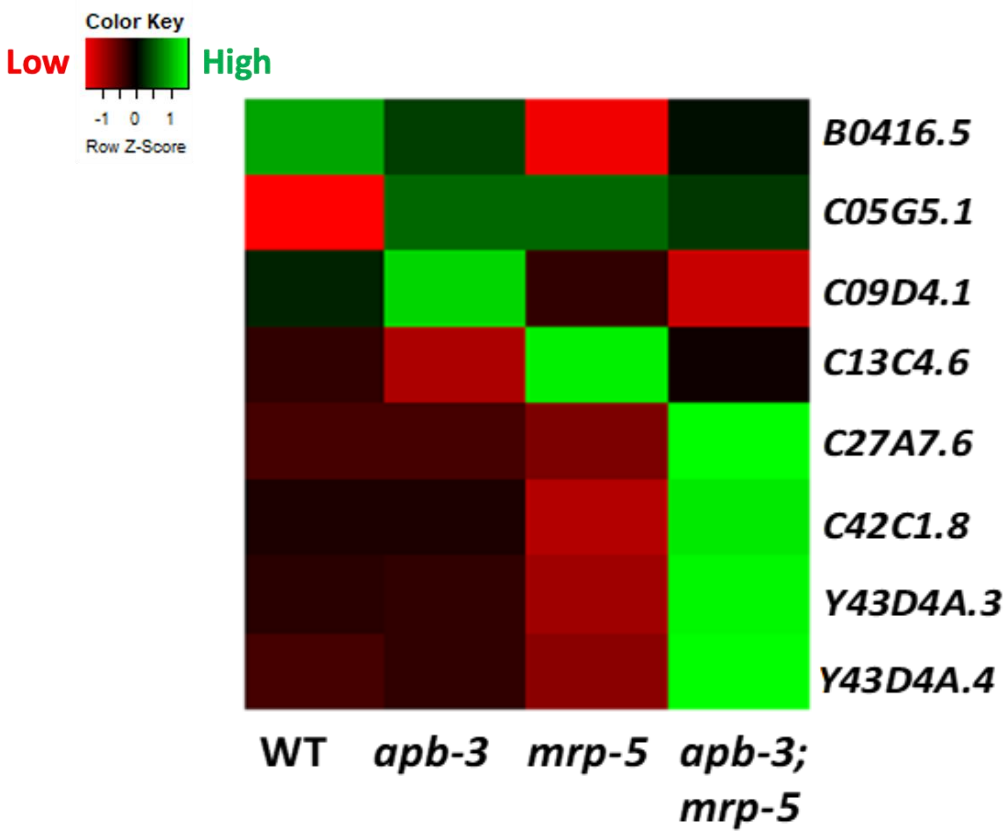

Figure 3.15. RNA-Seq analysis revealed upregulation of four SLC49A homologs in *C. elegans* in the suppressor strain (*apb-3;mrp-5*).

Expression of worm FLVCR homologs in WT, *apb-3(ok429)*, *mrp-5(ok2067)* and *mrp-5(ok2067);apb-3(ok429)* worms.

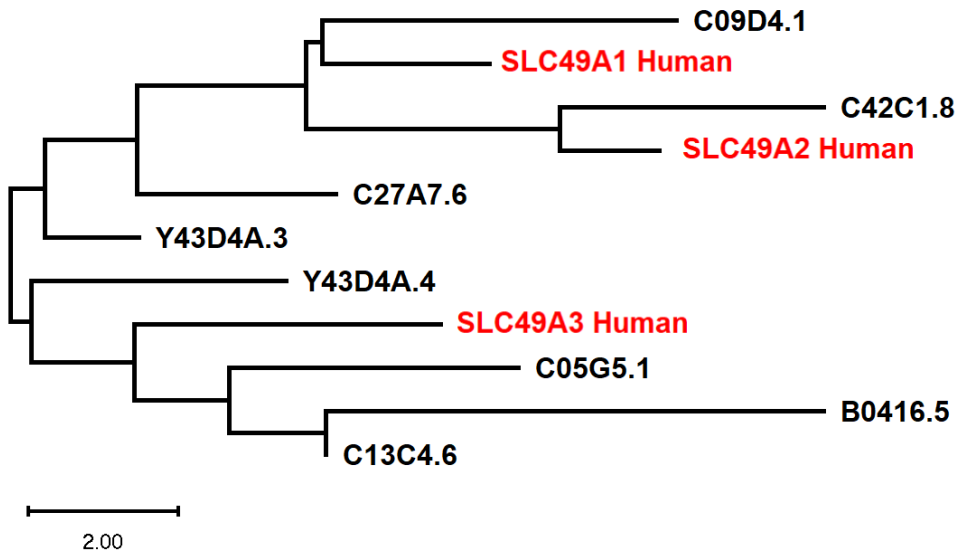

Figure 3.16. Phylogenetic analysis of SLC49A homologs in *C. elegans* and humans

Phylogenetic tree of the FLVCR family members in *C. elegans* and humans (red). Protein sequences were aligned using ClustalW and a phylogenetic tree was generated using the Neighbor-Joining method in MEGA. The tree is drawn to scale. The evolutionary distances are in the units of the number of amino acid substitutions per site.

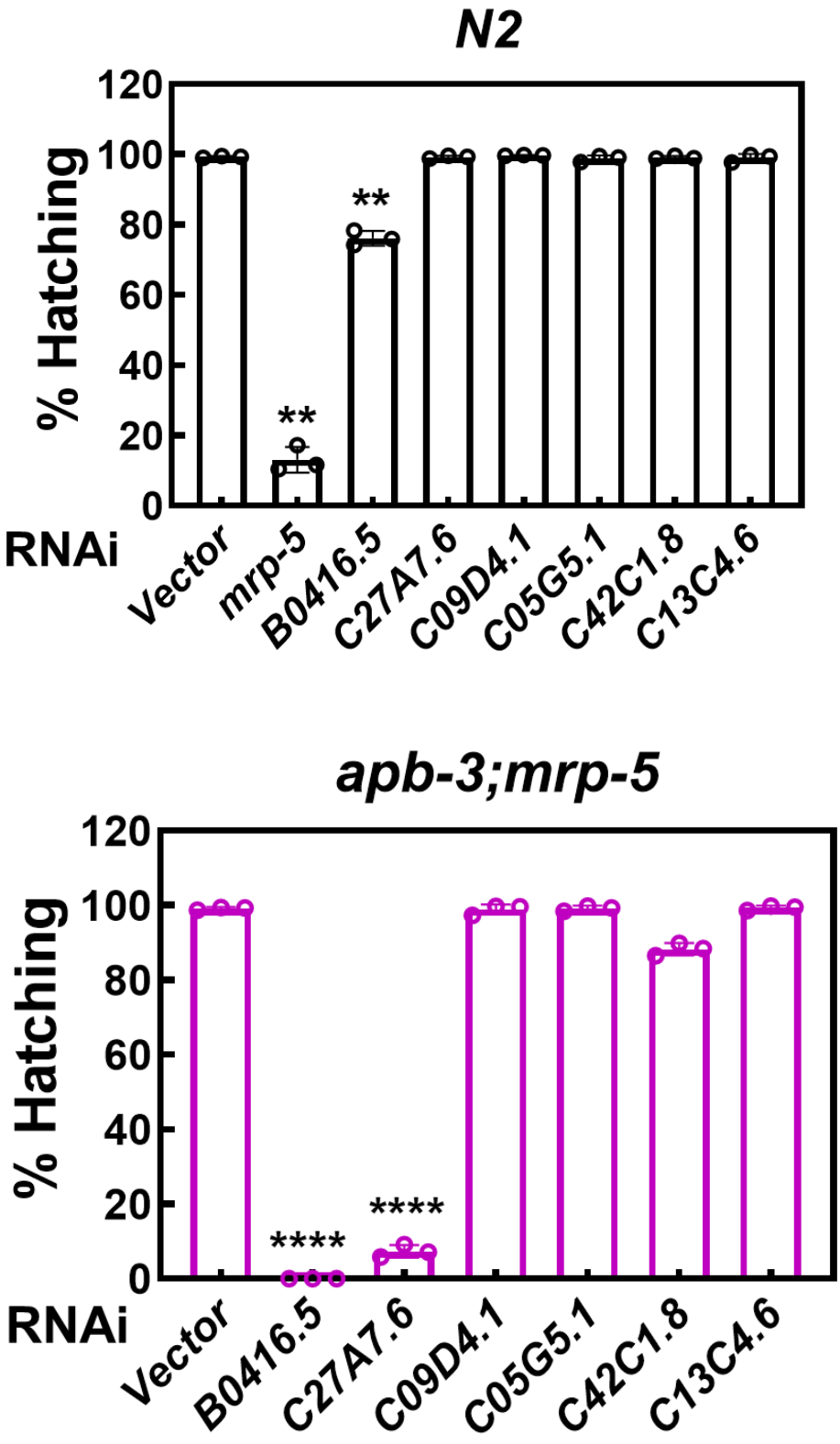
N2
% Hatching
120
100
80
60
40
20
0
**
**
RNAi
Vector
mrp-5
B0416.5
C27A7.6
C09D4.1
C05G5.1
C42C1.8
C13C4.6
apb-3;mrp-5
% Hatching
120
100
80
60
40
20
0
****
****
RNAi
Vector
B0416.5
C27A7.6
C09D4.1
C05G5.1
C42C1.8
C13C4.6

Figure 3.17. *B0416.5* and *C27A7.6* are essential in the suppressor strain.

Synchronized *N2* and *apb-3;mrp-5* worms were fed with dsRNA against each of the worm FLVCR homologs without any added heme on NGM plates. Once the P0 worms reached young adult stage, 5 worms were clonally picked and transferred to new RNAi plates, allowed to lay eggs for 24 h, and then removed. These worms were then transferred to new RNAi plates, and the eggs were scored for hatching after another 24 h. RNAi knockdown of *B0416.5* or *C27A7.6* is lethal in the suppressor strain, but not in wildtype worms.

A

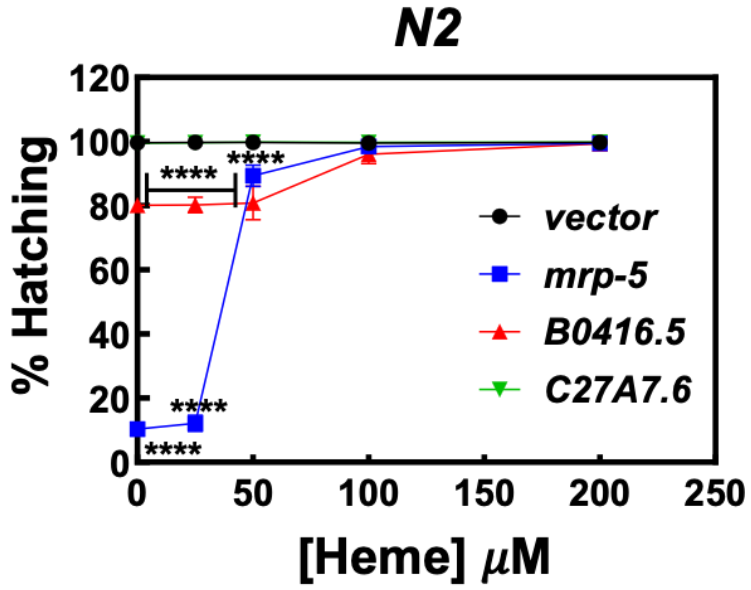
N2
% Hatching
[Heme] μM
vector
mrp-5
B0416.5
C27A7.6
****

B

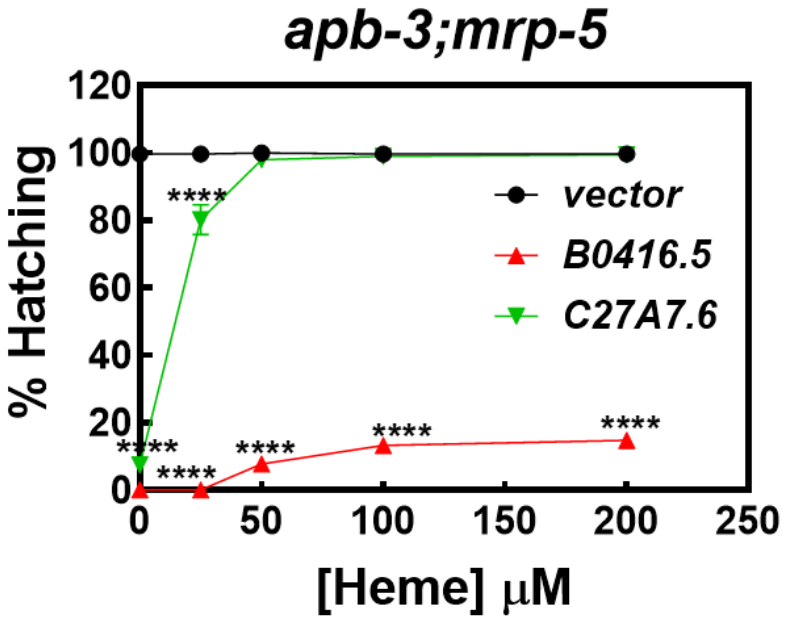
apb-3;mrp-5
% Hatching
[Heme] μM
vector
B0416.5
C27A7.6
****

C

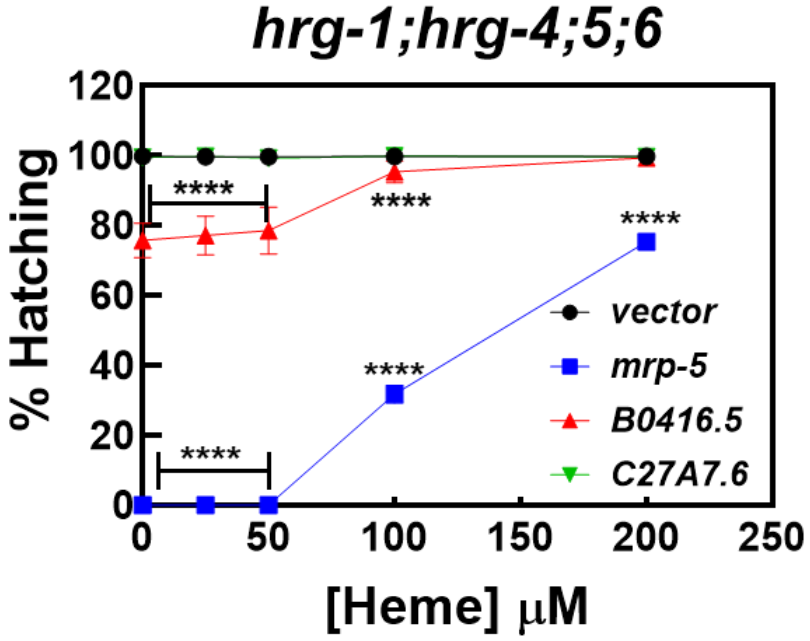
hrg-1;hrg-4;5;6
% Hatching
120
100
80
60
40
20
0
0
50
100
150
200
250
[Heme] μM
****
****
****
****
****
vector
mrp-5
B0416.5
C27A7.6

D

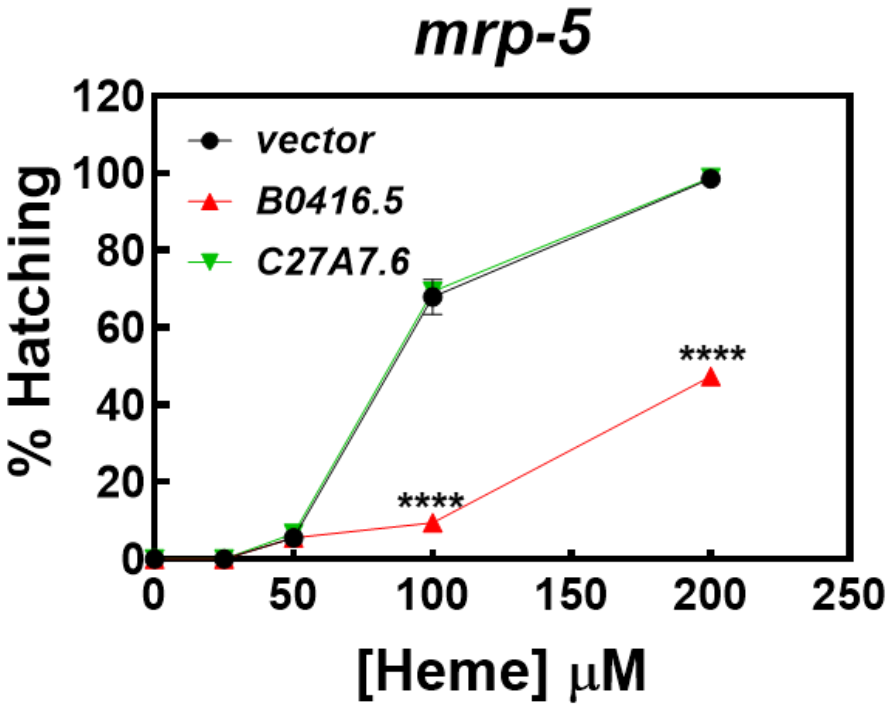
mrp-5
% Hatching
120
100
80
60
40
20
0
0
50
100
150
200
250
[Heme] μM
vector
B0416.5
C27A7.6
****
****

Figure 3.18. Heme dose response assays in different genetic backgrounds after RNAi depletion.

Synchronized worms were fed with dsRNA against each *vector, mrp-5, B0416.5* or *C27A7.6* supplemented with various heme concentrations on NGM plates. Once the P0 worms reached young adult stage, 5 worms were clonally picked and transferred to new RNAi plates, allowed to lay embryos for 24 h, and then removed. These worms were then transferred to new corresponding RNAi plates, and the embryos were scored for hatching after another 24 h.

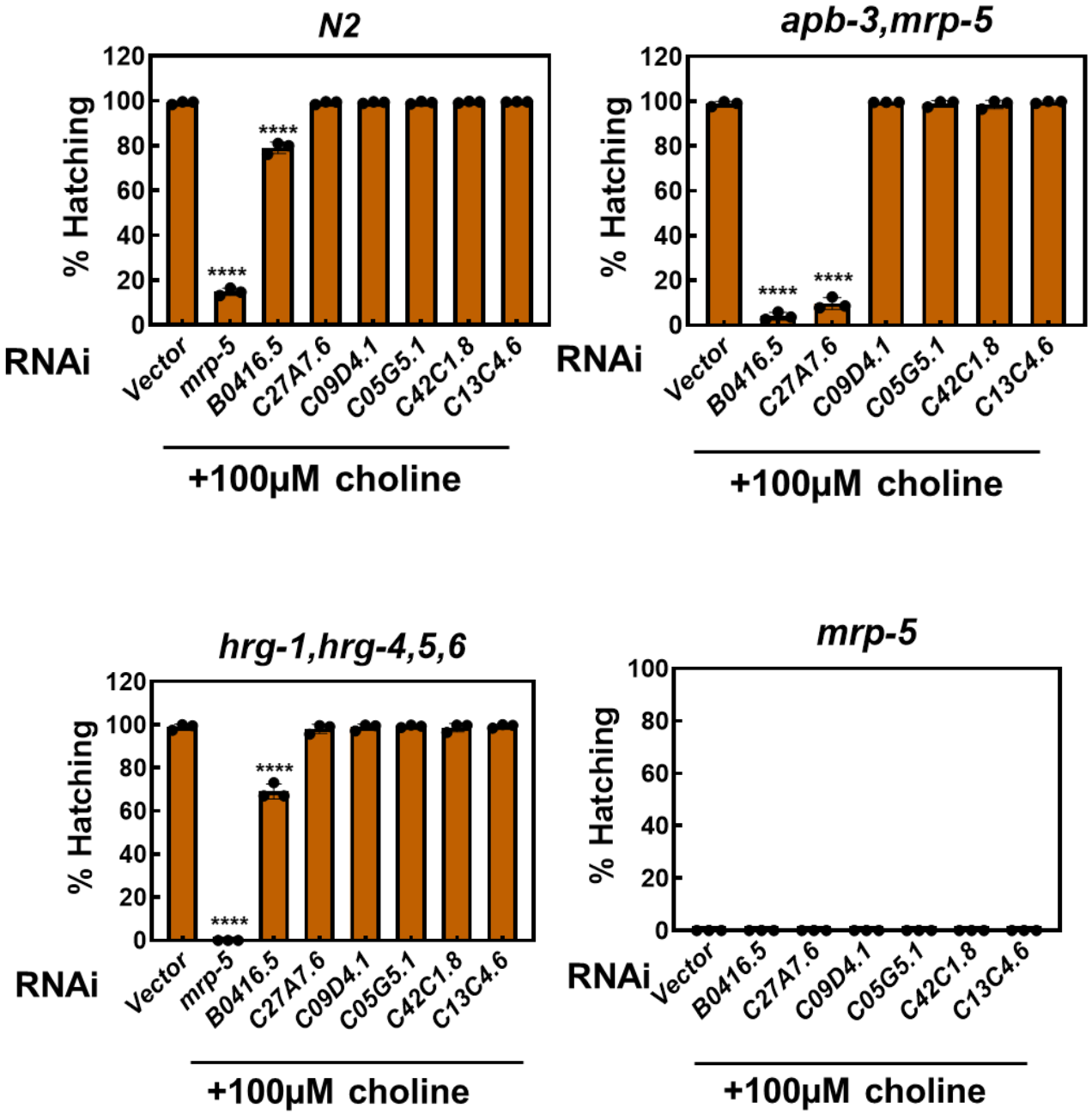
N2
% Hatching
120
100
80
60
40
20
0
****
****
RNAi
Vector
mrp-5
B0416.5
C27A7.6
C09D4.1
C05G5.1
C42C1.8
C13C4.6
+100µM choline
apb-3,mrp-5
% Hatching
****
****
RNAi
Vector
B0416.5
C27A7.6
C09D4.1
C05G5.1
C42C1.8
C13C4.6
+100µM choline
hrg-1,hrg-4,5,6
% Hatching
****
****
RNAi
Vector
mrp-5
B0416.5
C27A7.6
C09D4.1
C05G5.1
C42C1.8
C13C4.6
+100µM choline
mrp-5
% Hatching
100
80
60
40
20
0
RNAi
Vector
B0416.5
C27A7.6
C09D4.1
C05G5.1
C42C1.8
C13C4.6
+100µM choline

Figure 3.19. Choline supplementation does not rescue lethality caused by loss of *B0416.5* or *C27A7.6*.

Indicated worm strains were synchronized and fed with dsRNA against each of the worm SLC49A homologs in the presence of 100 μM supplemented choline chloride on NGM plates. Once the P0 worms reached young adult stage, 5 worms were clonally picked and transferred to new RNAi plates, allowed to lay embryos for 24 h, and then removed. These worms were then transferred to new RNAi plates, and the embryos were scored for hatching after another 24 h.

Tissue-specific expression of B0416.5 and C27A7.6

To determine the temporospatial location of the alternate heme transporters, we used CRISPR/Cas9 to generate transgenic strains in which GFP was integrated into the 3' end of the *B0416.5* or *C27A7.6* by homology directed repair. B0416.5::GFP *(IQH02)* localized to the basolateral and intracellular vesicular membrane compartments within the intestine, a pattern similar to that of MRP-5. In addition to the intestine, *B0416.5* was also expressed in the head, pharynx, embryo, oocyte, spermatogonia, and tail (Figure 3.20A). C27A7.6::GFP (*IQH01*) was largely restricted to the germline, primarily in the embryos and developing oocytes. Within the oocytes, C27A7.6 specifically localized to the plasma membrane as well as intracellular compartments (Figure 3.21A). RNAi knockdown of *B0416.5* and *C27A7.6* resulted in near complete loss of GFP; head and tail neurons were resistant to RNAi.

To delineate the mechanism underlying the functioning of these genes in the suppressor background, we performed RNAi knock down targeting either *apb-3*, *mrp-5*, or both. RNAi of *mrp-5* had no effect on B0416.5 protein localization and abundance, while *apb-3* depletion resulted in complete disappearance of B0416.5 from intracellular compartments. Co-depletion of *apb-3* and *mrp-5* partially restored the intracellular localization of B0416.5 to the LRO. We observed a larger and greater numbers of intracellular puncta containing C27A7.6::GFP in oocytes when *mrp-5* was depleted suggesting that *mrp-5* influences C27A7.6 trafficking or localization within the oocytes. Similarly, *apb-3*-targeted RNAi, also led to an increase in C27A7.6-positive puncta within oocytes. Notably, co-depletion of both *mrp-5* and *apb-3* resulted in even

larger vesicles in the oocytes (Figure 3.21B). These results indicate that the plasma membrane and vesicular localization of B0416.5 in the intestine and C27A7.6 in oocytes are altered in the suppressor and may influence their function(s) as a standby heme transporter (Figure 3.20B).

A


B0416.5::GFP
100µm

B

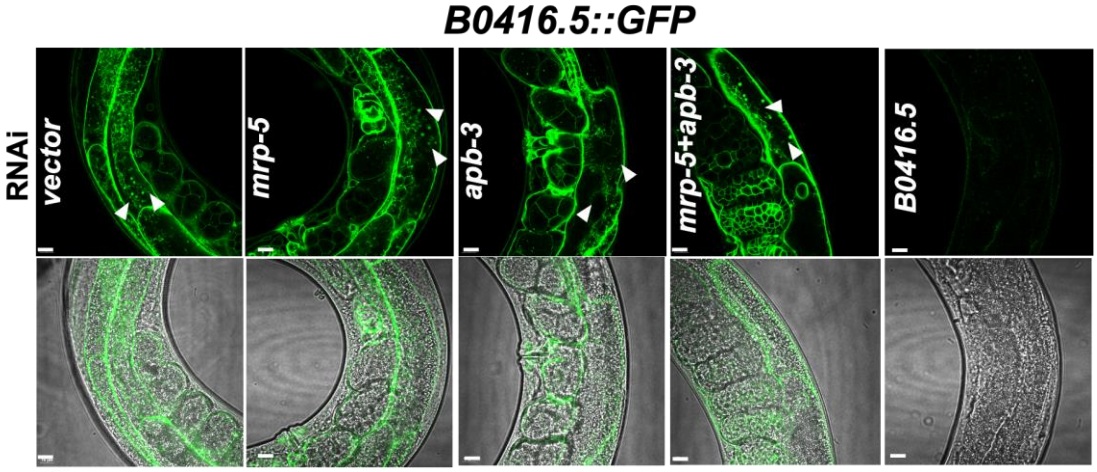
B0416.5::GFP
RNAi
vector
mrp-5
apb-3
mrp-5+apb-3
B0416.5

Figure 3.20. B0416.5 expression in *C. elegans.*

(A) Representative confocal image of a whole worm expressing *B0416.5::GFP*. B0416.5 is broadly expressed throughout the whole animal. Scale bar, 100 μm.

(B) Representative confocal images of intestine of *B0416.5::GFP* worms after being fed with the dsRNA to knock-down the indicated genes. White arrowheads represent the intracellular localization within the intestine. Scale bar, 10 μm.

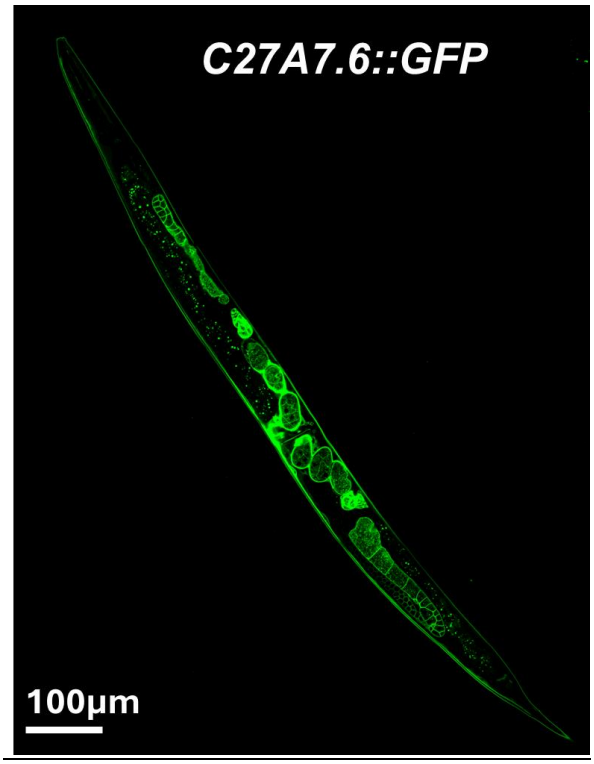
C27A7.6::GFP
100µm

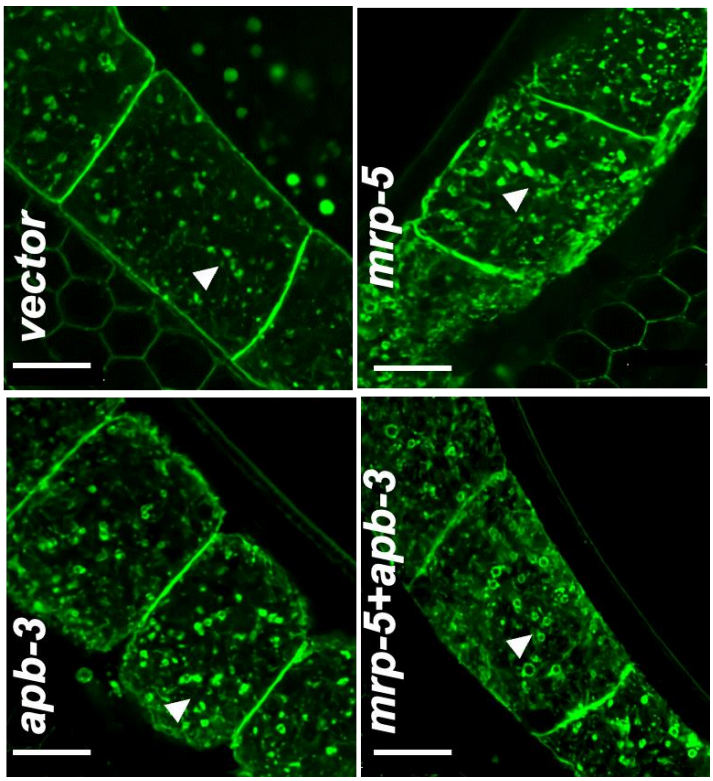
vector
mrp-5
apb-3
mrp-5+apb-3

Figure 3.21. C27A7.6 expression in *C. elegans*.

(A) Representative confocal image of a whole worm expressing *C27A7.6::GFP*. B0416.5 is primarily expressed within the germline, embryos, and spermatogonia. Scale bar, 100 μm.

(B) Representative confocal images of oocytes of *C27A7.6::GFP* worms after being fed with the dsRNA to knock-down the indicated genes. White arrowheads represent the intracellular localization within the intestine. Scale bar, 10 μm.

Chapter 4: Delineating the function of B0416.5 and C27A7.6

Summary

Genetic depletion of *mrp-5* and *ap-3* subunits increases systemic heme availability within the secretory pathway and engages two SLC49A homologs, *B0416.5* and *C27A7.6* as heme exporters. In mammalian cells, B0416.5 and C27A7.6 localize to the plasma membrane and LAMP1-positive compartments, mirroring their localization patterns in *C. elegans*. B0416.5 and C27A7.6 expression resulted in decreased total cellular heme and labile heme across intracellular compartments. Importantly, radioactive heme efflux assays confirmed that B0416.5 and C27A7.6 export heme. Live-cell imaging revealed that B0416.5 and C27A7.6 containing vesicles coalesce with HRG-1 and that cellular heme levels influenced their "kiss-and-run" interactions. These vesicular interactions represent a concerted mechanism for vesicular heme transfer between heme importers and exporters and establish an organismal model for heme homeostasis in metazoa.

Results

Expression and localization of B0416.5 and C27A7.6 in mammalian cells

To examine the cell biological role of *B0416.5* and *C27A7.6*, we tagged these transporters with HA and GFP at their C-terminus and expressed them in HEK293 cells. Immunoblotting of cell lysates transfected with these plasmids confirmed that both proteins were expressed at their predicted molecular weight (Figure 4.1). Confocal microscopy of HeLa cells transfected with *B0416.5* and *C27A7.6* revealed a dual localization pattern of plasma membrane, as they colocalized with wheat germ agglutin (WGA), as well as in intracellular LAMP1-positive compartments. This dual localization observed in mammalian cells mirrors the localization patterns observed in *C. elegans*. Since B0416.5 and C27A7.6 colocalize with LAMP1, a marker for late endosomes and lysosomes, where HRG-1 the heme importer is also known to reside, we further investigated their interaction with HRG-1 (Figures 4.2 and 4.3). Confocal microscopy revealed colocalization of both B0416.5 and C27A7.6 with *C. elegans* HRG-1 (CeHRG-1), suggesting that these heme transporters may functionally associate in these intracellular compartments.

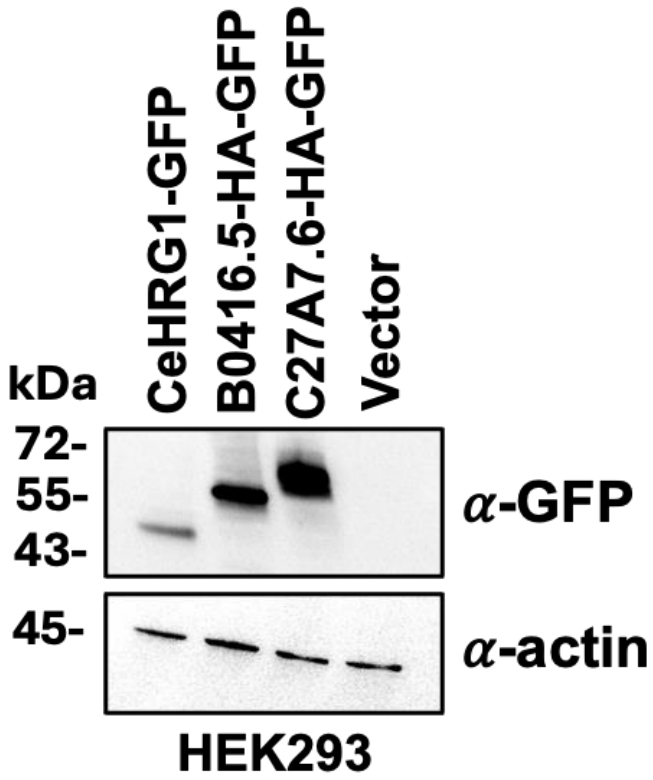

Figure 4.1. Western blot analysis of HEK293 cells expressing B0416.5 and C27A7.6 proteins.

HEK293 cells were transfected with plasmids encoding B0416.5, C27A7.6, and *C. elegans* HRG-1 (CeHRG1), all tagged with GFP at their C-terminus along with empty vector pcDNA3.1. Immunoblot analysis with anti-GFP antibody reveal cell lysates expressing the indicated proteins.

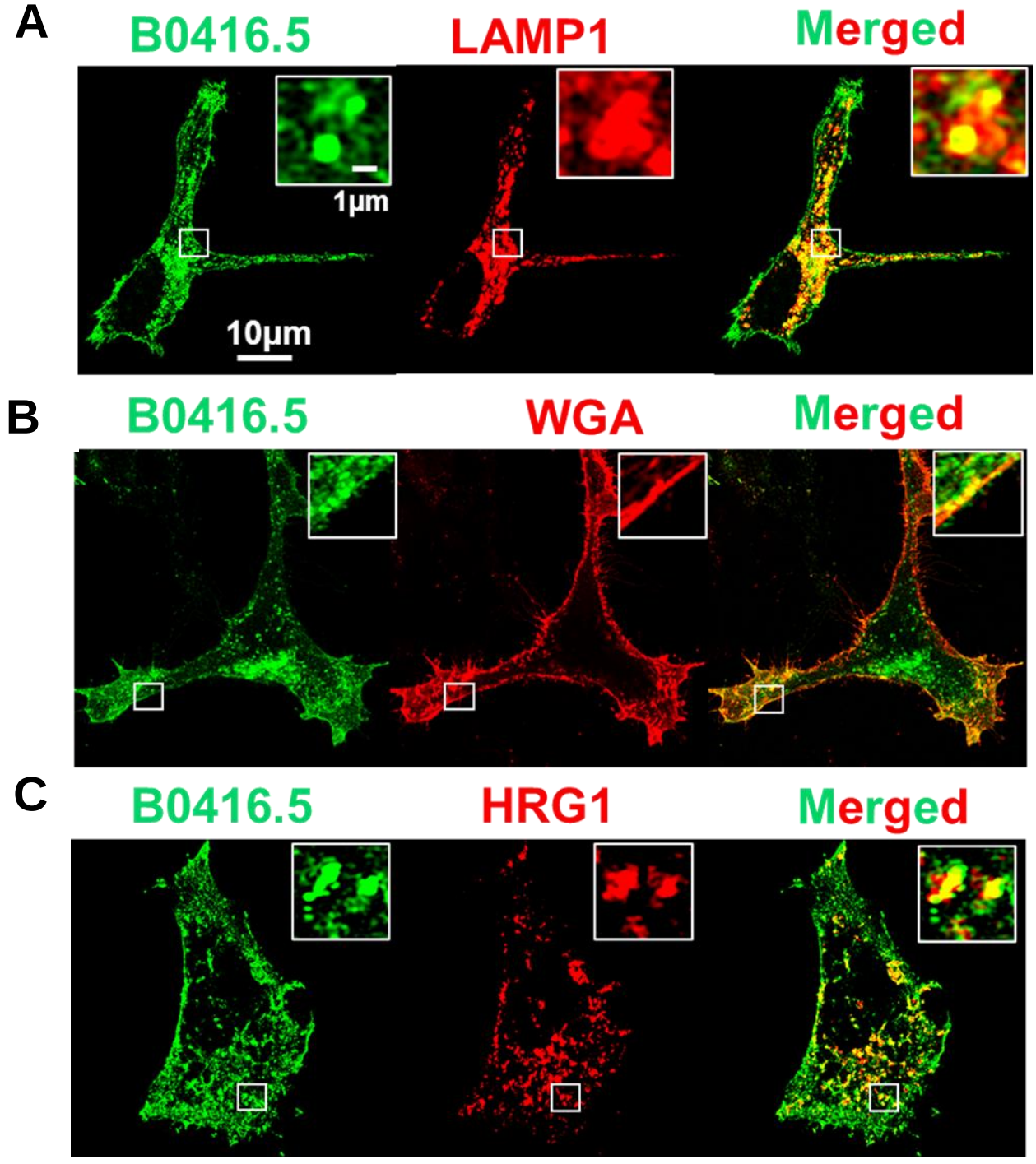
A
B0416.5
LAMP1
Merged
1μm
10μm
B
B0416.5
WGA
Merged
C
B0416.5
HRG1
Merged

Figure 4.2. B0416.5 localizes to the plasma membrane and endolysosomal compartments.

Confocal microscope images of HeLa cells transfected with B0416.5-HA-GFP. WGA is used as a plasma membrane marker (A) and Lamp1 (B) as late endosomal and lysosomal compartments. B0416.5 also colocalizes with the *C. elegans* heme importer HRG-1 (C). Scale bar, 10 μm. White boxes represent insets. Inset scale bar, 1 μm.

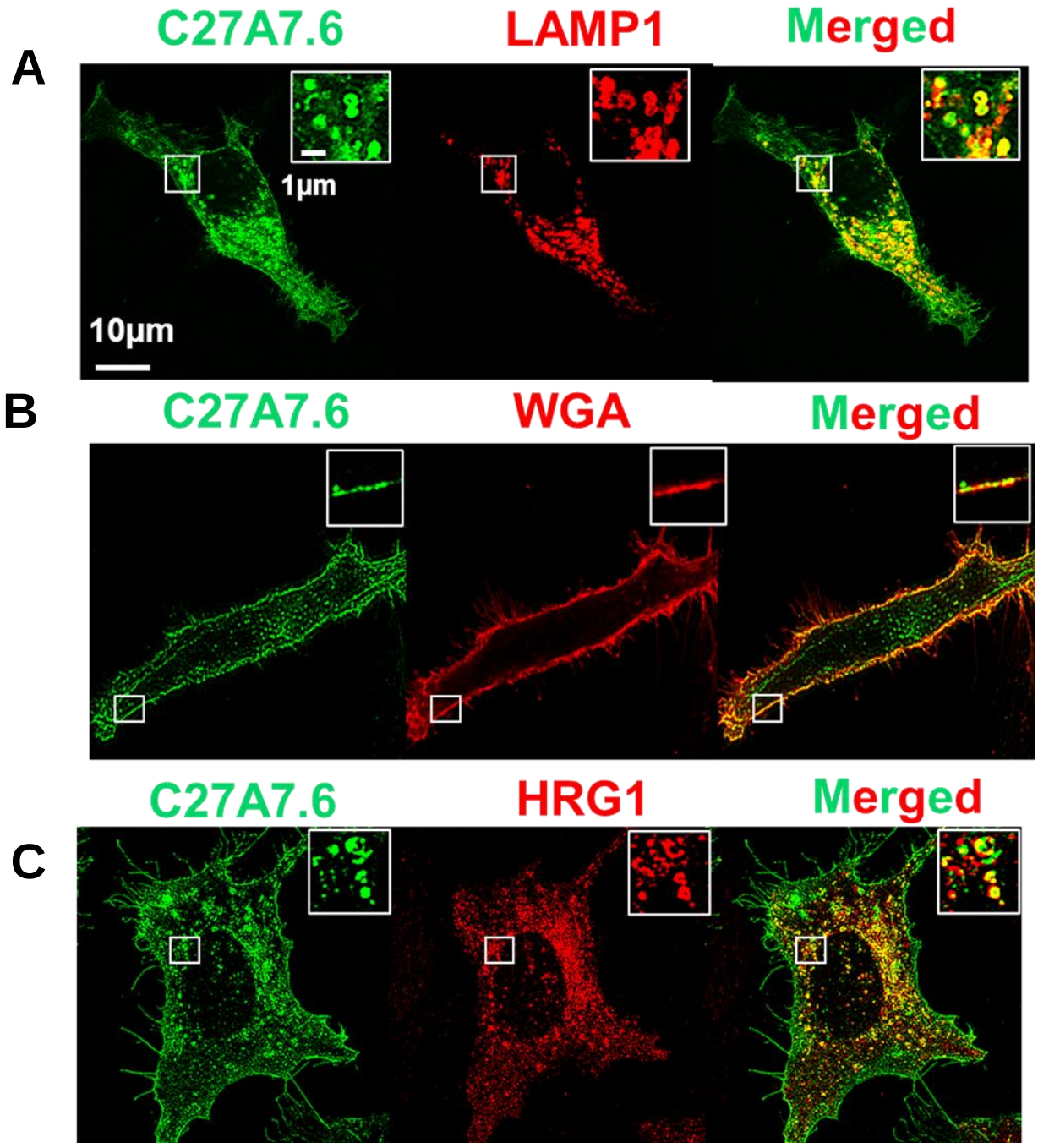
A
C27A7.6
LAMP1
Merged
1μm
10μm
B
C27A7.6
WGA
Merged
C
C27A7.6
HRG1
Merged

Figure 4.3. C27A7.6 localizes to the plasma membrane and endolysosomal compartments.

Confocal microscope images of HeLa cells transfected with C27A7.6-HA-GFP. WGA is used as a plasma membrane marker (A) and Lamp1 (B) as late endosomal and lysosomal compartments. C27A7.6 also colocalizes with the *C. elegans* heme importer HRG-1 (C). Scale bar, 10 μm. White boxes represent insets. Inset scale bar, 1 μm.

B0416.5 and C27A7.6 reduce overall heme content

To assess if B0416.5 and C27A7.6 could alter intracellular heme levels, we measured the total heme content within mammalian cells using the oxalic acid method. This assay relies on the chelation of Fe^{2+} from heme by oxalic acid leaving behind protoporphyrin IX, which can be measured by fluorescence spectroscopy. Thus, protoporphyrin IX fluorescence is a proxy for heme within the cell. To investigate the potential heme export function of a protein, we first needed to ensure sufficient heme import into cells. HEK293 cells were either singly transfected with the heme importer (CeHRG-1) or exporter (MRP-5, B0416.5 or C27A7.6), or both. Cells were depleted of their endogenous heme stores by addition of succinyl acetone (SA), an inhibitor of the second enzyme, ALAD, in the heme synthesis pathway followed by addition of 10 μM exogenous heme. HRG-1 transfected cells displayed a darker pellet color, while cells co-transfected with HRG-1 and exporters exhibited a lighter color. This color difference directly correlated with total heme content as only HRG-1 transfected cells showed the highest heme content compared to singly transfected cells. Cells co-transfected with HRG-1 plus a heme exporter showed significantly reduced total heme (Figure 4.4)

B

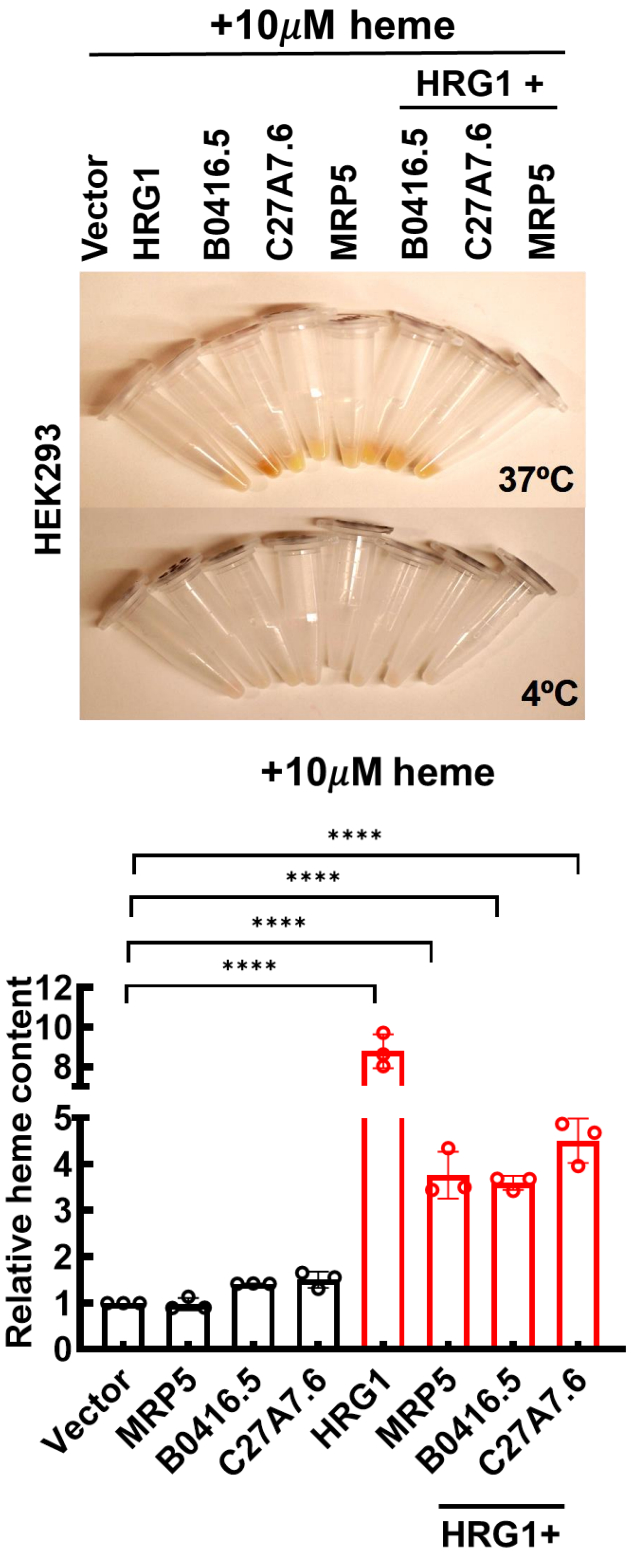
+10μM heme
HRG1 +
Vector
HRG1
B0416.5
C27A7.6
MRP5
B0416.5
C27A7.6
MRP5
HEK293
37ºC
4ºC
+10μM heme
****
****
****
****
Relative heme content
12
10
8
5
4
3
2
1
0
Vector
MRP5
B0416.5
C27A7.6
HRG1
MRP5
B0416.5
C27A7.6
HRG1+

Figure 4.4. Total heme content analysis reveals decreased heme with cells co-transfected with the heme importer HRG-1, and potential heme exporter candidates.

(A) Representative images of cell pellets. Images depict cell pellets from each transfected group. Compared to the darker pellet observed in the HRG-1 transfected cells, the pellets from co-transfected groups appear visibly paler, suggesting a potential decrease in intracellular heme content.

(B) Quantification of the total heme content, as measured by the oxalic acid method. All values have been normalized to the vector. Error bars represent mean ± SEM from three independent experiments. One-way ANOVA. **** $p<0.0001$.

We next examined the subcellular labile heme content using HRP and APX based reporter assays. HRP was engineered with a signal sequence to be targeted to the ER, while APX was targeted to either the mitochondria or cytosol. Both holo-HRP and holo-APX, require heme as a cofactor for their enzymatic activity. Thus, the activity of these reporter enzymes reflects the amount of labile heme present within each targeted organelle [18]. HEK293 cells transfected with the heme importer HRG-1 and exporters B0416.5 or C27A7.6 were then subjected to heme deprivation with SA followed by supplementation with 1 μM or 10 μM heme (Figure 4.5). As expected, under heme deprivation, no peroxidase reporter activity was detected in the ER, cytosol, and mitochondria. In low heme (1 μM) conditions, cells co-transfected with HRG-1 and heme exporters, displayed a lower reporter activity in the ER and cytosol compared to cells transfected with HRG-1 alone. This suggests that the presence of exporters either influences heme distribution or reduces its availability for these enzymes. However, at higher heme concentrations (10 μM), a more pronounced effect was observed; cells expressing HRG-1 and B0416.5 or C27A7.6 resulted in significantly lower reporter activity in the ER, cytosol, and mitochondria. These findings provide evidence that B0416.5 and C27A7.6 might function as heme exporters as these transporters influence labile heme levels within the cell causing an overall decrease.

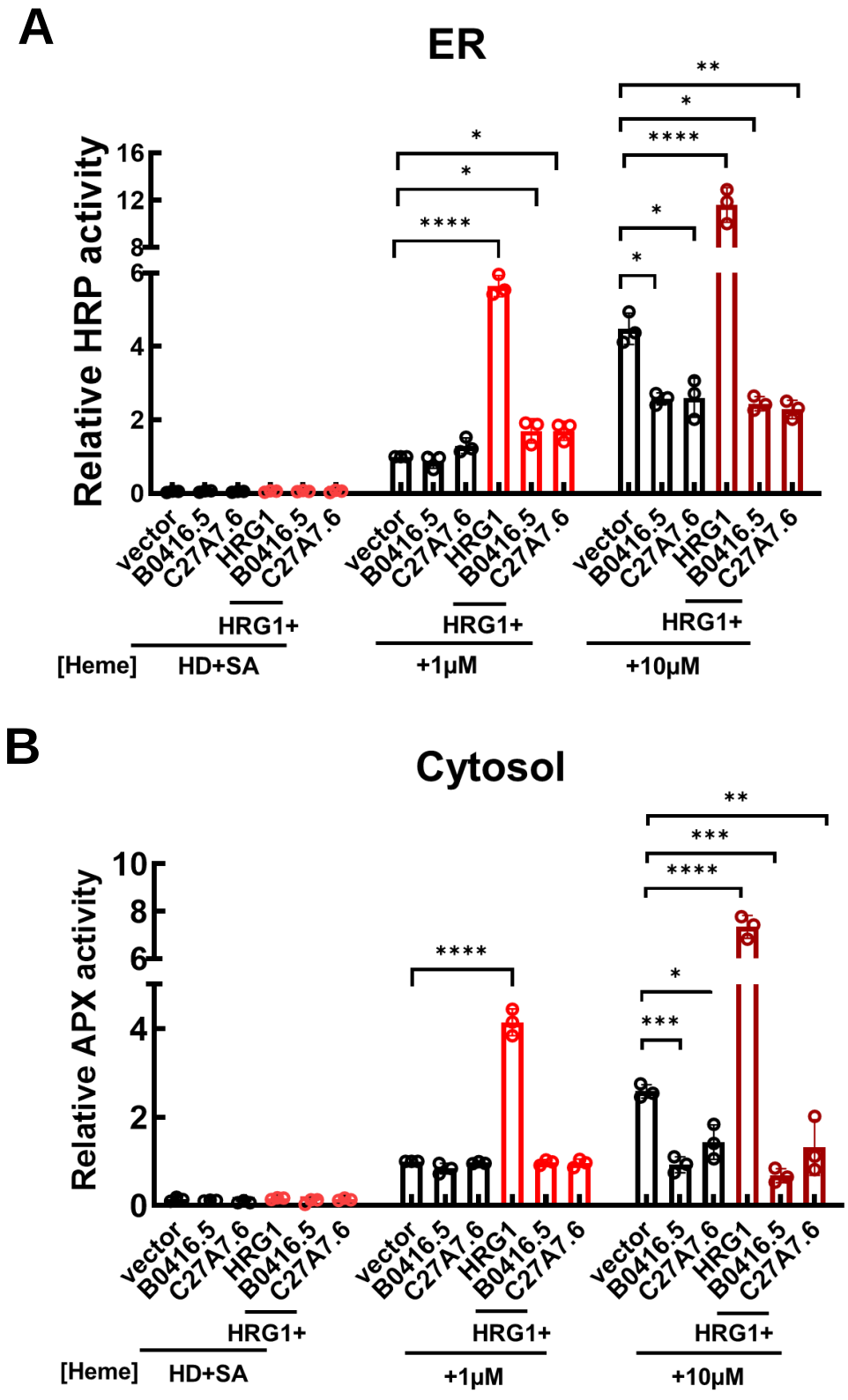
A
ER
Relative HRP activity
16
12
8
6
4
2
0
vector
B0416.5
C27A7.6
HRG1
B0416.5
C27A7.6
HRG1+
[Heme]
HD+SA
+1μM
+10μM
B
Cytosol
Relative APX activity
10
8
6
4
2
0

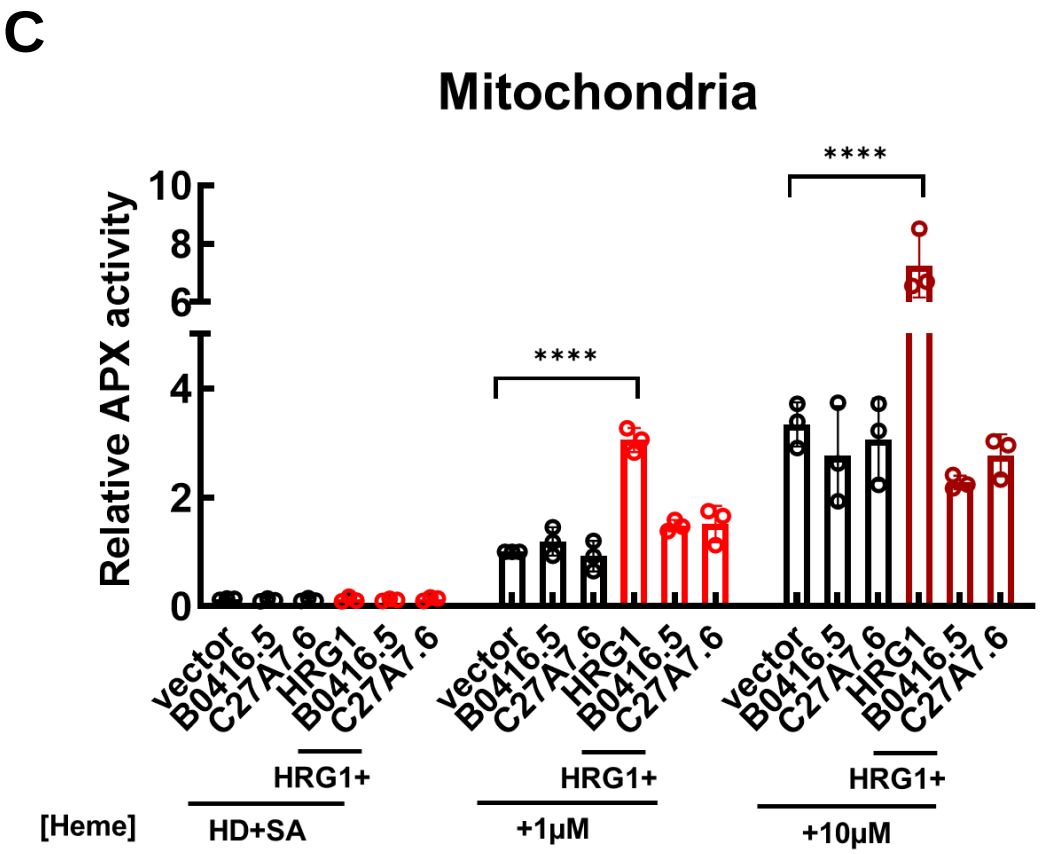

Figure 4.5. Heme-dependent enzymatic reporter assays demonstrate potential heme export by B0416.5 and C27A7.6, influencing overall labile heme levels within the cell.

HEK293 cells were transfected with ER-HRP (A), cytosol-APX (B) and mitochondria-APX (C), along with the indicated constructs, then grown for 24 h in heme-depleted plus succinyl acetone (HD+SA) for complete heme deprivation. Indicated amounts of heme were then added back and incubated for another 24 h. Cell lysates were harvested and analyzed for peroxidase activity, which was normalized to protein concentration of each sample, and then to the vector at 1 μM heme. Error bars represent mean ± SEM from three independent experiments. One-way ANOVA. *, $p<0.05$, **$p<0.01$, ***$p<0.001$, **** $p<0.0001$

Given that the APX reporter assay revealed the most prominent heme efflux in the cytosolic compartment, we decided to delve deeper into this finding. We further investigated the cytosolic APX activity across a broader range of heme concentrations, extending the analysis up to 50 μM heme. Across all tested heme concentrations (from 0 μM to 50 μM), cells co-transfected with the heme importer HRG-1 and the potential exporters B0416.5 or C27A7.6 displayed lower cytosolic APX activity compared to cells transfected with HRG-1 alone (Figure 4.6). This suggests an efflux of heme from the cytosol in the presence of the suspected exporters. However, the impact of the exporters on cytosolic heme levels is concentration dependent. Intriguingly, the activity of the co-transfected samples dropped below the vector only at heme concentrations 10 μM or higher. At higher concentrations (10 μM and above), the export activity by B0416.5 and C27A7.6 appeared to be more robust, leading to a significant decrease in cytosolic heme compared to not only HRG-1, but even vector alone. These results indicate that the exporters become more efficient in egressing heme when there is a larger pool of available heme within the cell.

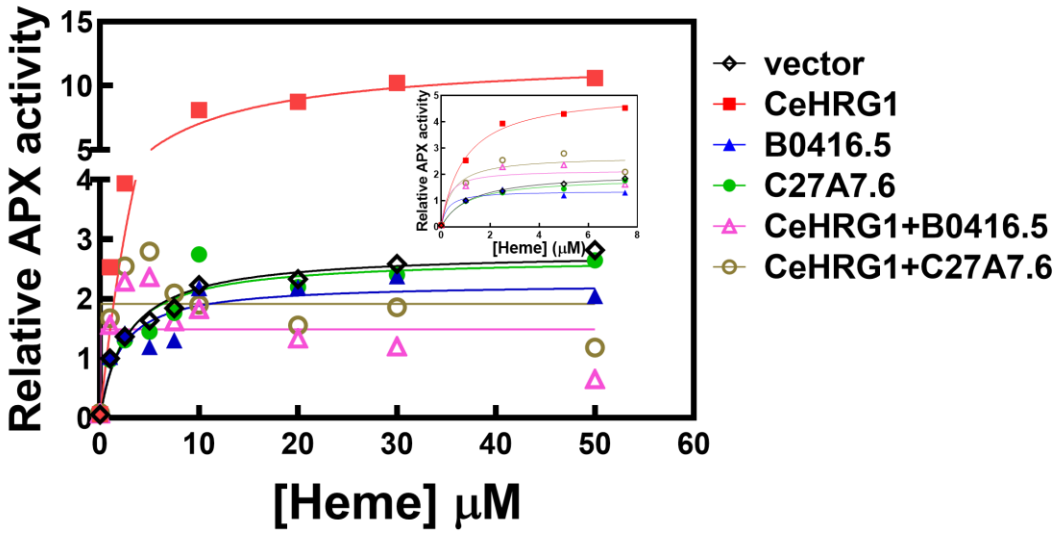

Figure 4.6. Heme dose response of cytosolic APX-based reporter assay.

HEK293 cells were transfected with cytosol-APX, along with the indicated constructs, then grown for 24 h in heme-depleted plus succinyl acetone (HD+SA) for complete heme deprivation. Indicated amounts of heme were then added back and incubated for another 24 h. Cell lysates were harvested and analyzed for peroxidase activity, which was normalized to protein concentration of each sample, and then to the vector at 1 μM heme. n=3. Error bars represent mean ± SEM from three independent experiments.

To ensure that the observed effects in the APX reporter assays stemmed solely from the ectopic CeHRG-1, we analyzed HRG1 abundance in HEK293 cells in response to heme as previous studies have shown that intracellular heme increases HRG1 in mammalian cells. Endogenous HRG1 remained unaltered across the different heme conditions in HEK293 cells (Figure 4.7). This result strengthens the conclusion that the effects observed in the APX assays were a direct consequence of the overexpressed HRG-1, and not due to the influence of endogenous HRG1.

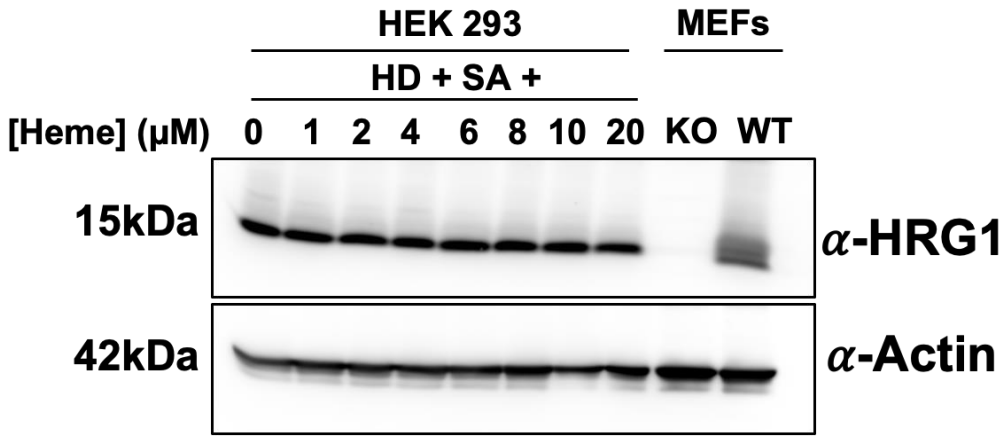

Figure 4.7. Endogenous HRG1 levels remain unchanged across different heme concentrations in HEK293 cells.

HEK293 cells treated with the indicated heme concentrations for 24 h, were lysed and subjected to immunoblotting with HRG1-specific antibody. Murine embryonic fibroblasts (MEFs) derived from wildtype (WT) and knockout (KO) mice were used as controls. As expected, HRG1 protein was absent in the HRG1 KO MEF lysate. In HEK293 cells, no changes in endogenous HRG1 protein levels were observed across different heme concentrations. α-actin served as a loading control.

B0416.5 and C27A7.6 act as *bona fide* heme exporters

To directly validate the heme export function of B0416.5 and C27A7.6, we employed radioactive [^{55}Fe]-heme, which offers a direct measure of export activity compared to the indirect assessment provided by reporter assays. To investigate heme export by B0416.5 and C27A7.6, we first established heme uptake parameters using 5 μM [^{55}Fe]-heme over 30 h in HEK293 cells transfected with CeHRG-1. This experiment revealed a significant and sustained heme uptake by cells expressing CeHRG-1 over the 30 h period. From this pilot experiment, we determined that 6 h of [^{55}Fe]-heme uptake with HRG-1 provided sufficient signal and efficient heme loading for subsequent heme export studies (Figure 4.8).

To assess heme export by B0416.5 and C27A7.6, we established [^{55}Fe]-heme efflux assays, which will allow quantification of [^{55}Fe]-heme released from cells after heme loading. We first conducted a series of six different transfections: empty vector control, transfected with either HRG-1, B0416.5 or C27A7.6, and co-transfected with HRG-1 plus B0416.5 or C27A7.6. To ensure a uniform level of intracellular heme, each condition was incubated with [^{55}Fe]-heme for 6 h, followed by a washout to remove any unbound heme, and then incubated with chase media devoid of additional heme for 24 h to monitor heme export. After the chase period, both cell lysates and culture media were collected and radioactivity in both fractions were measured using a liquid scintillation counter. Cells co-transfected with HRG-1 and either B0416.5 or C27A7.6 displayed a decrease in [^{55}Fe]-heme in the cell lysates with a concomitant increase in

radioactivity in the growth media. Cells supplemented with heme (10 μM, 20 μM, and 50 μM) showed a heme-dependent decrease of radiolabeled signal within cells and a corresponding increase in media. This suggests that the heme export function of B0416.5 and C27A7.6 is more prominent when a sufficient amount of intracellular heme pool is available. Overall, these findings provide direct evidence that both B0416.5 and C27A7.6 indeed function as heme exporters (Figure 4.9).

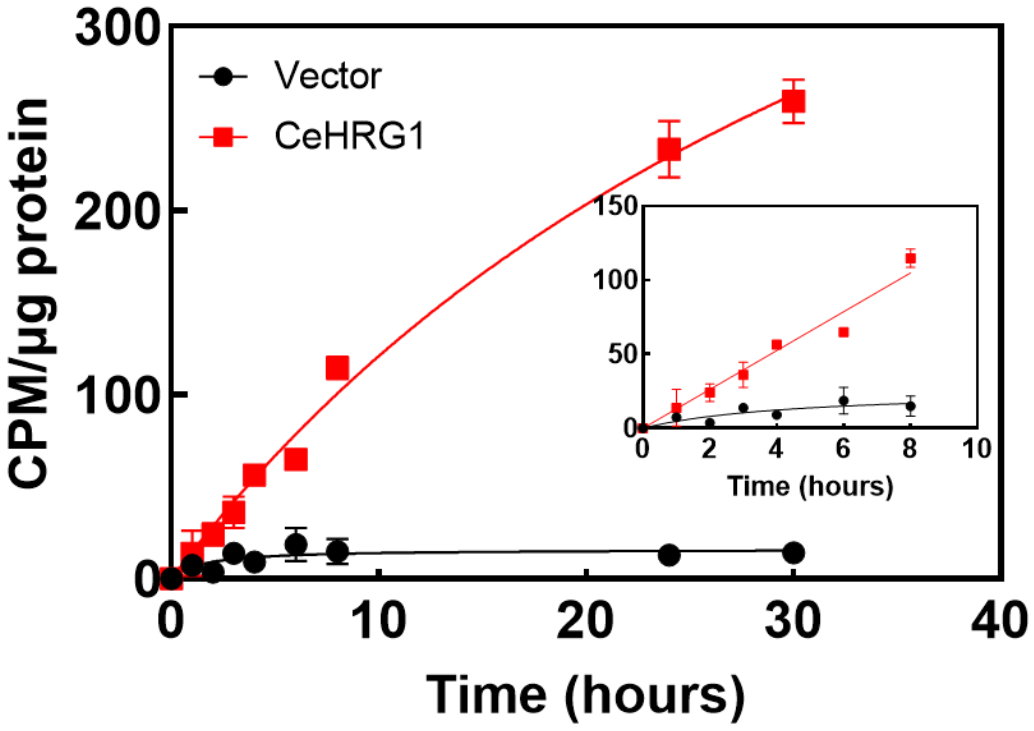

Figure 4.8. HRG-1 meditated heme uptake over time.

HEK293 cells transfected with empty vector or *C. elegans* HRG-1 (CeHRG1) and treated with 5 µM [^{55}Fe]-heme for 30 h. Cells were harvested and lysed at different time points, and the amount of radioactivity was measured as counts per minute (CPM), normalized to the protein concentration of each sample. Error bars represent mean ± SEM.

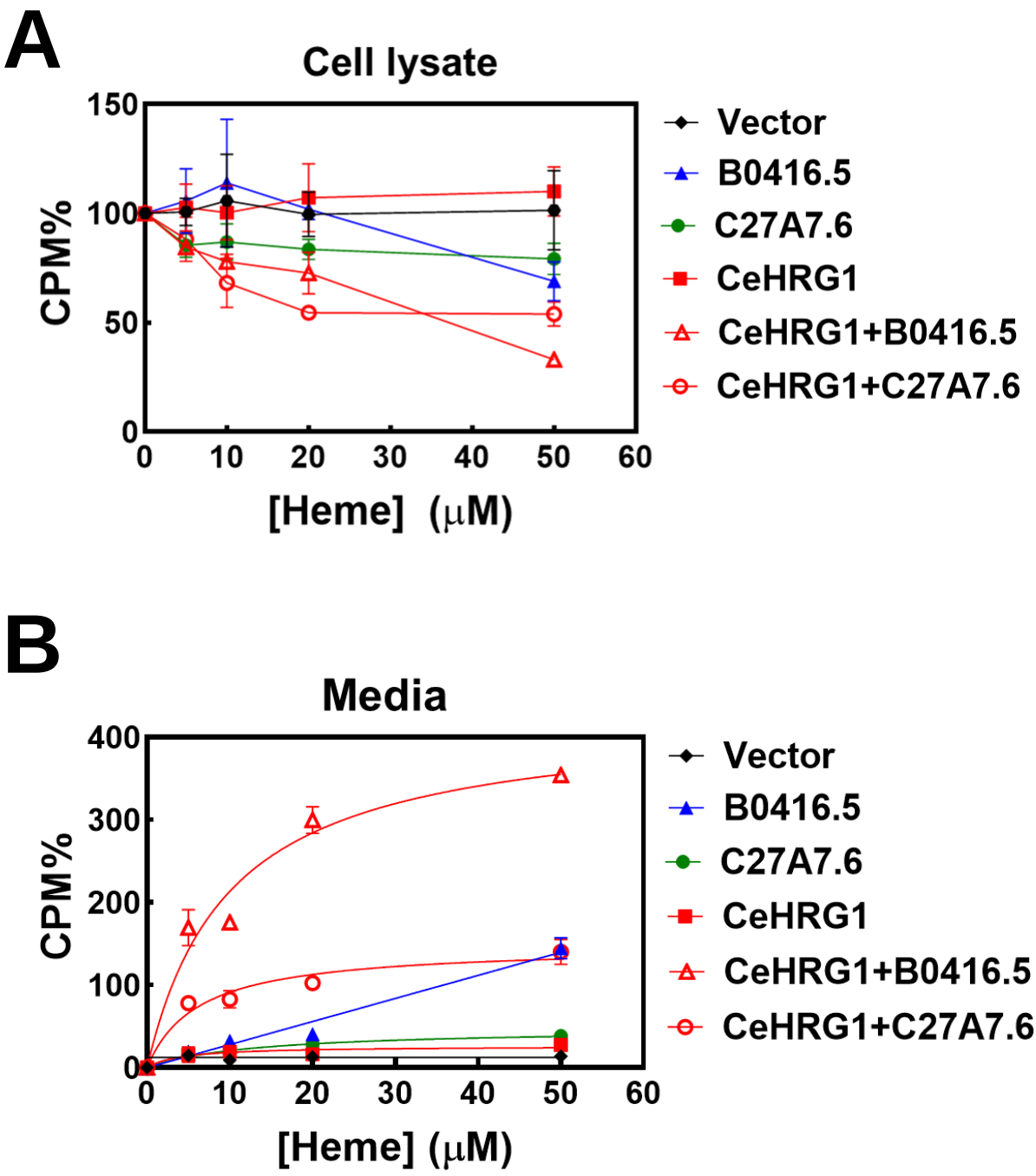
A
Cell lysate
150
100
50
0
CPM%
0
10
20
30
40
50
60
[Heme] (μM)
Vector
B0416.5
C27A7.6
CeHRG1
CeHRG1+B0416.5
CeHRG1+C27A7.6
B
Media
400
300
200
100
0
CPM%
0
10
20
30
40
50
60
[Heme] (μM)
Vector
B0416.5
C27A7.6
CeHRG1
CeHRG1+B0416.5
CeHRG1+C27A7.6

Figure 4.9. B0416.5 and C27A7.6 function as heme exporters.

HEK293 cells were transfected with the indicated constructs and loaded with different concentrations of [^{55}Fe]-heme for 6 h. Following a wash step, cells were incubated with a heme-free media for another 24 h, after which radioactivity was measured in both the cell lysates and the culture media. Compared to the empty vector or HRG1 alone, co-transfection with HRG1 and either B0416.5 or C27A7.6 showed a decrease in cell lysate radioactivity, and a corresponding increase in media radioactivity, indicating heme export. Error bars represent mean ± SEM.

Heme export function of B0416.5 and C27A7.6 is not affected by choline

Recent studies have shown that human FLVCR1/SLC49A1 and FLVCR2/SLC49A2 are choline importers [59-63]. To explore whether the *C. elegans* homologs B0416.5 and C27A7.6 might also function in choline transport, we utilized the cytosolic APX assay. This assay yielded the most significant reduction in heme levels within the cytosol when cells expressed B0416.5 or C27A7.6 plus HRG-1. We measured the APX activity under various heme (1 μM, 10 μM, 30 μM), choline (1 μM, 10 μM, 30 μM), and a combination of heme and choline. Notably, the presence of choline regardless of the concentration or its combination with heme, did not exert any significant influence on the cytosolic APX activity. These observations suggest that the B0416.5 or C27A7.6 are unlikely to import choline and that choline does not impact their heme export function (Figure 4.10).

A

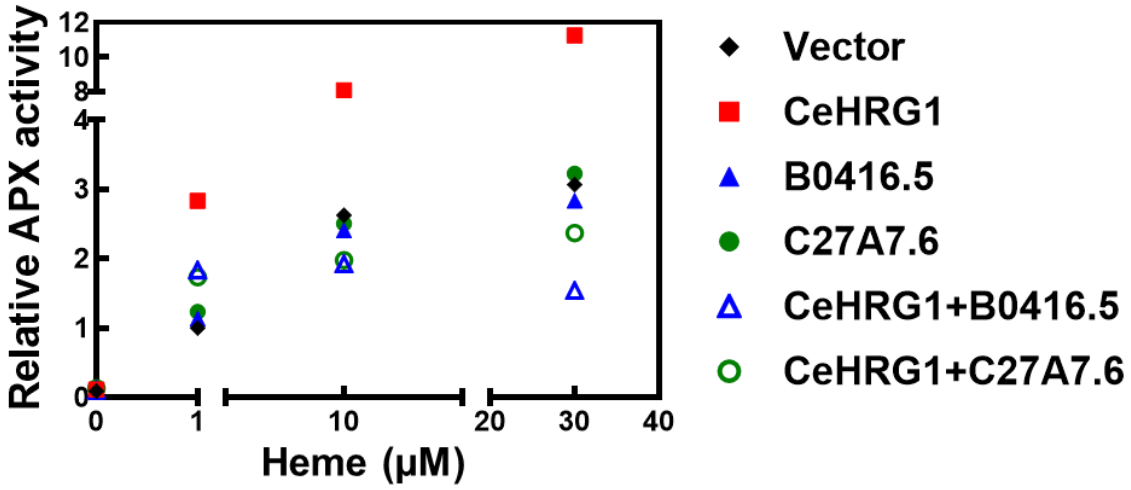
Relative APX activity
12
10
8
4
3
2
1
0
0
1
10
20
30
40
Heme (μM)
Vector
CeHRG1
B0416.5
C27A7.6
CeHRG1+B0416.5
CeHRG1+C27A7.6

B

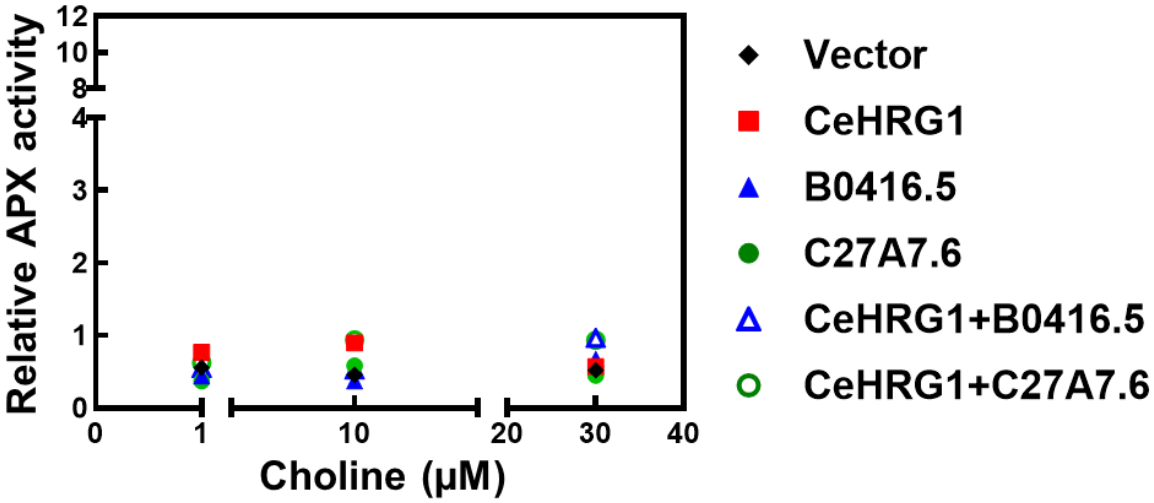
Relative APX activity
12
10
8
4
3
2
1
0
0
1
10
20
30
40
Choline (μM)
Vector
CeHRG1
B0416.5
C27A7.6
CeHRG1+B0416.5
CeHRG1+C27A7.6

C

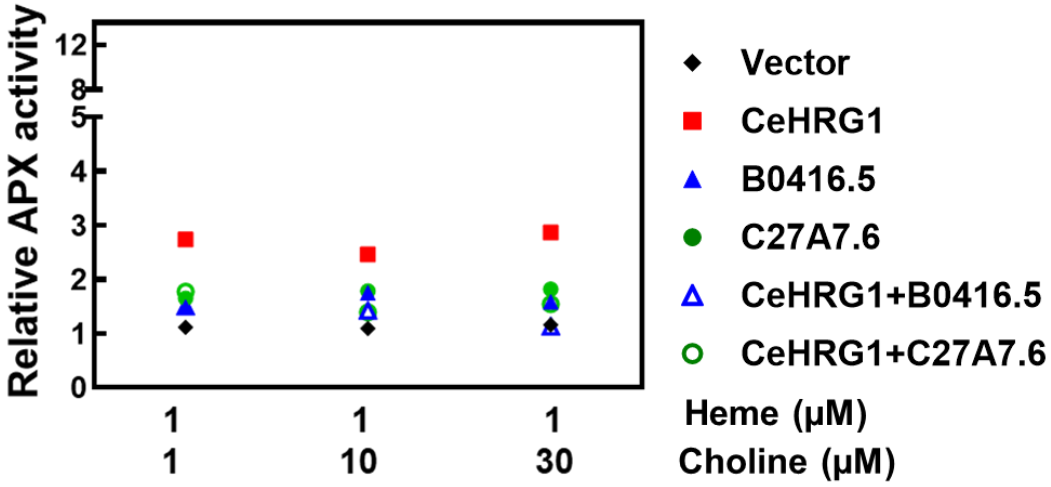
Relative APX activity
12
8
5
4
3
2
1
0
1
1
1
10
1
30
Heme (μM)
Choline (μM)
Vector
CeHRG1
B0416.5
C27A7.6
CeHRG1+B0416.5
CeHRG1+C27A7.6

D

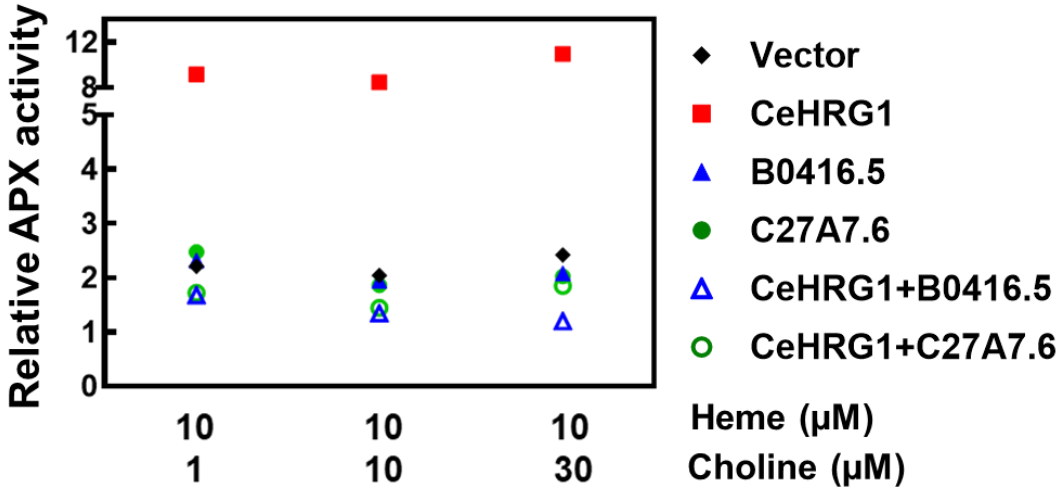
Relative APX activity
12
8
5
4
3
2
1
0
10
1
10
10
10
30
Heme (μM)
Choline (μM)
Vector
CeHRG1
B0416.5
C27A7.6
CeHRG1+B0416.5
CeHRG1+C27A7.6

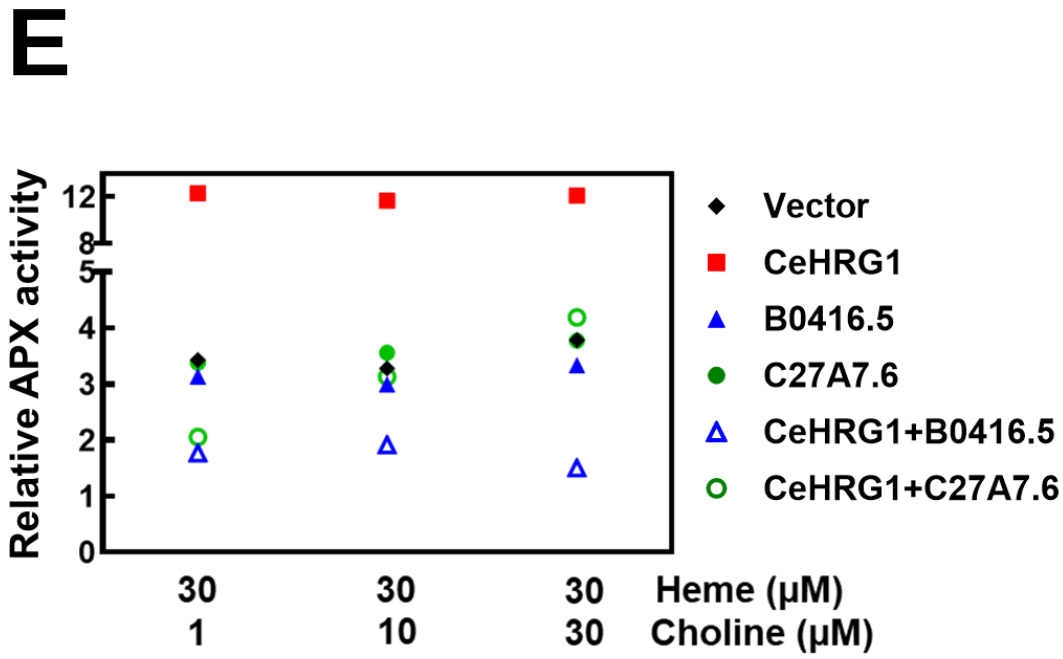

Figure 4.10. Heme export function of *C. elegans* homologs B0416.5 and C27A7.6 is not influenced by choline.

HEK293 cells were transfected with cytosolic APX along with the indicated constructs and exposed to various treatments: heme only (A), choline only (B) , or a combination of heme and choline, as illustrated (C-E). Cells were harvested and lysed and the APX activity measured was normalized to the protein concentration of each sample.

Coalescence between import and export vesicles facilitates heme transfer

To gain further insight into the interplay between heme import and export, we monitored the real-time dynamics of CeHRG-1-mCherry co-expressed with either B0416.5-GFP or C27A7.6-GFP in HeLa cells using live-cell microscopy. Spinning disc confocal imaging revealed frequent occurrence of "kiss-and-run" events between the HRG-1 and B0416.5 or C27A7.6 containing vesicles (Figure 4.11). Under complete heme deprivation, the duration of these vesicle fusions was significant shorter (< 1 sec), compared to cells supplemented with 50 μM heme, where they remained coalesced for around 20 sec. These transient interactions, characterized by brief fusion between the vesicles, suggest a potential mechanism for direct heme transfer between import and export compartments.

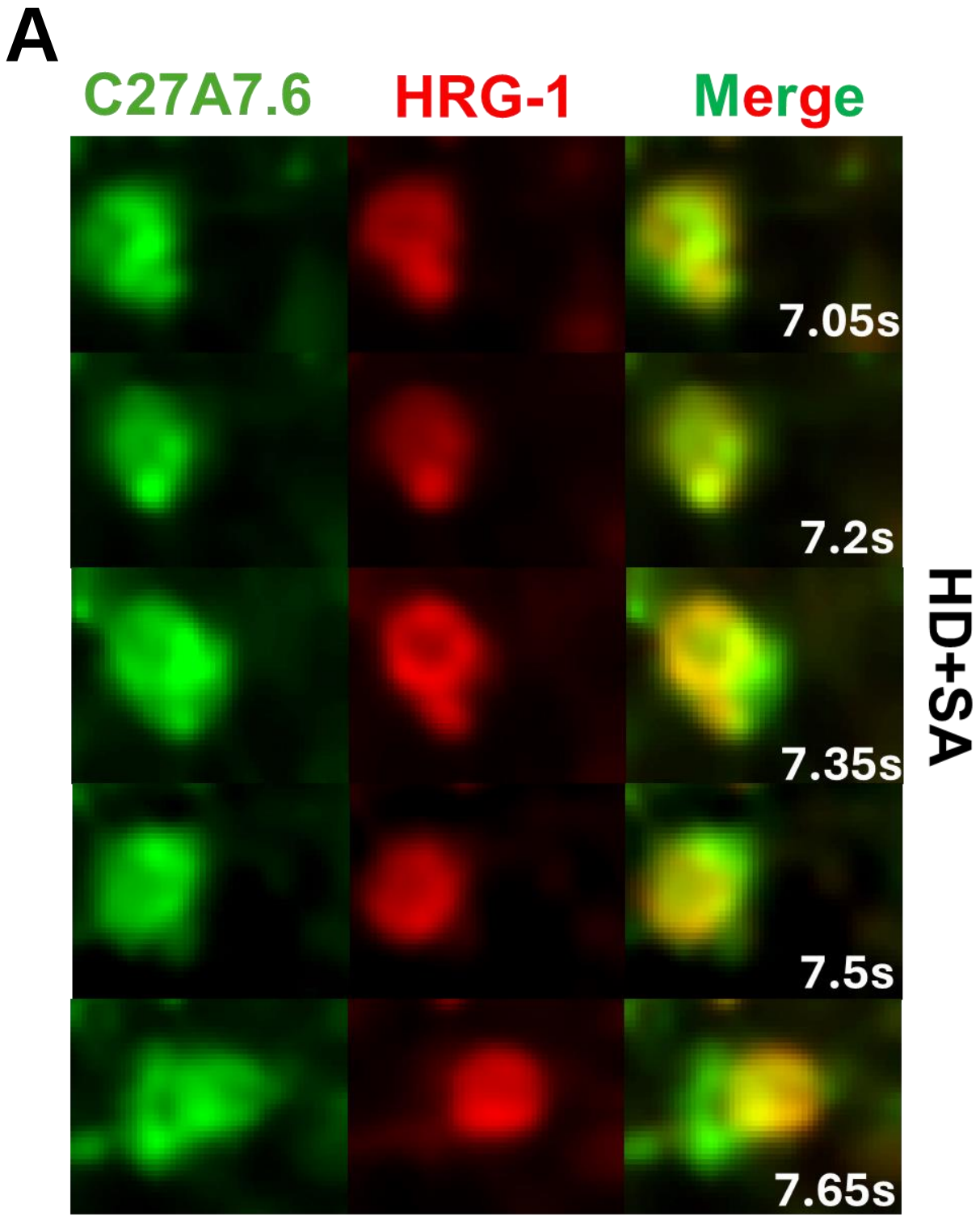
A
C27A7.6
HRG-1
Merge
7.05s
7.2s
7.35s
7.5s
7.65s
HD+SA

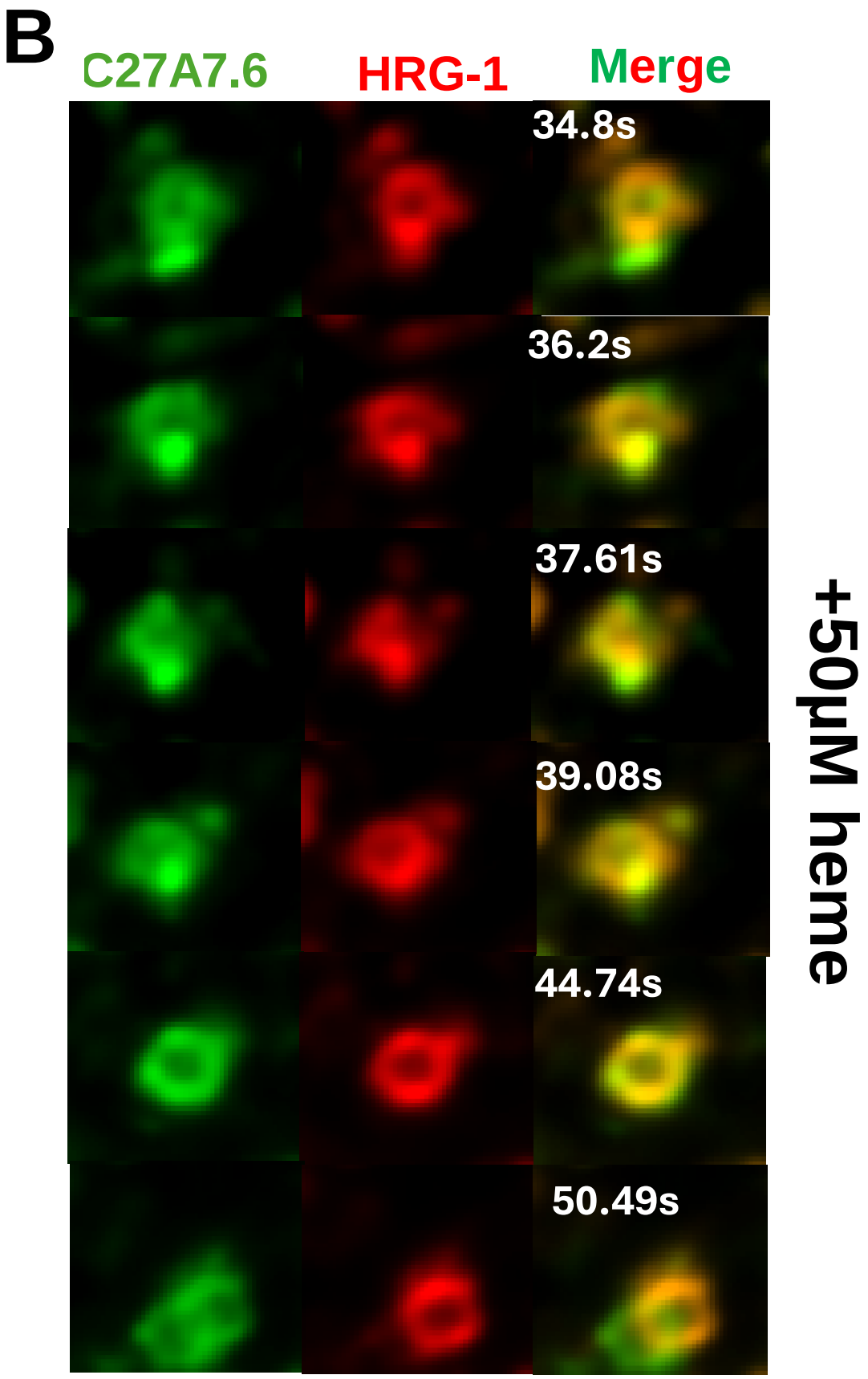
B
C27A7.6
HRG-1
Merge
34.8s
36.2s
37.61s
39.08s
44.74s
50.49s
+50uM heme

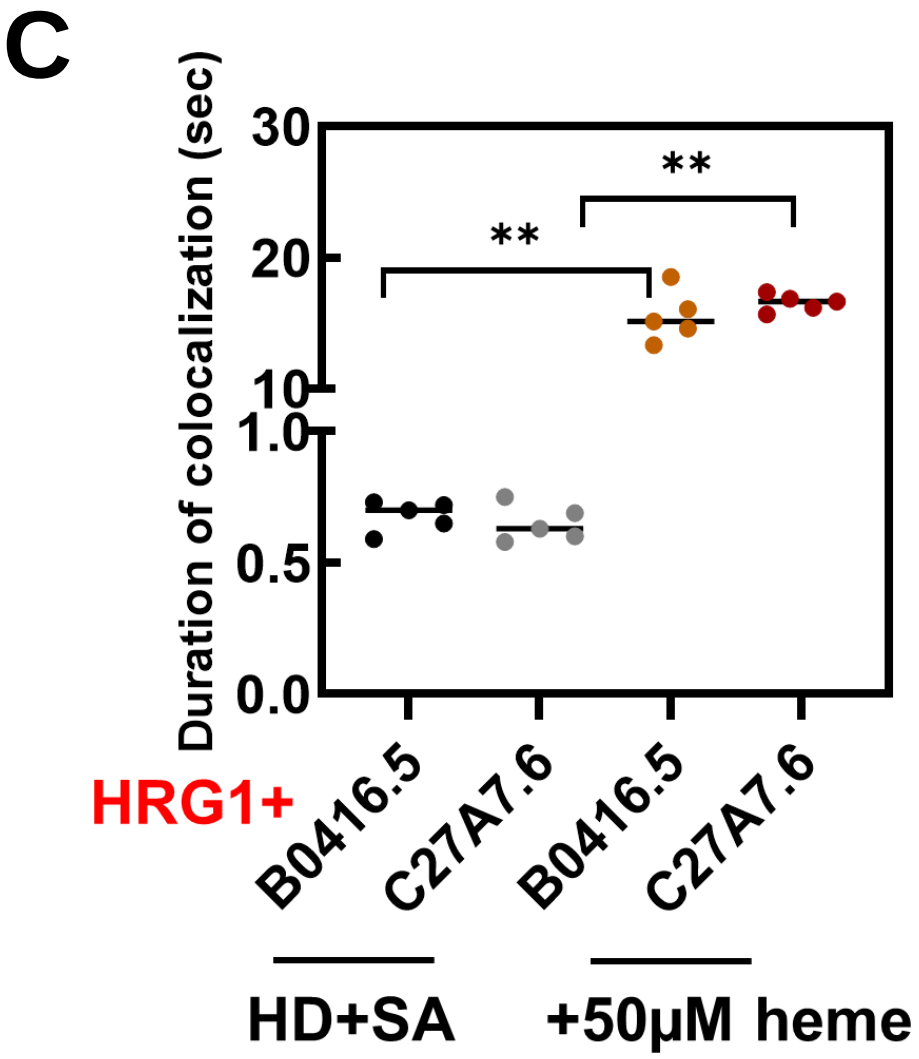

Figure 4.11. Live-cell imaging reveals heme availability-dependent "kiss-and-run" interactions between heme importer and exporter vesicles.

HeLa cells were co-transfected with HRG-1-mCherry (heme importer) and C27A7.6-HA-GFP (heme exporter). Live cell imaging using spinning disc microscope was performed to visualize interactions between these vesicles under different heme conditions:

(A) Under complete heme deprivation (HD) in the presence of succinylacetone (SA), HRG-1 (red) and C27A7.6 (green) vesicles exhibit brief transient interactions (less than one second).

(B) When supplemented with 50 μM heme, the same vesicles show a more prolonged association, remaining fused for almost 15 sec.

(C) Quantification of the duration of coalescence between heme importer (HRG-1) and exporter vesicles under heme depleted and heme supplemented conditions. Each dot represents five vesicles within the same cell.

Chapter 5: Discussion

Proposed model for interplay between heme import, storage, and export

Iron deficiency is the most common nutritional disorder globally, affecting both developing and developed nations, with 30 % of the world's population being iron-deficient [72,73]. While dietary factors such as acidic pH of the stomach and metal-chelating compounds in food can hinder iron absorption, heme-iron offers a more readily absorbed source of iron. However, heme being a multifaceted molecule is hydrophobic and cytotoxic while being essential in diverse biological processes. Hence its levels need to be tightly regulated to maintain systemic heme homeostasis. Understanding heme transport and trafficking is vital from both a nutritional and cellular perspective. By uncovering the mechanisms governing heme transport, we can gain valuable insights into potential strategies for addressing this widespread health concern.

In the current study, our forward genetic screen conducted on *mrp-5* null mutants unraveled a novel heme trafficking pathway mediated by cargo sorting AP-3 complexes as well as previously unknown heme exporters that share homology with human SLC49A3. Loss of the intestinal heme exporter *mrp-5* shows embryonic lethality which can be rescued by heme supplementation, suggesting the existence of alternate heme export pathways. To uncover these alternate heme export pathways, we conducted a forward genetic screen using *mrp-5* null mutants and identified LOF mutations of AP-

3 subunits that can completely bypass the *mrp-5* deficiency. We propose the following model for this suppression. In WT worms after heme is imported via the apical membrane of the intestine, it can either be stored and/or exported. Storage occurs within LROs, where the heme importer HRG-1 imports heme from these subcellular compartments into the cytosol. Heme export is mediated by MRP-5, which is primarily present on the basolateral membrane of the intestine (or plasma membrane of a non-polarized cell), thus ensuring adequate heme supply to the extra intestinal tissues. This helps maintain systemic heme homeostasis, and hence viability of the organism (Figure 5.1A). In the absence of *mrp-5*, the heme export pathway is impaired, resulting in more heme accumulation within the cell, specifically within the LRO, which in turn targets the heme importer HRG-1 for degradation. In the context of *C. elegans*, *mrp-5* deficiency results in heme trapped within the intestine resulting in heme deprivation in the extra-intestinal tissues, ultimately leading to embryonic lethality (Figure 5.1B). Interestingly, loss of AP-3 subunits disrupts the heme storage pathway since AP-3 is involved in formation of the LROs. This in turn leads to HRG-1 localizing to intermediate pre-LRO compartments, instead of the LROs (Figure 5.1C). However, in the absence of both AP-3 and *mrp-5*, the HRG-1 levels and localization are partially restored in the late endocytic compartments as SLC49A3 homologs facilitate heme export from the intestines. Based on their localization in *C. elegans*, B0416.5 mediates heme export from the intestine and C27A7.6 mediates maternal heme export to the developing oocytes owing to its localization in the germline (Figure 5.1C). Overall, this study sheds light on a previously unknown pathway for heme trafficking in *C. elegans*

and provides insights into how heme transporters work synergistically with adaptor proteins to maintain a fine balance between heme import, storage, and export.

A

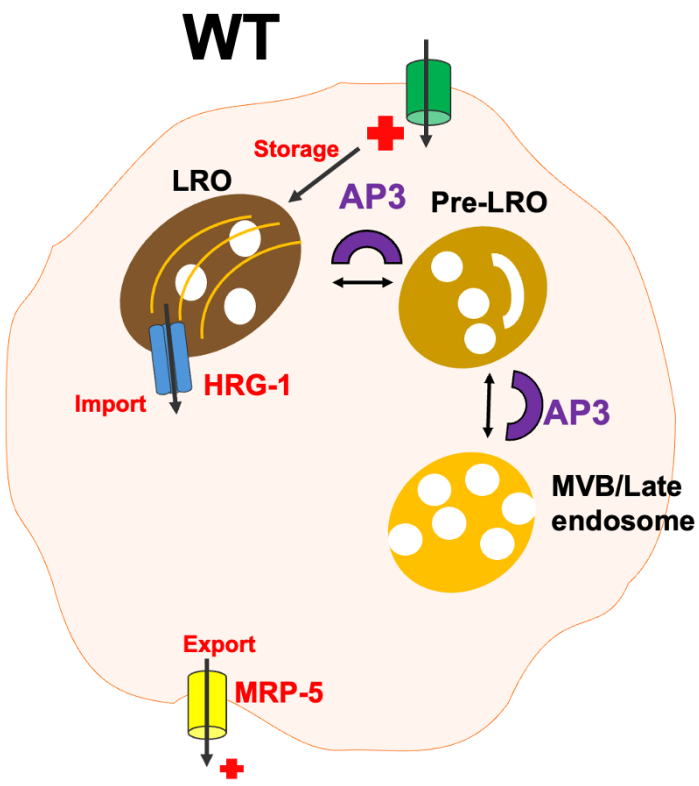
WT
Storage
LRO
AP3
Pre-LRO
Import
HRG-1
AP3
MVB/Late
endosome
Export
MRP-5

B

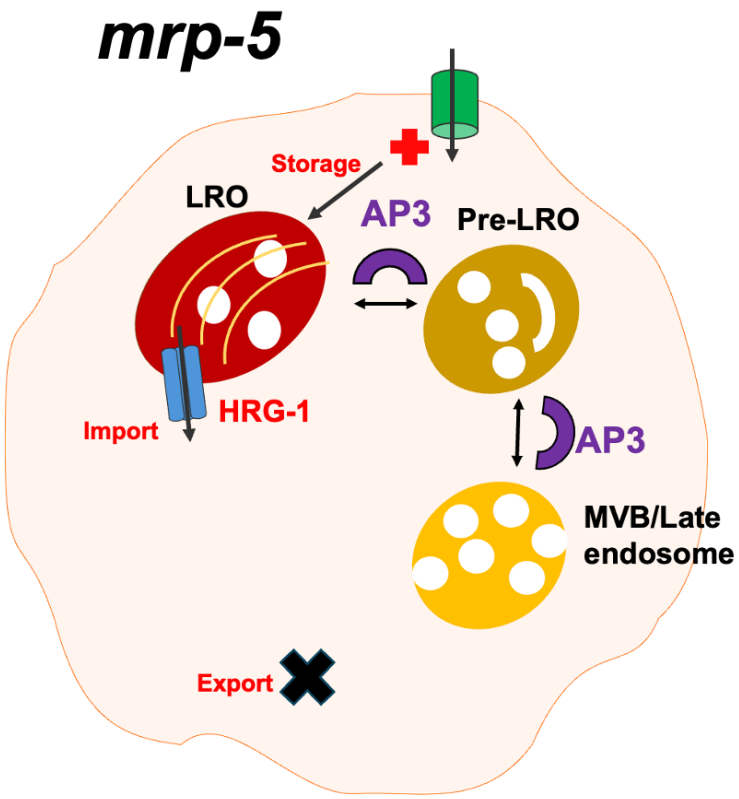
mrp-5
Storage
LRO
AP3
Pre-LRO
Import
HRG-1
AP3
MVB/Late
endosome
Export

C

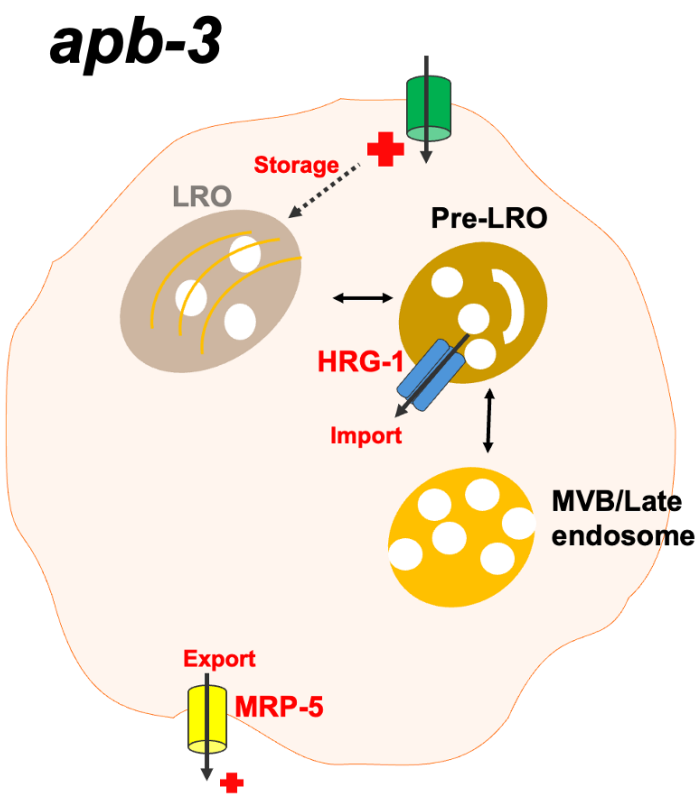
apb-3
Storage
LRO
Pre-LRO
HRG-1
Import
MVB/Late
endosome
Export
MRP-5

D

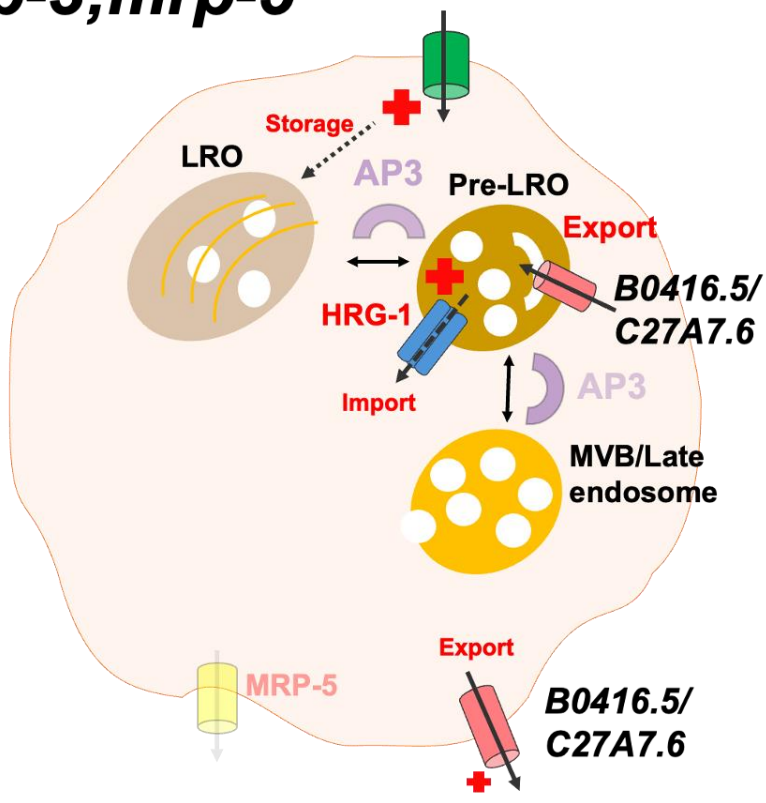
apb-3;mrp-5
Storage
LRO
AP3
Pre-LRO
Export
B0416.5/
C27A7.6
HRG-1
Import
AP3
MVB/Late
endosome
Export
MRP-5
B0416.5/
C27A7.6

Figure 5.1. Proposed model for the interplay between heme import, storage and export

(A) In wildtype conditions, heme storage occurs within lysosomal-related organelles (LROs). HRG-1 imports heme from the LROs into the cytosol. Heme export is mediated by MRP-5.

(B) Loss of *mrp-5* impairs heme export, resulting in heme accumulation in the LROs. This triggers HRG-1 degradation.

(C) AP-3 deficiency disrupts LRO formation, hindering heme storage. HRG-1 mis-localizes to intermediate compartments instead of LROs.

(D) In the absence of both *mrp-5* and *AP-3* subunit, HRG-1 levels and localization partially recover, allowing heme import from the subcellular compartments into the cytosol. Heme export is mediated by B0416.5 and C27A7.6, novel transporters homologous to human SLC49A3 protein.

Human SLC49A3 as a promising candidate for mammalian heme exporter

Our research sheds light on a new chapter in heme export with the identification of B0416.5 and C27A7.6 as crucial heme exporters in *C. elegans*. Their homology with the human SLC49A, also known as FLVCRs, family of proteins opens intriguing connections to the existing FLVCR research and challenges some previous assumptions. For more than two decades, FLVCR1 has been established for its role in cellular heme export. However, studies in the past year by multiple research groups have implicated human FLVCR1 and FLVCR2 in choline import and elucidated the structural mechanisms underlying the binding of these FLVCRs to choline while ignoring their heme transport functions and the possibility that FLVCRs could transport both heme and choline. Interestingly, the closely related SLC49A3 has remained completely uncharacterized, unlike its well-studied homologs FLVCR1/SLC49A1 and FLVCR2/SLC49A2. The identification of B0416.5 and C27A7.6 in *C. elegans* as heme exporters with homology to SLC49A3 marks a significant breakthrough. Both B0416.5 and C27A7.6 exhibit sequence similarity (47 %) with each other and share sequence similarity with human SLC49A3 (45 % for B0416.5 and 35 % for C27A7.6), thus suggesting similar functionality. The predicted AlphaFold3 model further strengthens this connection by positioning heme at the center of the SLC49A3 structure, nestled between its two predicted six-transmembrane domain (TMD) bundles (Figure 5.2). This reinforces the possibility that SLC49A3 functions as a heme exporter. The predicted topologies of human FLVCR1 and FLVCR2, show no interactions with heme (Figure 5.3).

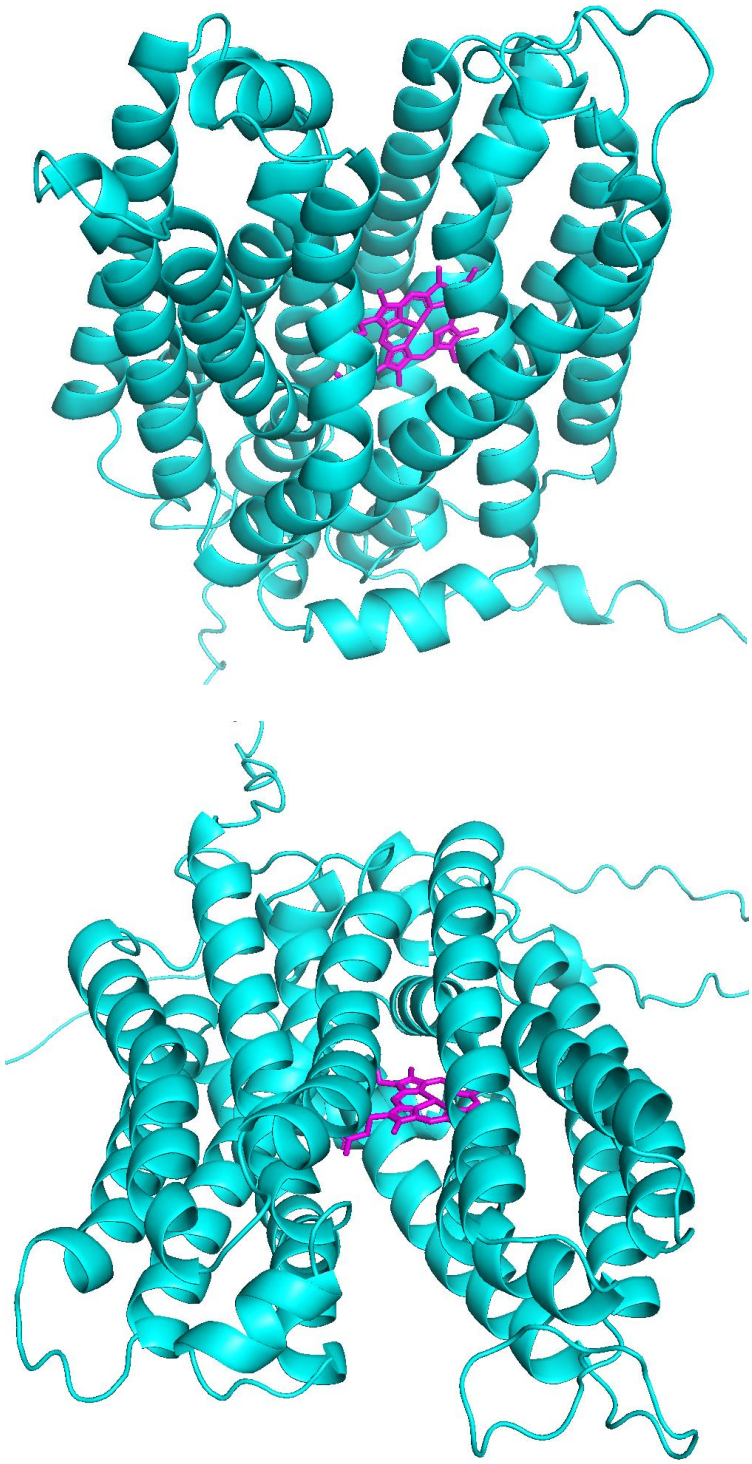

Figure 5.2. Predicted AlphaFold modeling to show interaction between human SLC49A3 (cyan) and heme (magenta)

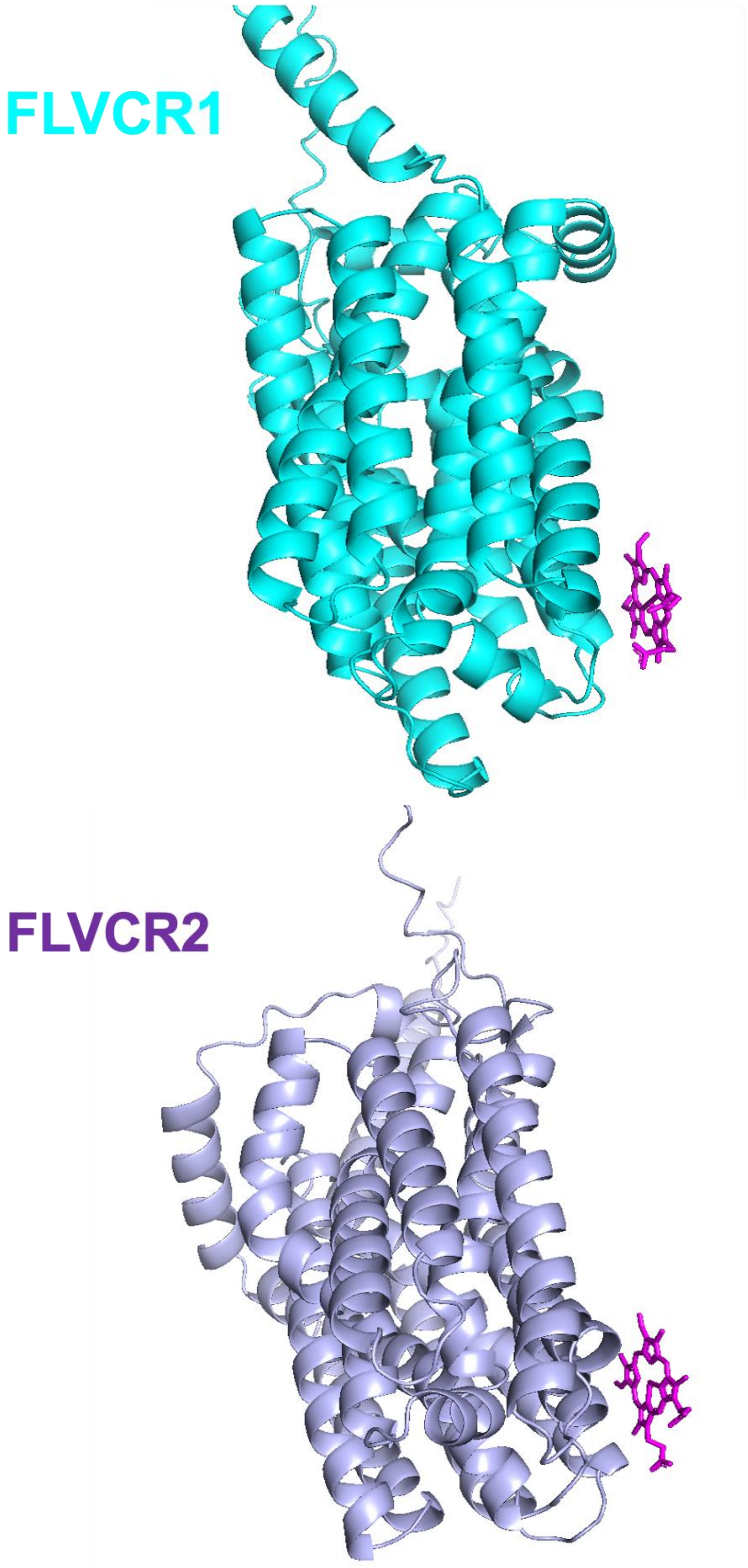

Figure 5.3. Predicted AlphaFold modeling showed no interaction between human FLVCR1 (top) or FLVCR2 (bottom) with heme (magenta).

B0416.5 and C27A7.6 can export exogenous heme

While FLVCR1 has been associated with endogenous heme synthesis in various studies using cell and animal models, its role in exogenous heme export remains unclear. Previous studies suggest that exogenous heme is targeted for degradation rather than export by FLVCR1 [74]. For instance, reduced *FLVCR1a* expression and increased heme oxygenase activity is observed in animals suffering from sickle-cell anemia, potentially indicating degradation of exogenous heme [75]. Most studies have used high doses of exogenous heme, which are non-physiological, thus making interpretation difficult [49]. On the other hand, our research using mammalian cells and SLC49A3 homologs offers new perspectives. We observed robust heme export activity at low concentrations of heme with the export increasing proportionally with added heme, suggesting a dose-dependent response. Moreover, our experiments ensured proper heme loading into cells using the heme importer HRG-1. Importantly, all our assays were conducted in the presence of succinyl acetone, a heme synthesis inhibitor, thus eliminating confounding factors from *de novo* heme synthesis. Our findings from heme export assays, coupled with the cellular co-localization of these transporters with the heme importer HRG-1, provide compelling evidence of their function as heme exporters.

LRO compartments facilitate Zinc transfer in *C. elegans*

Recent research in *C. elegans* has elucidated that a pair of zinc transporters regulate zinc import and export from the LROs to promote zinc homeostasis [76]. The study revealed that LROs are dynamic and respond to changes in the cytosolic zinc levels by engaging its two compartments, an acidified compartment and an expanded compartment, thereby facilitating the sorting of zinc transporters. This finding presents an intriguing parallel to our results. The colocalization of heme importer and exporter, influenced by heme itself, suggests a potential regulatory mechanism for heme homeostasis raising the possibility that specialized compartments might exist for heme to regulate the delivery and deployment of transporters for maintaining cellular heme homeostasis. Further investigation is necessary to gain valuable insights into understanding if this is a general mechanism deployed by cells to promote transport of metals and to prevent toxicity at the same time.

Tissue specific localization patterns of the exporters

The two homologs involved in heme export display different localization patterns. While B0416.5 is ubiquitous, C27A7.6 is present in the germline. This suggests a tissue-specific role for these two transporters. Depleting the AP-3 subunits, specifically affected the intestinal localization of B0416.5, without impacting its localization in other tissues. It is possible that B0416.5 functions as a heme exporter not only in the intestine but also in other tissues. Future experiments using tissue-specific depletion of

B0416.5 could help dissect its function in other organs. The presence of C27A7.6 in the germline suggests its potential role in exporting heme to developing oocytes. All our lethality experiments were conducted using F1 generation worms and the impact of C27A7.6 RNAi on F2 generation has not been explored. We believe that owing to its germline localization C27A7.6 might be instrumental for maternal export of heme to developing oocytes, which can be confirmed only if we deplete the maternal heme stores. This would also explain why a very low concentration of heme (10 μM) can override the lethality caused by C27A7.6 RNAi in the suppressor strain, as that seems to be enough for the embryos to hatch and lay progeny. Perhaps knockdown of *hrg-3*, the heme chaperone for maternal heme delivery, along with C27A7.6 will result in a more severe phenotype. Further studies investigating subsequent generations are needed to confirm this hypothesis.

Chapter 6: Conclusions and future directions

Conclusions

While heme synthesis has been extensively studied, mechanisms governing heme transport and trafficking remain elusive. The goal of this study was to identify novel heme export pathways and key players in this pathway in order to gain valuable insights into how organisms maintain systemic heme homeostasis. The major findings of this study are outlined below:

1. *mrp-5* null mutants display embryonic lethality which can be rescued by the addition of heme. This suggests the existence of alternate heme export pathways that function in the absence of *mrp-5*. To uncover these pathways, an EMS-based forward genetic screen on *mrp-5* null mutants was performed and identified loss of function mutations of adaptor protein subunits (AP-3) as strong suppressors of lethality. Genetic knockdown of any of these AP-3 subunits completely bypassed the lethality caused by *mrp-5* deficiency without the addition of exogenous heme.

2. Depletion of AP-3 subunits act as strong suppressors of *mrp-5* lethality. RNAi depletion of *mrp-5* in a heme sensitized strain results in complete lethality that cannot be reversed by heme supplementation. However, combinatorial RNAi

of *mrp-5* along with any of the adaptor protein subunits can rescue the death by ~30 %. Furthermore, 50 μM heme supplementation completely bypassed the lethal phenotype.

3. Loss of *mrp-5* along with AP-3 subunits increases systemic heme availability specifically in the secretory pathway without altering cytosolic heme levels. Using tissue specific enzymatic reporter worm strains, we show co-depleting *mrp-5* and *AP-3* subunits leads to a significant increase in labile heme levels across all tissues including the intestine, hypodermis and muscle. It is noteworthy that loss of AP-3 subunits prevents the *mrp-5* induced heme decrease in the hypodermis and neurons.

4. Coordinated function of the heme exporter MRP-5 and AP-3 is critical for proper localization and abundance of heme importer HRG-1 within the intestine. Loss of AP-3 subunits disrupt LRO formation, leading to HRG-1 mis-localization. Because of impaired heme export caused by *mrp-5* deficiency, more heme accumulates within the intestine resulting in degradation of HRG-1. Our experiments revealed that overexpression of HRG-1 rescues the embryonic lethality associated with *mrp-5*. Conversely, depleting HRG-1 in the suppressor strain negates the rescue effect, underscoring the importance of HRG-1 levels in dictating *mrp-5* lethality.

5. RNA-Seq analyses revealed human SLC49A3 homologs B0416.5 and C27A7.6 as heme exporters in the suppressor strain. Although lethality caused by loss of

C27A7.6 in the suppressor strain was rescued by heme supplementation, lethality caused by loss of B0416.5 was irreversible. While the tissue localization pattern was different for B0416.5 and C27A7.6 (intestine and germline respectively), they shared the same intracellular localization (plasma membrane and intracellular vesicles). These act as backup transporters when the primary pathway mediated via MRP-5 is compromised.

6. Suppression of *mrp-5* lethality by loss of AP-3 complex is specific to heme homeostasis and does not affect other essential trace nutrient pathways. To test the specificity of this suppression we chose the copper export pathway given its parallels with the heme export pathway in *C. elegans*. Loss of the copper exporter *cua-1* leads to embryonic lethality which can be rescued by copper supplementation. CUA-1 also traffics between the basolateral membrane and endocytic vesicles in the intestine. Unlike *mrp-5* lethality, loss of AP-3 subunits fails to rescue the lethality caused by defective copper export, suggesting that the suppression mediated by AP-3 on *mrp-5* is heme specific.

7. Our cell biological assays confirmed the heme export function of the SLC49A3 homologs B0416.5 and C27A7.6. Peroxidase reporter-based assays revealed that both these proteins cause an overall decrease in labile heme across different organelles including the ER, mitochondria, and cytosol. Radioactive efflux experiments with [^{55}Fe]-heme provide direct evidence that cells provided with

heme via HRG-1 are efficient in exporting the heme when they express B0416.5 and C27A7.6.

8. Live-cell imaging revealed “kiss-and-run” events between HRG-1 (import) and B0415.5/C27A7.6 (export) vesicles. The interaction dynamics between the import and export vesicles is influenced by cellular heme levels. High heme concentrations result in longer duration of coalescence between the import and export vesicles, thus indicating a potential mechanism for direct vesicular heme transfer.

9. Given the recent publications implicating human FLVCR1 (SLC49A1) and FLVCR2 (SLC49A2) in choline import, we determined if choline has any effect on the SLC49A3 homologs in *C. elegans* and in mammalian cells. In worms, choline supplementation did not rescue the embryonic lethality caused by lack of B0416.5 or C27A7.6. Likewise, there was no impact of choline on the heme efflux activity of either of the heme transporters, as revealed by the cytosol targeted peroxidase reporter assay.

Future directions

Delineating the role of human SLC49A3

One of the most pressing questions that remain is to understand if the function of SLC49A3 in humans is conserved as observed for its *C. elegans* counterpart. First, we propose to do overexpression studies in mammalian cells to determine if the protein is expressed and localizes to similar intracellular compartment as the worm homologs. We also plan to determine the localization of SLC49A3 in polarized MDCKII or CacoII intestinal cell lines, to gain further insights into its trafficking pattern. Conducting heme-based functional assays would then provide insights to understand if the human SLC49A3 plays any role in heme homeostasis. Employing peroxidase-based reporter assays as well as radioactive heme assays in the presence of a heme importer to allow heme loading will allow us to directly assess if it indeed exports heme. Microscopy studies using human HRG-1 and co-localization with SLC49A3 would further support the heme export function of human SLC49A3. Additionally, we plan to generate SLC49A3 knockout mammalian cells, to determine if this results in an abrogated heme export out of the cells.

Following in vitro characterization, in vivo studies by generating knock-out zebrafish and mice models will be instrumental. Given the recent connection between human FLVCR1/FLVCR2 and choline, SLC49A3 becomes a promising candidate for the primary mammalian heme exporter. Importantly, MRP5 and MRP9 knockout mice show no obvious heme-dependent phenotypes, beyond male reproductive dysfunction.

Additionally, the function of human FLVCR1 as a heme exporter is under question, especially after structural data elucidated the binding of FLVCR1 and FLVCR2 with choline. In the light of these recent developments, future research will need to focus on the in vivo characterization of SLC49A3 knockout vertebrate models including but not limited to erythropoiesis, iron metabolism and various tissue-specific analysis.

Dissecting the tissue-specific role of B0416.5 and AP-3 complex in *C. elegans*

The exporter B0416.5 is ubiquitously expressed in *C. elegans.* We are yet to explore its heme-export function beyond the intestine. Conducting tissue-specific depletions of B0416.5 in the suppressor background will enable us to dissect its function in each tissue. This will allow us to gain a precise understanding of its role as a heme exporter in different tissues.

Similar to B0416.5, AP-3 complex is also expressed in nearly all worm tissues. Although all our results showed that knockdown of either of the four subunits can restore *mrp-5* deficiency, the specific contribution of each subunit within different tissues remains unknown. Using tissue-specific knockdowns, we will be able to systematically study the role of AP-3 complexes in heme homeostasis. Conversely, we will resurrect AP-3 expression in specific tissues while the rest of the animal lacks the protein. This will provide temporospatial insights into the tissue-specific function of AP-3 complex in regulating heme homeostasis.

Heme transport by MRP-5

Although this study along with previous studies have delineated the role of MRP-5 in heme export in *C. elegans,* a key limitation is the lack of direct evidence for MRP-5 mediated heme transport. This has also been challenging because MRP-5 primarily localizes to intracellular compartments, making it difficult to measure the changes in heme concentrations within these compartments. One promising model to overcome this challenge is polarized MDCKII cells, since MRP-5 traffics to the basolateral membrane in these cells, thus eliminating the confounding factor of subcellular localization. Additionally, use of the fluorescent heme analog ZnMP will allow us to determine if the heme indeed is accumulating within these intracellular compartments and it can be employed in other cellular models where MRP-5 localizes to subcellular compartments.

Significance

In most animals, heme is synthesized via a highly conserved eight-step pathway shared between the mitochondria and cytosol [77]. The final step of the heme synthesis pathway occurring in the mitochondrial matrix involves the insertion of iron into the protoporphyrin IX ring to produce heme [78]. After its synthesis is complete, this heme needs to be exported out of the mitochondria to different cellular compartments, where it is incorporated into hemoproteins ensuring vital biological functions [79]. Since

heme is hydrophobic and cytotoxic, heme trafficking within and between cells needs to be tightly regulated by a network of transporters and chaperones.

In this study, we have uncovered a novel heme trafficking pathway, which plays a key role in maintaining systemic heme homeostasis. Our forward genetic screen conducted on *mrp-5* null mutants identified LOF mutations in cargo sorting adaptor protein complex (AP-3) subunits that can completely suppress the embryonic lethality caused by *mrp-5* deficiency without any exogenous heme. This suppression is governed by two mechanisms: First, AP-3 can suppress the *mrp-5* associated death by dictating the HRG-1 levels and localization. Our results show that loss of the heme exporter MRP-5 also leads to a concomitant loss of the heme importer HRG-1. As heme accumulates within the intestine due to impaired export, HRG-1 is targeted for degradation. Loss of AP-3 subunits can resurrect the HRG-1 levels as well as localization in the absence of *mrp-5*. Furthermore, overexpression of *hrg-1* bypasses the lethality caused by loss of *mrp-5*. Conversely, depletion of *hrg-1* in the suppressor strain (*apb-3;mrp-5*) can negate the suppression. Thus, HRG-1 levels dictate *mrp-5* lethality. Second, our RNA-Seq analysis reveals that the suppressor strain engages SLC49A3 homologs, B0416.5 and C27A7.6, as backup heme exporters for survival. These homologs show different tissue localizations in *C. elegans* but localize to similar intracellular compartments chiefly the plasma membrane and endocytic vesicles. Additionally, our cell biology assays validate the heme export function of both B0416.5 and C27A7.6 as demonstrated by [^{55}Fe]-heme efflux from the cells into the media establishing a framework for radioactive heme efflux assays. Our live-cell imaging experiments

revealed a “kiss-and-run” mechanism between the import (HRG-1) and export (B0416.5/C27A7.6) vesicles, which are influenced by heme levels potentially facilitating heme transfer to prevent toxicity.

The field of heme export has always been an area of active research since studies over the past two decades have elucidated the role of human FLVCR1 as the primary mammalian heme exporter given its function in erythropoiesis as well as in other tissues including liver, endothelial cells and intestine. However, research in the past year has shown that both FLVCR1 and FLVCR2 import choline thus raising questions about their physiological substrate. Our work identifies SLC49A3 as a promising candidate for mammalian heme export. This is supported by direct evidence of heme export activity of the *C. elegans* homologs as well as structural modeling suggesting human SLC49A3 can bind heme, unlike its close relatives SLC49A1 or SLC49A2. Overall, this work sheds light on a novel heme trafficking pathway in *C. elegans* and identifies a promising candidate as a mammalian heme exporter, paving the way for future research into its role in mammalian systems and heme-related diseases.

Appendix I

Strain name	Genotype	Description	Source
N2	WT	Used as wildtype strain	CGC
N2; *mrp-5(ok2067ok2067)*	*mrp-5(ok2067/ok2067)*	*mrp-5 (ok2067/ok2067)* allele in the N2 background	VC1599 was outcrossed to N2 3x times [26]
RB662	*apb-3(ok429/ok429)*	*apb-3* mutant	CGC
IQ1901	*mrp-5(ok2067/ok2067) ; apb-3(ok429/ok429)*	AP-3, *mrp-5* Suppressor mutant	Crossing *mrp-5(ok2067ok2067)* to RB662 *[64]*
IQ1005	*mrp-5(ok2067/ok2067); apm-3(ih1005/ih1005)*	*mrp-5* suppressor mutant; mapped	EMS mutagenesis of N2; *mrp-5(ok2067ok2067)* [64]
IQ6111	P_{hrg-1}*::HRG-1-mCherry::unc-54 UTR*	HRG-1 transcriptional reporter, intestinal expression	[36]
IQ6112	P_{vha-6}*::HRG-1-mCherry::unc-54 UTR*	HRG-1translational reporter, intestinal expression	Bombardment
IQ9101	P_{vha-6}*::HRP-mcherry::unc-54 UTR*; *lin-15B(n744/n744)*	RNAi Hypersensitive Intestinal HRP (ER) reporter	[18]
IQ9102	P_{dpy-7}*::HRP-mcherry::unc-54 UTR*; *lin-15B(n744/n744*	RNAi Hypersensitive Hypodermal HRP (ER) reporter	[18]
IQ9104	$P_{unc-119}$*::HRP-mcherry::unc-54 UTR*; *lin-15B(n744/n744*	RNAi Hypersensitive Neuronal HRP (ER) reporter	[18]
IQ9006	P_{vha-6}*::APX-EGFP::unc-54 UTR*	Intestinal APX (cytosol) reporter	Bombardment
VP303	P_{nhx-2}*::rde-1(ne213)*	Intestine-specific RNAi	CGC
IQH01	*C27A7.6::GFP*	Translational reporter of C27A7.6	This study
IQH02	*B0416.5::GFP*	Translational reporter of B0416.5	This study

QKO	*hrg-1;hrg-4;-5;-6*	Quadruple knockout	Generated by CRISPR
NYL1269	$P_{F53F4.13}$*::GFP (yadIs48)*	Amphid sheath glial reporter strain	Dong Lab [70]
NYL2499	$P_{F53F4.13}$*::GFP (yadIs48);mrp-5(yad138)*	*mrp-5* LOF amphid sheath glial reporter strain	Dong Lab [70]
CZ333	P_{unc-25}*::SNB-1::GFP (juls1)*	GABA synapses reporter strain	Dong Lab [70]

Appendix II

Oligonucleotides used in this study

Purpose	Name	Sequence
Genotyping *IQH01*	5' C27 exon7	ATCCTGCCGGTGTTGCCCTCG
	3’ GFPnovo2	GTGCCCATTAACATCACCATCT
	5’ C27 exon 14	ATATCGTCGTCTAGAACTGG
	3' C27 after 3’UTR	CACGGGAAGCAATTCGAGATTCAGTG
Genotyping *IQH02*	5’ B04 exon 1	ATGGGCGCTGATGATGGTGC
	5’ B04 exon 4	CGGTGTACAAGCGATTGGAAGC
	3’ B04 after 3’UTR	CTCATCCGTAAGTAACGAGAATCCCG
	3’ GFPnovo2	GTGCCCATTAACATCACCATCT
B0416.5 amplification	5’ XhoI B0416.5 ORF	CGTACGCTCGAGATGGGCGCTGATGGTG
	3’ BamHI-B0416.5 ORF	CTGCCAGGATCCGCAGCATAATCAGGAACATCGT ATGGGTATTTCTTCTGAAGAGGTTCAAC

Appendix III

Constructs synthesized using TWIST

C27A7.6-HA-GFP

GGATCCAAAAAAATGGAAAACGACAGTGGTGTAGATCAACCGCTGTTGATGGGATCG
GCGATCAACAAAGAAGCCGTCGCCGCAGATAAGGATACTTCGGCAAATGAAGGAATC
AGCGAAAATAGTGTTATATACAAGGTCTACCCAGCTCGATGGCTCGTTCTAGCTGTT
TGTTGCTTTCTTGCTCTTTCAAACGCAATGCAATGGATAAGCTTCAGCTCTCTATCC
GACGAAGTTCAGATATATTATAGAGGACGTCCAGCCAACGGGAGCATTGATGTATCA
CTTGTCACGAATCAAATTTTCCAGTTTGTCGCCGTGTTCACTGGATTTGGTGGAATG
TACATAACTGATAACAAAGGAATAAAAACGGCTGGTCTTCTTGGTACAACTTTAAAT
GTAATTGGAGCATCGATTCGGATGATTGCCTCGATTCCTTTCATAAAATCACATTTT
GTTCGTGAATGTCTTCTTCATGCAGGATCGTTTATCGCTGCTTCAGCACAAGCATTC
TTTTTAGTTCTTCCATCAAAAATTGCTGAATGCTGGTTCCCTGGTGATCAGAGAGCA
ATTGCAAATGTACTTTCTTTTGTTGCAAATCCTGCCGGTGTTGCCCTCGGAACAATT
GTGCCATCCATTCTTTTTGGTCACAATAAGACTATTGATTCGAATAGTTGGATGTTC
TTCACATTTACTCTTGGAATGGAATGTCTAGCCTTGTTCCCATTTGTTCTAGCACTA
TTCGTTCGAACTAAACTGCCACCCACTCCACCATCAGCTTCTTCTGCTGCTCATCAG
AACAACATTGGTTTCTTTAAATCTATTCTTCAATGTATTTTTAATGCTCAATTTTTC
ATCCAAATGACTCTCTTTGCATTTGCGTTTTCGCTTCTGTGGAGTCTAATGATTTTC
CTCGATGGTCCACTCAAAGATCAAGGTTATGAGATGGCTGGATATCCAACTGCCGTG
TGTGCAATCGTTGGCACGTTAACATCACTGCTCGCTGGTCATATTGCCGACAAAACA
CGCAAGTTCAAGGAAATAATCAGAGTTTGTACTGTTGGATTTTCATGTTCAGTCATT
ACATTGAGAATGTTCCTAAATCAACCACGGACTGGGCTCTTTGATAGCATAATCGTT
TACACTCTTTGTGGATGTCTCGGTGCCTTTTCAATACCTCAATTCCCGATTGGAGTG
GAACTTGGTGTTGAGACGACATTCCCAGTAATGGAAGCAACGTCATCAGGTGTTCTT
GTTATATTCGGATCGCTTTTCATGTTCATTATTCCATTTGCACAAAATTACACAGAA
AAGTTGCACTTGTTCTATGCACAATCTTGGAAATTTGCTCTCGATGTAACATGTGGG
CTCTCAATTGTATCTGTCATCTTATCACTGTTCTTTTTGAGACCACGATATCGTCGT
CTAGAACTGGAAAATGCCAAATTGGCATTAGAAAATGAGGAACCTGTTACAGCTCGA
ACGGCTGCGTCGGATATCGAAATGCGATACCCATACGATGTTCCTGATTATGCTGAA
TTCATGGTGAGCAAGGGCGAGGAGCTGTTCACCGGGGTGGTGCCCATCCTGGTCGAG
CTGGACGGCGACGTAAACGGCCACAAGTTCAGCGTGTCCGGCGAGGGCGAGGGCGAT
GCCACCTACGGCAAGCTGACCCTGAAGTTCATCTGCACCACCGGCAAGCTGCCCGTG
CCCTGGCCCACCCTCGTGACCACCCTGACCTACGGCGTGCAGTGCTTCAGCCGCTAC
CCCGACCACATGAAGCAGCACGACTTCTTCAAGTCCGCCATGCCCGAAGGCTACGTC
CAGGAGCGCACCATCTTCTTCAAGGACGACGGCAACTACAAGACCCGCGCCGAGGTG
AAGTTCGAGGGCGACACCCTGGTGAACCGCATCGAGCTGAAGGGCATCGACTTCAAG
GAGGACGGCAACATCCTGGGGCACAAGCTGGAGTACAACTACAACAGCCACAACGTC

TATATCATGGCCGACAAGCAGAAGAACGGCATCAAGGTGAACTTCAAGATCCGCCAC
AACATCGAGGACGGCAGCGTGCAGCTCGCCGACCACTACCAGCAGAACACCCCCATC
GGCGACGGCCCCGTGCTGCTGCCCGACAACCACTACCTGAGCACCCAGTCCGCCCTG
AGCAAAGACCCCAACGAGAAGCGCGATCACATGGTCCTGCTGGAGTTCGTGACCGCC
GCCGGGATCACTCTCGGCATGGACGAGCTGTACAAGTAAGAATTCTAGGCGGCCGC

B0416.5-FLAG

GAATTCATGGGCGCTGATGATGGTGCCATAAGTGCGGATAAGGTGGATATTCGACTG
CAGCCACTCAACAAGAACGGAGCACAAGACGAGACTGATGAAGAAGCAGCAGATCAA
ATCCAACTTCGTGTCTACAAGCAGAGATGGATTGTTCTTCTTGCCGTTGCTCTTCTC
AACAACACAAACACAATGTCTTGGATTGGATACGCCCCGTCTGGAAACTACGTCAAT
AGCTTCTATGGAGAGAGCAGTGCCGCTTGGCTATCCATGGTGTACATGATGTGTACA
ATCCCGGTTGGAATGTTCGCCATGTGGGCTGGTCGTGAATGGGGTCTCCGAACGGCG
GTGCTCATTGCCGGATGGGCCAATGGAATTGGAGCTGTTATTCGTGTCATCTCATCA
TTGGACTTTGTTCCTCAGGATCTCCGTTTTCCAATCTGTATGACTGGACAAGGAATT
GCAGCCATTGCTTACCCATTCATTATGTTCCTTCCAACTAAGGTTGCTGGATCGTGG
TTCCCCGACACTCAACGTGCAATTGCCACAAGTATCGGAGTGATGTCTAACCCGCTT
GGAGTTTTGATGGCCAACTTGATCAGTCCTGCTATTGTGAAGTCTCCTGAACACGTC
ATTTGGCTCAACATCTTCACATGTGTTCCATCTCTGATTGCTATGCTGATTGCTACC
TTTGGAGTCAATCGCAGTGAACCTAAGATCCCACCAACCTTCAGCGCTAGTAAGCCA
CAAATGGACTTTGTCTCTGGAATGAAGTCATGCTTCTCCTCGAAACAATACATTATC
CTGCTCATCGTCATGGGTGGTGGTATTGGAATGTTCAATTGTCTGTACACTGTCATG
CTTGAGCTTTTGTGTCCATCTGGATACTCTAATTTTTTCTCTGGAGTATGTGCTGCT
CTTATGATTGTCGGAGGTGTATTCGGTGCCGCTGCAAGCAGTATCTTTGTGGATCGC
ACCAAGCTCTATGAGGAGACTCTCAAAATTGCTCTTGGAGCTGCAGTCATATTTGGC
TTGATTTTCCTTCAGCTCACTCTTCATCAAGGATACTCAGTTATTCTCGGTGTTACT
TGTCTTTTGTTTGGAGTTCTTGGACTGGCCACGTATCCAATTGGTTTGGAATTGGCT
TCGGAATGCACATTCCCAGTGTCTGAAGCTACTTCAACCGGACTCATTGTTTTGTCT
GGACAAATTCAAAGTGTCATCTACGTCTTCATTATGAAGAACTTTGCCCGTCCACTC
CAACCAGATCGCATGCACATTCAAGTCTGCCAACTCACCCCAGACGATACAATCAAT
ACACCAAAGGATAATACCATGTCCATCATGATTTTCTCACTTCTTGCTACACTTCTC
GTTCTTACACTTGTGGTCCTCTTCAAACCGGTCTACAAGCGATTGGAAGCTGAACGT
GGAAATCGTGCAACTGCTGACAAAGCAAAAGAGCTTTCAAATCAGAATAAGGACAGA
ATCACACTTCAAGCTGAAAGTGCCGTTGAACCTCTTCAGAAGAAATAA
GACTACAAAGACGATGACGACAAGGCGGCCGC

Appendix IV

RNA-Seq analysis revealed no trends for differentially expressed genes involved in other metabolic pathways between wildtype, *mrp-5* and suppressor strain.

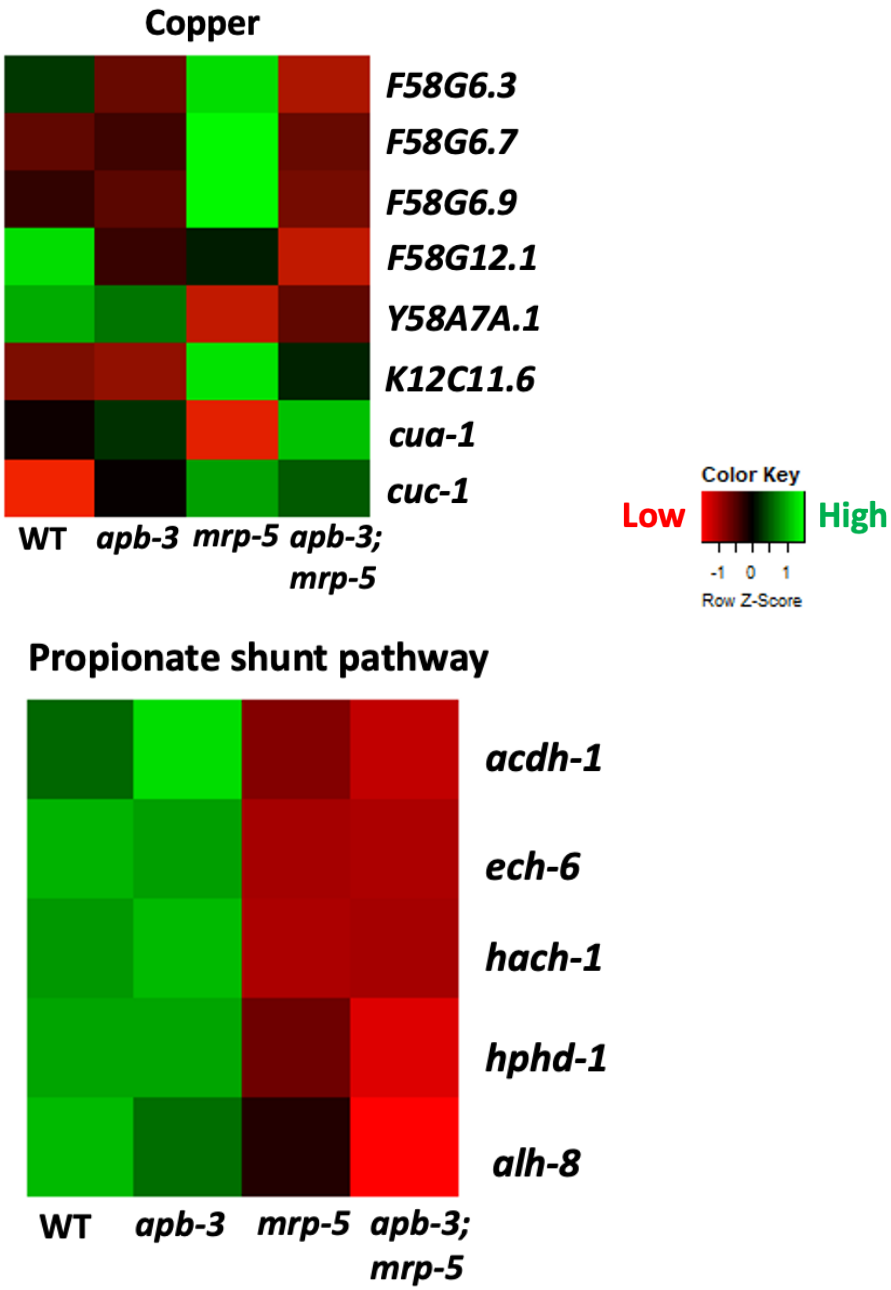

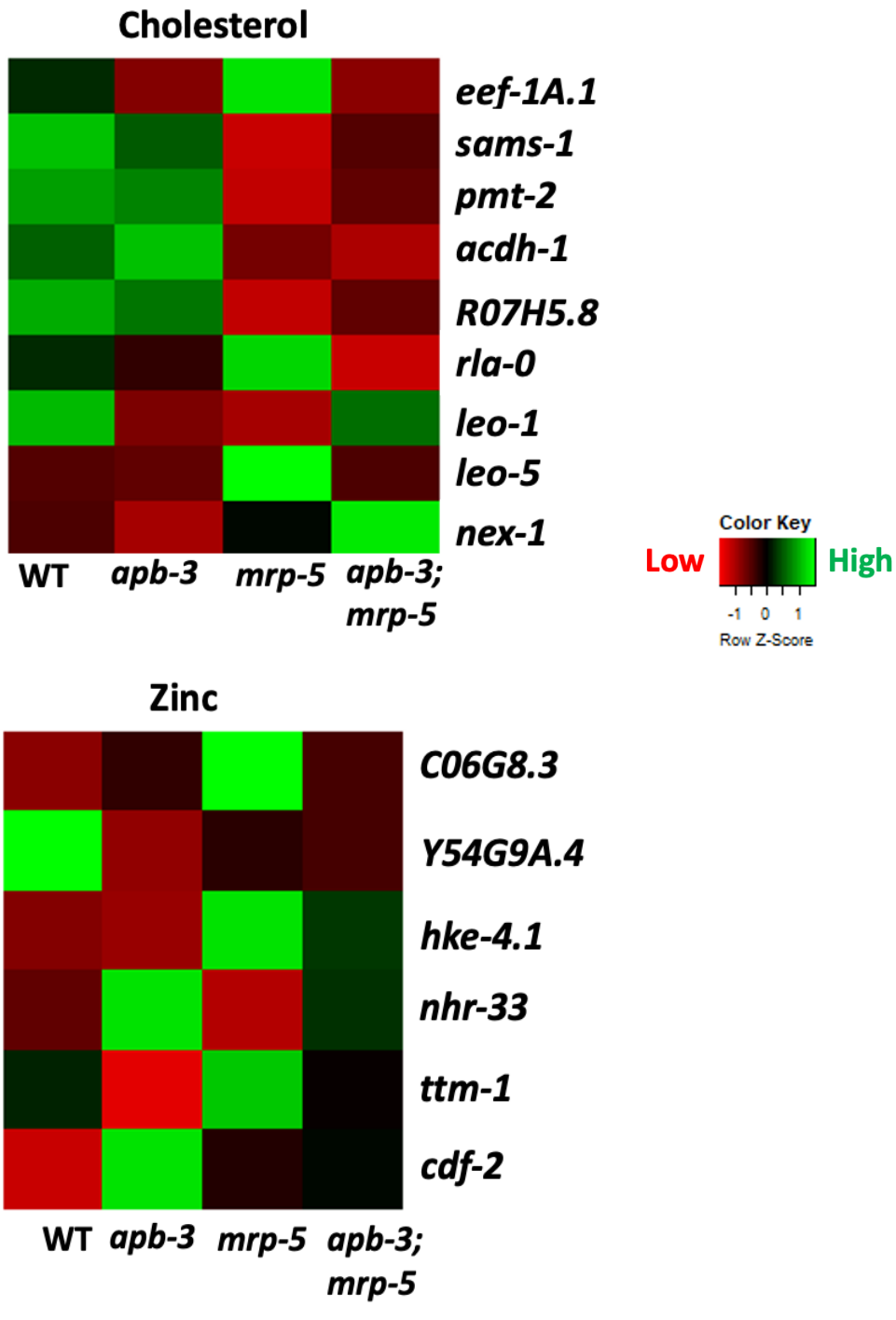
Cholesterol
eef-1A.1
sams-1
pmt-2
acdh-1
R07H5.8
rla-0
leo-1
leo-5
nex-1
WT
apb-3
mrp-5
apb-3; mrp-5
Color Key
Low
High
-1 0 1
Row Z-Score
Zinc
C06G8.3
Y54G9A.4
hke-4.1
nhr-33
ttm-1
cdf-2
WT
apb-3
mrp-5
apb-3; mrp-5

Appendix V

HRG-1 protein abundance is affected by loss of *mrp-5*, which can be partially restored by co-depletion of *AP-3* subunits.

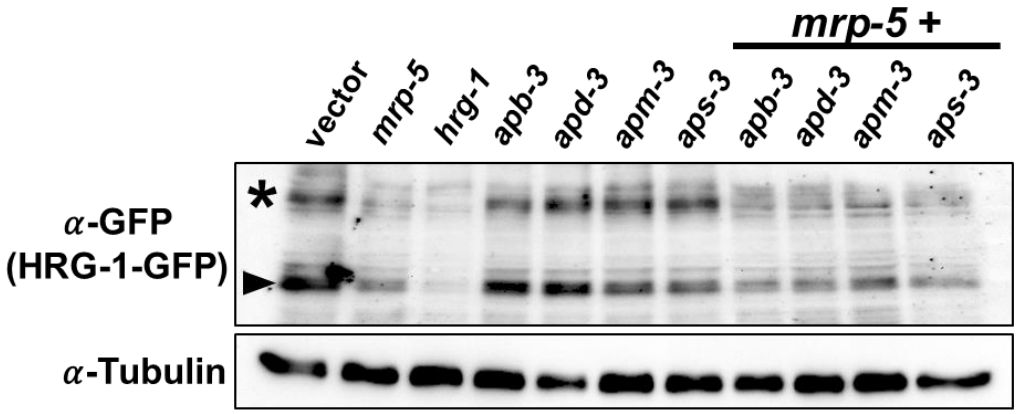

Bibliography

1. Dutt, S., Hamza, I., and Bartnikas, T. B.: Molecular Mechanisms of Iron and Heme Metabolism. *Annu Rev Nutr* 2022, 42:311-335.[PMID:35508203]
2. Heinemann, I. U., Jahn, M., and Jahn, D.: The biochemistry of heme biosynthesis. *Arch Biochem Biophys* 2008, 474(2):238-51.[PMID:18314007]
3. Severance, S., and Hamza, I.: Trafficking of heme and porphyrins in metazoa. *Chem Rev* 2009, 109(10):4596-616.[PMID:19764719]
4. Donegan, R. K., Moore, C. M., Hanna, D. A., and Reddi, A. R.: Handling heme: The mechanisms underlying the movement of heme within and between cells. *Free Radic Biol Med* 2019, 133:88-100.[PMID:30092350]
5. Chambers, I. G., Willoughby, M. M., Hamza, I., and Reddi, A. R.: One ring to bring them all and in the darkness bind them: The trafficking of heme without deliverers. *Biochim Biophys Acta Mol Cell Res* 2021, 1868(1):118881.[PMID:33022276]
6. Maio, N., Kim, K. S., Holmes-Hampton, G., Singh, A., and Rouault, T. A.: Dimeric ferrochelatase bridges ABCB7 and ABCB10 homodimers in an architecturally defined molecular complex required for heme biosynthesis. *Haematologica* 2019, 104(9):1756-1767.[PMID:30765471]
7. Piel, R. B., 3rd, Dailey, H. A., Jr., and Medlock, A. E.: The mitochondrial heme metabolon: Insights into the complex(ity) of heme synthesis and distribution. *Mol Genet Metab* 2019, 128(3):198-203.[PMID:30709775]
8. Fiorito, V., Allocco, A. L., Petrillo, S., Gazzano, E., Torretta, S., Marchi, S., Destefanis, F., Pacelli, C., Audrito, V., Provero, P., Medico, E., Chiabrando, D., Porporato, P. E., Cancelliere, C., Bardelli, A., Trusolino, L., Capitanio, N., Deaglio, S., Altruda, F., Pinton, P., Cardaci, S., Riganti, C., and Tolosano, E.: The heme synthesis-export system regulates the tricarboxylic acid cycle flux and oxidative phosphorylation. *Cell Rep* 2021, 35(11):109252.[PMID:34133926]
9. Liu, G., Sil, D., Maio, N., Tong, W. H., Bollinger, J. M., Jr., Krebs, C., and Rouault, T. A.: Heme biosynthesis depends on previously unrecognized acquisition of iron-sulfur cofactors in human amino-levulinic acid dehydratase. *Nat Commun* 2020, 11(1):6310.[PMID:33298951]
10. Chiabrando, D., Vinchi, F., Fiorito, V., Mercurio, S., and Tolosano, E.: Heme in pathophysiology: a matter of scavenging, metabolism and trafficking across cell membranes. *Front Pharmacol* 2014, 5:61.[PMID:24782769]
11. Dai, Y., Sweeny, E. A., Schlanger, S., Ghosh, A., and Stuehr, D. J.: GAPDH delivers heme to soluble guanylyl cyclase. *J Biol Chem* 2020, 295(24):8145-8154.[PMID:32358060]
12. Perally, S., Lacourse, E. J., Campbell, A. M., and Brophy, P. M.: Heme Transport and Detoxification in Nematodes: Subproteomics Evidence of Differential Role of Glutathione Transferases. *J Proteome Res* 2008.[PMID:18720983]

13. Watanabe, Y., Ishimori, K., and Uchida, T.: Dual role of the active-center cysteine in human peroxiredoxin 1: Peroxidase activity and heme binding. *Biochem Biophys Res Commun* 2017, 483(3):930-935.[PMID:28082197]
14. Vincent, S. H., and Muller-Eberhard, U.: A protein of the Z class of liver cytosolic proteins in the rat that preferentially binds heme. *J. Biol. Chem.* 1985, 260(27):14521-14528
15. Medlock, A. E., Shiferaw, M. T., Marcero, J. R., Vashisht, A. A., Wohlschlegel, J. A., Phillips, J. D., and Dailey, H. A.: Identification of the Mitochondrial Heme Metabolism Complex. *PLoS One* 2015, 10(8):e0135896.[PMID:26287972]
16. Galmozzi, A., Kok, B. P., Kim, A. S., Montenegro-Burke, J. R., Lee, J. Y., Spreafico, R., Mosure, S., Albert, V., Cintron-Colon, R., Godio, C., Webb, W. R., Conti, B., Solt, L. A., Kojetin, D., Parker, C. G., Peluso, J. J., Pru, J. K., Siuzdak, G., Cravatt, B. F., and Saez, E.: PGRMC2 is an intracellular haem chaperone critical for adipocyte function. *Nature* 2019, 576(7785):138-142.[PMID:31748741]
17. Hanna, D. A., Martinez-Guzman, O., and Reddi, A. R.: Heme Gazing: Illuminating Eukaryotic Heme Trafficking, Dynamics, and Signaling with Fluorescent Heme Sensors. *Biochemistry* 2017, 56(13):1815-1823.[PMID:28316240]
18. Yuan, X., Rietzschel, N., Kwon, H., Walter Nuno, A. B., Hanna, D. A., Phillips, J. D., Raven, E. L., Reddi, A. R., and Hamza, I.: Regulation of intracellular heme trafficking revealed by subcellular reporters. *Proc Natl Acad Sci U S A* 2016, 113(35):E5144-52.[PMID:27528661]
19. Sarkar, A., Carter, E. L., Harland, J. B., Speelman, A. L., Lehnert, N., and Ragsdale, S. W.: Ferric heme as a CO/NO sensor in the nuclear receptor Rev-Erbss by coupling gas binding to electron transfer. *Proc Natl Acad Sci U S A* 2021, 118(3).[PMID:33436410]
20. Faller, M., Matsunaga, M., Yin, S., Loo, J. A., and Guo, F.: Heme is involved in microRNA processing. *Nat Struct Mol Biol* 2007, 14(1):23-9.[PMID:17159994]
21. Barr, I., Smith, A. T., Chen, Y., Senturia, R., Burstyn, J. N., and Guo, F.: Ferric, not ferrous, heme activates RNA-binding protein DGCR8 for primary microRNA processing. *Proc Natl Acad Sci U S A* 2012, 109(6):1919-24.[PMID:22308374]
22. Korolnek, T., and Hamza, I.: Like iron in the blood of the people: the requirement for heme trafficking in iron metabolism. *Front Pharmacol* 2014, 5:126.[PMID:24926267]
23. Scorrano, L., De Matteis, M. A., Emr, S., Giordano, F., Hajnoczky, G., Kornmann, B., Lackner, L. L., Levine, T. P., Pellegrini, L., Reinisch, K., Rizzuto, R., Simmen, T., Stenmark, H., Ungermann, C., and Schuldiner, M.: Coming together to define membrane contact sites. *Nat Commun* 2019, 10(1):1287.[PMID:30894536]
24. Martinez-Guzman, O., Willoughby, M. M., Saini, A., Dietz, J. V., Bohovych, I., Medlock, A. E., Khalimonchuk, O., and Reddi, A. R.: Mitochondrial-nuclear heme trafficking in budding yeast is regulated by GTPases that control

mitochondrial dynamics and ER contact sites. *J Cell Sci* 2020, 133(10).[PMID:32265272]
25. Dietz, J. V., Willoughby, M. M., Piel, R. B., 3rd, Ross, T. A., Bohovych, I., Addis, H. G., Fox, J. L., Lanzilotta, W. N., Dailey, H. A., Wohlschlegel, J. A., Reddi, A. R., Medlock, A. E., and Khalimonchuk, O.: Mitochondrial contact site and cristae organizing system (MICOS) machinery supports heme biosynthesis by enabling optimal performance of ferrochelatase. *Redox Biol* 2021, 46:102125.[PMID:34517185]
26. Korolnek, T., Zhang, J., Beardsley, S., Scheffer, G. L., and Hamza, I.: Control of metazoan heme homeostasis by a conserved multidrug resistance protein. *Cell Metab* 2014, 19(6):1008-19.[PMID:24836561]
27. Chambers, I. G., Kumar, P., Lichtenberg, J., Wang, P., Yu, J., Phillips, J. D., Kane, M. A., Bodine, D., and Hamza, I.: MRP5 and MRP9 play a concerted role in male reproduction and mitochondrial function. *Proc Natl Acad Sci U S A* 2022, 119(6).[PMID:35121660]
28. Ponka, P., Sheftel, A. D., English, A. M., Scott Bohle, D., and Garcia-Santos, D.: Do Mammalian Cells Really Need to Export and Import Heme? *Trends Biochem Sci* 2017, 42(5):395-406.[PMID:28254242]
29. Chen, C., Samuel, T. K., Sinclair, J., Dailey, H. A., and Hamza, I.: An intercellular heme-trafficking protein delivers maternal heme to the embryo during development in C. elegans. *Cell* 2011, 145(5):720-31.[PMID:21620137]
30. Chen, C., Samuel, T. K., Krause, M., Dailey, H. A., and Hamza, I.: Heme utilization in the Caenorhabditis elegans hypodermal cells is facilitated by heme-responsive gene-2. *J Biol Chem* 2012, 287(12):9601-12.[PMID:22303006]
31. Nemeth, E., Tuttle, M. S., Powelson, J., Vaughn, M. B., Donovan, A., Ward, D. M., Ganz, T., and Kaplan, J.: Hepcidin regulates cellular iron efflux by binding to ferroportin and inducing its internalization. *Science* 2004, 306(5704):2090-3.[PMID:15514116]
32. Sinclair, J., Pinter, K., Samuel, T., Beardsley, S., Yuan, X., Zhang, J., Meng, K., Yun, S., Krause, M., and Hamza, I.: Inter-organ signalling by HRG-7 promotes systemic haem homeostasis. *Nat Cell Biol* 2017, 19(7):799-807
33. Zhang, D. L., Wu, J., Shah, B. N., Greutelaers, K. C., Ghosh, M. C., Ollivierre, H., Su, X. Z., Thuma, P. E., Bedu-Addo, G., Mockenhaupt, F. P., Gordeuk, V. R., and Rouault, T. A.: Erythrocytic ferroportin reduces intracellular iron accumulation, hemolysis, and malaria risk. *Science* 2018, 359(6383):1520-1523.[PMID:29599243]
34. Sinclair, J., and Hamza, I.: Lessons from bloodless worms: heme homeostasis in C. elegans. *Biometals* 2015, 28(3):481-9.[PMID:25724951]
35. Severance, S., Rajagopal, A., Rao, A. U., Cerqueira, G. C., Mitreva, M., El-Sayed, N. M., Krause, M., and Hamza, I.: Genome-wide analysis reveals novel genes essential for heme homeostasis in Caenorhabditis elegans. *PLoS Genet* 2010, 6(7):e1001044.[PMID:20686661]
36. Rajagopal, A., Rao, A. U., Amigo, J., Tian, M., Upadhyay, S. K., Hall, C., Uhm, S., Mathew, M. K., Fleming, M. D., Paw, B. H., Krause, M., and

Hamza, I.: Haem homeostasis is regulated by the conserved and concerted functions of HRG-1 proteins. *Nature* 2008, 453(7198):1127-31.[PMID:18418376]
37. O'Callaghan, K. M., Ayllon, V., O'Keeffe, J., Wang, Y., Cox, O. T., Loughran, G., Forgac, M., and O'Connor, R.: Heme-binding protein HRG-1 is induced by insulin-like growth factor I and associates with the vacuolar H+-ATPase to control endosomal pH and receptor trafficking. *J Biol Chem* 2010, 285(1):381-91.[PMID:19875448]
38. Yuan, X., Protchenko, O., Philpott, C. C., and Hamza, I.: Topologically conserved residues direct heme transport in HRG-1-related proteins. *J Biol Chem* 2012, 287(7):4914-24.[PMID:22174408]
39. Park, S. Y., and Guo, X.: Adaptor protein complexes and intracellular transport. *Biosci Rep* 2014, 34(4).[PMID:24975939]
40. Ma, Z., Islam, M. N., Xu, T., and Song, E.: AP-3 adaptor complex-mediated vesicle trafficking. *Biophys Rep* 2021, 7(2):91-100.[PMID:37288146]
41. Hermann, G. J., Scavarda, E., Weis, A. M., Saxton, D. S., Thomas, L. L., Salesky, R., Somhegyi, H., Curtin, T. P., Barrett, A., Foster, O. K., Vine, A., Erlich, K., Kwan, E., Rabbitts, B. M., and Warren, K.: C. elegans BLOC-1 functions in trafficking to lysosome-related gut granules. *PLoS One* 2012, 7(8):e43043.[PMID:22916203]
42. Abkowitz, J. L., Holly, R. D., and Grant, C. K.: Retrovirus-induced feline pure red cell aplasia. Hematopoietic progenitors are infected with feline leukemia virus and erythroid burst-forming cells are uniquely sensitive to heterologous complement. *J Clin Invest* 1987, 80(4):1056-63.[PMID:2821071]
43. Quigley, J. G., Yang, Z., Worthington, M. T., Phillips, J. D., Sabo, K. M., Sabath, D. E., Berg, C. L., Sassa, S., Wood, B. L., and Abkowitz, J. L.: Identification of a human heme exporter that is essential for erythropoiesis. *Cell* 2004, 118(6):757-66.[PMID:15369674]
44. Keel, S. B., Doty, R. T., Yang, Z., Quigley, J. G., Chen, J., Knoblaugh, S., Kingsley, P. D., De Domenico, I., Vaughn, M. B., Kaplan, J., Palis, J., and Abkowitz, J. L.: A heme export protein is required for red blood cell differentiation and iron homeostasis. *Science* 2008, 319(5864):825-8.[PMID:18258918]
45. Yang, Z., Philips, J. D., Doty, R. T., Giraudi, P., Ostrow, J. D., Tiribelli, C., Smith, A., and Abkowitz, J. L.: Kinetics and specificity of feline leukemia virus subgroup C receptor (FLVCR) export function and its dependence on hemopexin. *J Biol Chem* 2010, 285(37):28874-82.[PMID:20610401]
46. Chiabrando, D., Marro, S., Mercurio, S., Giorgi, C., Petrillo, S., Vinchi, F., Fiorito, V., Fagoonee, S., Camporeale, A., Turco, E., Merlo, G. R., Silengo, L., Altruda, F., Pinton, P., and Tolosano, E.: The mitochondrial heme exporter FLVCR1b mediates erythroid differentiation. *J Clin Invest* 2012, 122(12):4569-79.[PMID:23187127]
47. Fleming, M. D., and Hamza, I.: Mitochondrial heme: an exit strategy at last. *J Clin Invest* 2012, 122(12):4328-30.[PMID:23187133]

48. Mercurio, S., Petrillo, S., Chiabrando, D., Bassi, Z. I., Gays, D., Camporeale, A., Vacaru, A., Miniscalco, B., Valperga, G., Silengo, L., Altruda, F., Baron, M. H., Santoro, M. M., and Tolosano, E.: The heme exporter Flvcr1 regulates expansion and differentiation of committed erythroid progenitors by controlling intracellular heme accumulation. *Haematologica* 2015, 100(6):720-9.[PMID:25795718]
49. Vinchi, F., Ingoglia, G., Chiabrando, D., Mercurio, S., Turco, E., Silengo, L., Altruda, F., and Tolosano, E.: Heme exporter FLVCR1a regulates heme synthesis and degradation and controls activity of cytochromes P450. *Gastroenterology* 2014, 146(5):1325-38.[PMID:24486949]
50. Fiorito, V., Forni, M., Silengo, L., Altruda, F., and Tolosano, E.: Crucial Role of FLVCR1a in the Maintenance of Intestinal Heme Homeostasis. *Antioxid Redox Signal* 2015, 23(18):1410-23.[PMID:26067085]
51. Petrillo, S., Chiabrando, D., Genova, T., Fiorito, V., Ingoglia, G., Vinchi, F., Mussano, F., Carossa, S., Silengo, L., Altruda, F., Merlo, G. R., Munaron, L., and Tolosano, E.: Heme accumulation in endothelial cells impairs angiogenesis by triggering paraptosis. *Cell Death Differ* 2018, 25(3):573-588.[PMID:29229999]
52. Allocco, A. L., Bertino, F., Petrillo, S., Chiabrando, D., Riganti, C., Bardelli, A., Altruda, F., Fiorito, V., and Tolosano, E.: Inhibition of Heme Export and/or Heme Synthesis Potentiates Metformin Anti-Proliferative Effect on Cancer Cell Lines. *Cancers (Basel)* 2022, 14(5).[PMID:35267538]
53. Mistretta, M., Fiorito, V., Allocco, A. L., Ammirata, G., Hsu, M. Y., Digiovanni, S., Belicchi, M., Napoli, L., Ripolone, M., Trombetta, E., Mauri, P., Farini, A., Meregalli, M., Villa, C., Porporato, P. E., Miniscalco, B., Crich, S. G., Riganti, C., Torrente, Y., and Tolosano, E.: Flvcr1a deficiency promotes heme-based energy metabolism dysfunction in skeletal muscle. *Cell Rep* 2024, 43(3):113854.[PMID:38412099]
54. Meyer, E., Ricketts, C., Morgan, N. V., Morris, M. R., Pasha, S., Tee, L. J., Rahman, F., Bazin, A., Bessieres, B., Dechelotte, P., Yacoubi, M. T., Al-Adnani, M., Marton, T., Tannahill, D., Trembath, R. C., Fallet-Bianco, C., Cox, P., Williams, D., and Maher, E. R.: Mutations in FLVCR2 are associated with proliferative vasculopathy and hydranencephaly-hydrocephaly syndrome (Fowler syndrome). *Am J Hum Genet* 2010, 86(3):471-8.[PMID:20206334]
55. Duffy, S. P., Shing, J., Saraon, P., Berger, L. C., Eiden, M. V., Wilde, A., and Tailor, C. S.: The Fowler syndrome-associated protein FLVCR2 is an importer of heme. *Mol Cell Biol* 2010, 30(22):5318-24.[PMID:20823265]
56. Li, Y., Ivica, N. A., Dong, T., Papageorgiou, D. P., He, Y., Brown, D. R., Kleyman, M., Hu, G., Chen, W. W., Sullivan, L. B., Del Rosario, A., Hammond, P. T., Vander Heiden, M. G., and Chen, J.: MFSD7C switches mitochondrial ATP synthesis to thermogenesis in response to heme. *Nat Commun* 2020, 11(1):4837.[PMID:32973183]
57. Khan, A. A., and Quigley, J. G.: Heme and FLVCR-related transporter families SLC48 and SLC49. *Mol Aspects Med* 2013, 34(2-3):669-82.[PMID:23506900]

58. Tsuchiya, M., Tachibana, N., Nagao, K., Tamura, T., and Hamachi, I.: Organelle-selective click labeling coupled with flow cytometry allows pooled CRISPR screening of genes involved in phosphatidylcholine metabolism. *Cell Metab* 2023, 35(6):1072-1083 e9.[PMID:36917984]
59. Kenny, T. C., Khan, A., Son, Y., Yue, L., Heissel, S., Sharma, A., Pasolli, H. A., Liu, Y., Gamazon, E. R., Alwaseem, H., Hite, R. K., and Birsoy, K.: Integrative genetic analysis identifies FLVCR1 as a plasma-membrane choline transporter in mammals. *Cell Metab* 2023, 35(6):1057-1071 e12.[PMID:37100056]
60. Ha, H. T. T., Sukumar, V. K., Chua, J. W. B., Nguyen, D. T., Nguyen, T. Q., Lim, L. H. K., Cazenave-Gassiot, A., and Nguyen, L. N.: Mfsd7b facilitates choline transport and missense mutations affect choline transport function. *Cell Mol Life Sci* 2023, 81(1):3.[PMID:38055060]
61. Son, Y., Kenny, T. C., Khan, A., Birsoy, K., and Hite, R. K.: Structural basis of lipid head group entry to the Kennedy pathway by FLVCR1. *Nature* 2024,
62. Nguyen, X. T. A., Le, T. N. U., Nguyen, T. Q., Thi Thuy Ha, H., Artati, A., Leong, N. C. P., Nguyen, D. T., Lim, P. Y., Susanto, A. V., Huang, Q., Fam, L., Leong, L. N., Bonne, I., Lee, A., Granadillo, J. L., Gooch, C., Yu, D., Huang, H., Soong, T. W., Chang, M. W., Wenk, M. R., Adamski, J., Cazenave-Gassiot, A., and Nguyen, L. N.: MFSD7c functions as a transporter of choline at the blood-brain barrier. *Cell Res* 2024, 34(3):245-257.[PMID:38302740]
63. Cater, R. J., Mukherjee, D., Gil-Iturbe, E., Erramilli, S. K., Chen, T., Koo, K., Santander, N., Reckers, A., Kloss, B., Gawda, T., Choy, B. C., Zhang, Z., Katewa, A., Larpthaveesarp, A., Huang, E. J., Mooney, S. W. J., Clarke, O. B., Yee, S. W., Giacomini, K. M., Kossiakoff, A. A., Quick, M., Arnold, T., and Mancia, F.: Structural and molecular basis of choline uptake into the brain by FLVCR2. *Nature* 2024,
64. Beardsley, S. (2016), pp. 130, University of Maryland, College Park, United States -- Maryland
65. Rao, A. U., Carta, L. K., Lesuisse, E., and Hamza, I.: Lack of heme synthesis in a free-living eukaryote. *Proc Natl Acad Sci U S A* 2005, 102(12):4270-5.[PMID:15767563]
66. Vanfleteren, J. R.: Nematode growth factor. *Nature* 1974, 248(445):255-7.[PMID:4819421]
67. Nass, R., and Hamza, I.: The nematode C. elegans as an animal model to explore toxicology in vivo: solid and axenic growth culture conditions and compound exposure parameters. *Curr Protoc Toxicol* 2007, Chapter 1:Unit1 9.[PMID:20922756]
68. Epstein, H. F., and Shakes, D. C. (eds) (1995) Caenorhabditis elegans: Modern Biological Analysis of an Organism Vol. 48. Methods in Cell Biology. Edited by Wilson, L., and Matsudaira, P., Academic Press, San Diego
69. Qadota, H., Inoue, M., Hikita, T., Koppen, M., Hardin, J. D., Amano, M., Moerman, D. G., and Kaibuchi, K.: Establishment of a tissue-specific RNAi system in C. elegans. *Gene* 2007, 400(1-2):166-73.[PMID:17681718]

70. Zhang, A., Ackley, B. D., and Yan, D.: Vitamin B12 Regulates Glial Migration and Synapse Formation through Isoform-Specific Control of PTP-3/LAR PRTP Expression. *Cell Rep* 2020, 30(12):3981-3988 e3.[PMID:32209461]
71. Chun, H., Sharma, A. K., Lee, J., Chan, J., Jia, S., and Kim, B. E.: The Intestinal Copper Exporter CUA-1 Is Required for Systemic Copper Homeostasis in Caenorhabditis elegans. *J Biol Chem* 2017, 292(1):1-14.[PMID:27881675]
72. Kumar, S. B., Arnipalli, S. R., Mehta, P., Carrau, S., and Ziouzenkova, O.: Iron Deficiency Anemia: Efficacy and Limitations of Nutritional and Comprehensive Mitigation Strategies. *Nutrients* 2022, 14(14).[PMID:35889932]
73. Kumar, A., Sharma, E., Marley, A., Samaan, M. A., and Brookes, M. J.: Iron deficiency anaemia: pathophysiology, assessment, practical management. *BMJ Open Gastroenterol* 2022, 9(1).[PMID:34996762]
74. Fiorito, V., and Tolosano, E.: Unearthing FLVCR1a: tracing the path to a vital cellular transporter. *Cell Mol Life Sci* 2024, 81(1):166.[PMID:38581583]
75. Vinchi, F., De Franceschi, L., Ghigo, A., Townes, T., Cimino, J., Silengo, L., Hirsch, E., Altruda, F., and Tolosano, E.: Hemopexin therapy improves cardiovascular function by preventing heme-induced endothelial toxicity in mouse models of hemolytic diseases. *Circulation* 2013, 127(12):1317-29.[PMID:23446829]
76. Mendoza, A. D., Dietrich, N., Tan, C. H., Herrera, D., Kasiah, J., Payne, Z., Cubillas, C., Schneider, D. L., and Kornfeld, K.: Lysosome-related organelles contain an expansion compartment that mediates delivery of zinc transporters to promote homeostasis. *Proc Natl Acad Sci U S A* 2024, 121(7):e2307143121.[PMID:38330011]
77. Dailey, H. A.: Terminal steps of haem biosynthesis. *Biochem Soc Trans* 2002, 30(4):590-5.[PMID:12196143]
78. Tsiftsoglou, A. S., Tsamadou, A. I., and Papadopoulou, L. C.: Heme as key regulator of major mammalian cellular functions: Molecular, cellular, and pharmacological aspects. *Pharmacol. Ther.* 2006, 111(2):327-345
79. Severance, S., Chen, C., and Hamza, I. (2011) Eukaryotic Heme Trafficking Vol. 15: Biochemistry of Tetrapyrroles. 1-48. Handbook of Porphyrin Science. Edited by Kadish, K. M., Smith, K. M., and Guilard, R. 15 vols., World Scientific Publishing Co.